AD NUMBER
AD370261
CLASSIFICATION CHANGES
TO: unclassified
FROM: confidential
LIMITATION CHANGES
TO: Approved for public release, distribution unlimited
FROM: Distribution authorized to U.S. Gov't. agencies only; Administrative/Operational Use; FEB 1954. Other requests shall be referred to Defense Atomic Support Agency, Washington, DC 20301.
AUTHORITY
DNA ltr, 18 Feb 1982; DNA ltr, 18 Feb 1982

SECURITY MARKING

The classified or limited status of this report applies to each page, unless otherwise marked.
Separate page printouts MUST be marked accordingly.

THIS DOCUMENT CONTAINS INFORMATION AFFECTING THE NATIONAL DEFENSE OF THE UNITED STATES WITHIN THE MEANING OF THE ESPIONAGE LAWS, TITLE 18, U.S.C., SECTIONS 793 AND 794. THE TRANSMISSION OR THE REVELATION OF ITS CONTENTS IN ANY MANNER TO AN UNAUTHORIZED PERSON IS PROHIBITED BY LAW.

NOTICE: When government or other drawings, specifications or other data are used for any purpose other than in connection with a definitely related government procurement operation, the U. S. Government thereby incurs no responsibility, nor any obligation whatsoever; and the fact that the Government may have formulated, furnished, or in any way supplied the said drawings, specifications, or other data is not to be regarded by implication or otherwise as in any manner licensing the holder or any other person or corporation, or conveying any rights or permission to manufacture, use or sell any patented invention that may in any way be related thereto.

B / ~/9858

[redacted]

WT-734

Copy No. 184 A

(1)

Operation UPSHOT-KNOTHOLE

~~NEVADA PROVING GROUNDS~~

~~March-June 1953~~

~~FORMERLY RESTRICTED DATA~~
HANDLE AS RESTRICTED DATA IN FOREIGN DISSEMINATION
SECTION 144b, ATOMIC ENERGY ACT 1954

Classification (Cancelled) (Changed to ...)
By authority of ...
By ... Date 11 JUL 1957

Project 3.22

EFFECTS ON ENGINEER BRIDGING EQUIPMENT

CONFIDENTIAL

Classification ~~(Cancelled)~~ (Changed to
By Authority of DASASC-3 memo 19 Jan 62
By ... Date 23 Jan 62

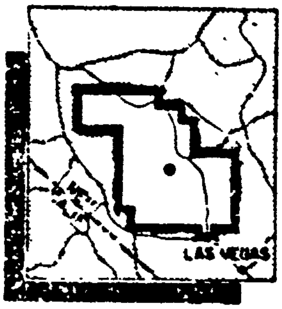

MAR 17 1966

HEADQUARTERS FIELD COMMAND, ARMED FORCES SPECIAL WEAPONS PROJECT
SANDIA BASE, ALBUQUERQUE, NEW MEXICO

U. S. GOVERNMENT AGENCIES MAY OBTAIN COPIES OF THIS REPORT DIRECTLY FROM DDC. OTHER QUALIFIED DDC USERS SHALL REQUEST THROUGH

Director
Defense Atomic Support Agency
Washington, D. C. 20301

[redacted]

GROUP 3
Downgraded at 12 year intervals;
Not automatically declassified

If this report is no longer needed, return it to
AEC Technical Information Service
P. O. Box 401
Oak Ridge, Tennessee

[redacted]

WT-734

This document consists of [redacted] pages

No. [redacted] of [redacted] Copies, Series A

2.7

OPERATION UPSHOT-KNOTHOLE

Project 3.22

EFFECTS ON ENGINEER BRIDGING EQUIPMENT

[redacted]

By

Gerald T. Moore, [redacted]

February 1954

FORMERLY RESTRICTED DATA

RESTRICTED

[redacted]

contents in any manner to an unauthorized person is prohibited.

"This document contains information affecting the National Defense of the United States within the meaning of the Espionage Laws, Title 18, U.S.C., Secs. 793 and 794. Its transmission or the revelation of its contents in any manner to an unauthorized person is prohibited by law."

Engineer Research and Development Laboratories
Fort Belvoir, Virginia

[redacted]

GROUP 3
Downgraded at 12 year intervals;
Not automatically declassified

ABSTRACT

The purpose of Project 3.22, Operation UPSHOT-KNOTHOLE, was to indicate the vulnerability of Army prefabricated fixed bridging to atomic blast and to determine means to reduce the vulnerability. To accomplish this, two 100-ft Bailey bridge spans were erected such that one was exposed to Shot 9 and both were exposed to Shot 10 of the test series; and two single bay sections of bridging were erected to afford a comparison between Bailey and T6 bridging. The presence of a precursor wave and high dynamic pressures in the region of interest for Shot 10 severely limited the value of the results of that part of the experiment. Results indicate that an anchor cable would be the best means of limiting the response of such a bridge.

FOREWORD

This report is one of the reports presenting the results of the 78 projects participating in the Military Effects Tests Program of Operation UPSHOT-KNOTHOLE, which included 11 test detonations. For readers interested in other pertinent test information, reference is made to WT-782, Summary Report of the Technical Director, Military Effects Program. This summary report includes the following information of possible general interest:

1. An overall description of each detonation, including yield, height of burst, ground zero location, time of detonation, ambient atmospheric conditions at detonation, etc., for the 11 shots.
2. Compilation and correlation of all project results on the basic measurements of blast and shock, thermal radiation, and nuclear radiation.
3. Compilation and correlation of the various project results on weapons effects.
4. A summary of each project, including objectives and results.
5. A complete listing of all reports covering the Military Effects Tests Program.

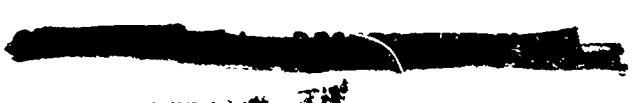

PREFACE

This report embraces all of the work accomplished under Project 3.22, Operation UPSHOT-KNOTHOLE, including test work and analysis work. The report is presented as the first attempt to determine quantitatively the response of Army prefabricated fixed bridging to an atomic blast. Some analytical work has been included for which there is no corresponding test data for purposes of correlation.

A section on blast effects has been included in the first chapter, and a description of the type of bridging tested appears in Chapter 2.

ACKNOWLEDGMENTS

The aid of all of those who were instrumental in making possible this report is gratefully acknowledged. In particular, indebtedness is expressed to the following personnel of the Engineer Research and Development Laboratories:

Maj William G. Krats, WOJG Y. L. Smith, and M/Sgt A. J. Barry for the conception and planning of the project.
Mr. Norman G. Hansen, for his many helpful suggestions and for his part in writing the appendices.
Capt Virgil S. Adkins, for overseeing most of the construction and and administrative matters.
Capt Walter J. Slamk, for his suggestions in the preparation of the final draft.
SFC Robert E. Bowman,
SFC Robert C. Nelson, and
Cpl William Lovelady, for aiding in the many construction and supply problems.
Cpl Charles T. Messinger, for his work in the mathematics.
Cpl Bruce R. Detmers, for his patience in the preparation of the many fine drawings.
Mary Anne Hunter and
Betty E. Serot, for their excellent job of preparing the report.

Many thanks are also due the following:

Dr. Robert J. Hansen, of the Massachusetts Institute of Technology, for his technical guidance.
The members of AFSWP, Program 9, for the technical photography.
Personnel of the Ballistic Research Laboratories, for the acceleration measurements.
Personnel of the Stanford Research Institute and the Naval Ordnance Laboratory for their part in the basic instrumentation; and
Officers and men of the 412th Engineer Construction Battalion, for their cooperative efforts in effecting the construction work.

CONTENTS

ILLUSTRATIONS

TABLES

CHAPTER 1

INTRODUCTION

1.1 OBJECTIVES

The major objective of Project 3.22, Operation UPSHOT-KNOTHOLE, was to determine the effects of atomic bomb blast on military type prefabricated fixed bridging. Specifically, the following objectives were sought:

1. To determine the loading resulting from the blast;
2. To determine which structural components are the weakest and will be damaged at the lowest level of loading;
3. To determine what level of damage may be tolerated without causing progressive failure;
4. To establish analytical methods which may be generally used to calculate the response of truss structures to atomic bomb blast; and,
5. To investigate practical methods of limiting the structural response of a Bailey bridge to blast loading.

1.2 SCOPE

The test work accomplished as part of this project involved subjecting three bridge structures to Shot 9 and the same three structures plus a fourth to Shot 10. High speed photography and acceleration measurements recorded the response of two of the bridges.

The bridge was represented by a relatively simple mechanical system whose response to an idealized forcing function was calculated by analytic means. The results are correlated with test results insofar as is possible.

1.3 BACKGROUND

Subsequent to the use of the atomic bomb at Hiroshima and Nagasaki, it became apparent that a program of investigation into defense against atomic warfare as applied in the strategic and tactical operations of any possible future enemy should be undertaken. As a part of this program, the effects of nuclear detonation upon many kinds of tactical

equipment and structures have been studied. This part of the program has, in general, encompassed three types of investigations. They are:

1. An investigation into blast and radiation phenomena occurring in ground and air media in the vicinity of a detonation (or in the water media where applicable).

2. An investigation of the forces on or impulses imparted to test items by the blast wave.

3. A study of the reaction of the various test items to the resulting forces, impulses, or thermal radiation intensities.

At the outset of the program (and even before Hiroshima) attempts were made at theoretical analysis which would, by considering the energy and momentum relations and the thermodynamic properties of the medium, predict the blast phenomena. This medium was generally air, and it is the blast wave in air that is of interest here. Reference 12, Resume of the Theory of Plant Shock and Adiabatic Waves with Applications to the Theory of Shock Tubes, published in March, 1950, by the Ballistics Research Laboratories and Ref 13, Operation GREENHOUSE Scientific Directors' Report, Annex 3.3, U. S. Air Force Structures, Appendix E, Section I, WT-59, develop this theory. Reference 1, The Effects of Atomic Weapons, prepared under the direction of the Los Alamos Scientific Laboratory, presents an excellent description of a nuclear detonation with its associated blast, thermal, and radiation phenomena. Reference 2, The Capabilities of Atomic Weapons, Department of the Army Technical Manual, TM 23-200, presents up-to-date weapons effects data in graphical form.

It is by no means implied here that the basic phenomena are completely or even nearly completely understood. As is brought out further in this report, much remains to be learned of blast phenomena for detonations at relatively low altitudes.

Much experimental and analytical work has been accomplished and is at the present being undertaken to form criteria which will make possible accurate calculations of the force of the blast wave on all types of structures. In addition to tests involving relatively large test structures being subjected to atomic blasts, laboratory tests of simple geometric shapes or model structures in shock tubes and wind tunnels have been conducted. Of particular interest here is the work done at the Massachusetts Institute of Technology in the latter part of 1950 and early 1951 on truss bridges, Ref 8, Behavior of Truss Bridges Under Blast from an Atomic Bomb. Model bridge trusses and floor sections were tested separately and together mounted on force-sensing supports in a wind tunnel. In this way, such effects as shielding of one truss by another as a function of the spacing between the two trusses and the effect of the angle between the direction of blast propagation and the centerline of the bridge were determined. After the forces were determined, a response analysis of the prototype bridge was made.

1.4 THEORY

The major phenomena associated with an atomic burst may be catalogued as blast phenomena, thermal radiation phenomena, and gamma and neutron radiation phenomena. It is the effects of blast which are of primary importance with a bridge structure. The nuclear reaction which

occurs when an atomic bomb is detonated is accompanied by the release of a vast quantity of energy, a large portion of which heats and vaporizes the materials of which the weapon is composed. The high pressure of the vaporized materials thus created gives rise to an outward movement, and a radially expanding, spherical shock wave is initiated. The blast manifests itself at a point near the ground as a sudden rise in pressure from ambient atmospheric pressure to a peak whose value depends on the size of the weapon and the distance to the point in question. The passage of the blast wave is accompanied by high velocity winds traveling in the direction of blast propagation and a decay in pressure back to ambient. This series of events is termed the positive phase, and the duration of the events is the positive phase duration. After reaching ambient, the overpressure continues to drop to a negative value somewhat less in magnitude than the corresponding peak positive overpressure. It then slowly rises to ambient. This latter series of events is the negative phase.

In the absence of precursor or similar effects, the ideal blast wave overpressure may be represented approximately by the equation

$$p(t) = P_{so}\left(1 - \frac{t}{t_1}\right)\epsilon^{-K\frac{t}{t_1}} \qquad (11)$$

where $p(t)$ = free stream overpressure (pressure above atmospheric) as a function of time
P_{so} = peak overpressure
t_1 = positive phase duration
K = a number which experimentally has been shown to vary from about 0.2 to 2.2

It will be noted that, in the equation, $t = 0$ is taken to be the time at which the wave arrives at the point in question. The relation is illustrated in Fig. 1.1.

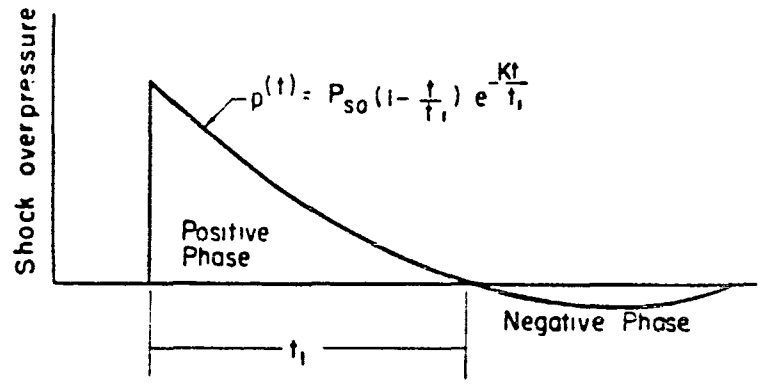

Fig. 1.1 Shock Overpressure-Time Curve Showing Positive and Negative Phases

The interpretation of the blast wave in terms of a forcing function is not as easy to express analytically as is the blast wave itself. The force on a structure begins with the incidence of the blast wave on the surface of the structure and can be broken down into two components: the shock force, F_s , and the drag force, F_d. The F_s is attributed to the force of the blast front on the structure and is initially the reflected pressure of the blast wave multiplied by the area of the structure normal to the direction of blast propagation. The reflected pressure rapidly decays to side-on (free stream) pressure, and F_s accordingly decays. When the shock front reaches and begins to travel down the rear face of the structure, pressure builds up on that face and soon reaches side on value. Thus, the shock force on the front face is soon opposed by an equal and opposite force on the rear face, and the net value of F_s on the structure becomes zero. The length of time that a net shock force is acting on the structure is, therefore, dependent on the time it takes the shock front to pass from the front face to the rear face, and so is dependent on the depth of the structure in the direction of blast propagation. Since for structures of small depth the shock force acts for such a short period of time compared to the response time of the structure, it is quite often convenient to consider the shock impulse, I_s , rather than the shock force. It has been found that the shock impulse varies very nearly linearly with the initial side-on overpressure, P_{so} , for any given structural member; and, therefore, a quantity may be introduced which is a constant property of the structure considered (Chapter 3, Ref 8). This quantity is the ratio of unit impulse to peak overpressure, where unit impulse is the impulse per unit of area upon which the shock front is incident. The shock impulse imparted to the structure on passage of the blast wave is thus given by the following equation:

$$I_s = \left(\frac{I_o}{P_{so}}\right) P_{so} A \qquad (1.2)$$

where I_o = unit impulse (impulse delivered to the structure per unit area)
A = area exposed to the shock front
$\left(\frac{I_o}{P_{so}}\right)$ = ratio of unit impulse to peak overpressure (a property of the structure)

Values of the ratio of unit impulse to peak pressure may be tabulated for different structures and are presented in Fig. 1.2 as a function of dimensions for a rectangular section.

The drag force results from the high velocity winds immediately following the shock front. The force is expressed by the equation

$$F_d = C_d q A_{eff} \qquad (1.3)$$

where: C_d = drag coefficient, a non-dimensional constant
A_{eff} = area effective in resisting drag pressure
q = dynamic drag pressure

The dynamic pressure, q , is defined mathematically through the relation

$$q = \frac{1}{2} \rho v^2 \qquad (1.4)$$

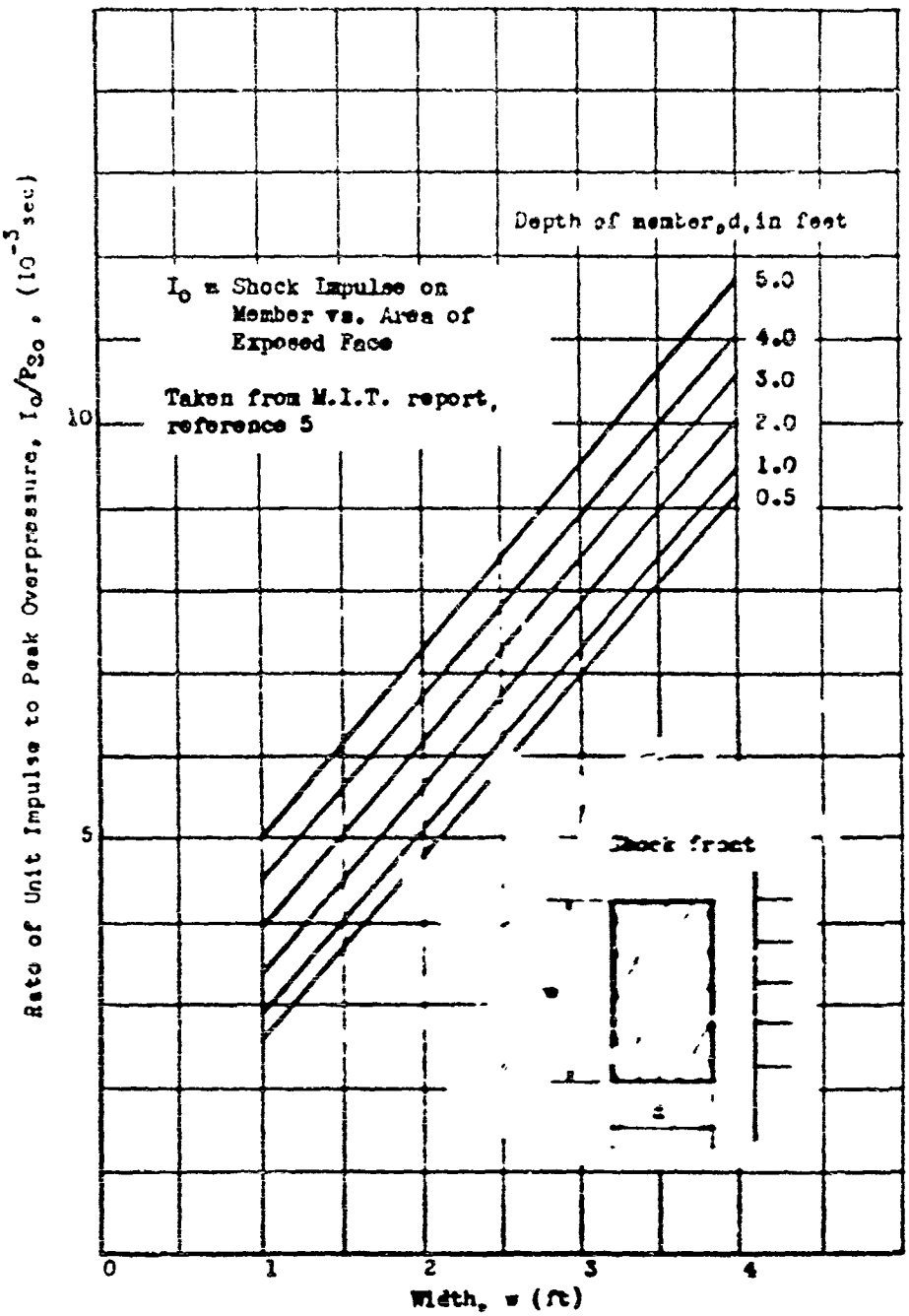

Fig. 1.2 Shock Impulse as a Function of Width and Depth of Member Subject to Normal Shock

where: ρ = density of the medium (air)
v = velocity of the medium (wind velocity)

For an ideal plane adiabatic shock wave, ρ and v are single valued functions of p for any particular ambient atmospheric pressure; so, for any instantaneous value of p, there exists a corresponding value of q. The relation is

$$q = \frac{5/2\, p^2}{7P_0 + p} \qquad (1.5)$$

where: P_0 = atmospheric pressure.

Thus, from the overpressure-time curve and from Fig. 1.3, a dynamic pressure-time curve may be constructed. It should be remembered that this curve is derived assuming the validity of Equation 1.5. Under certain circumstances significant deviations from this curve have been observed, and values of q actually realised have been higher than would be indicated by the corresponding value of p. (See Section 4.2.1 and Fig. 4.10.)

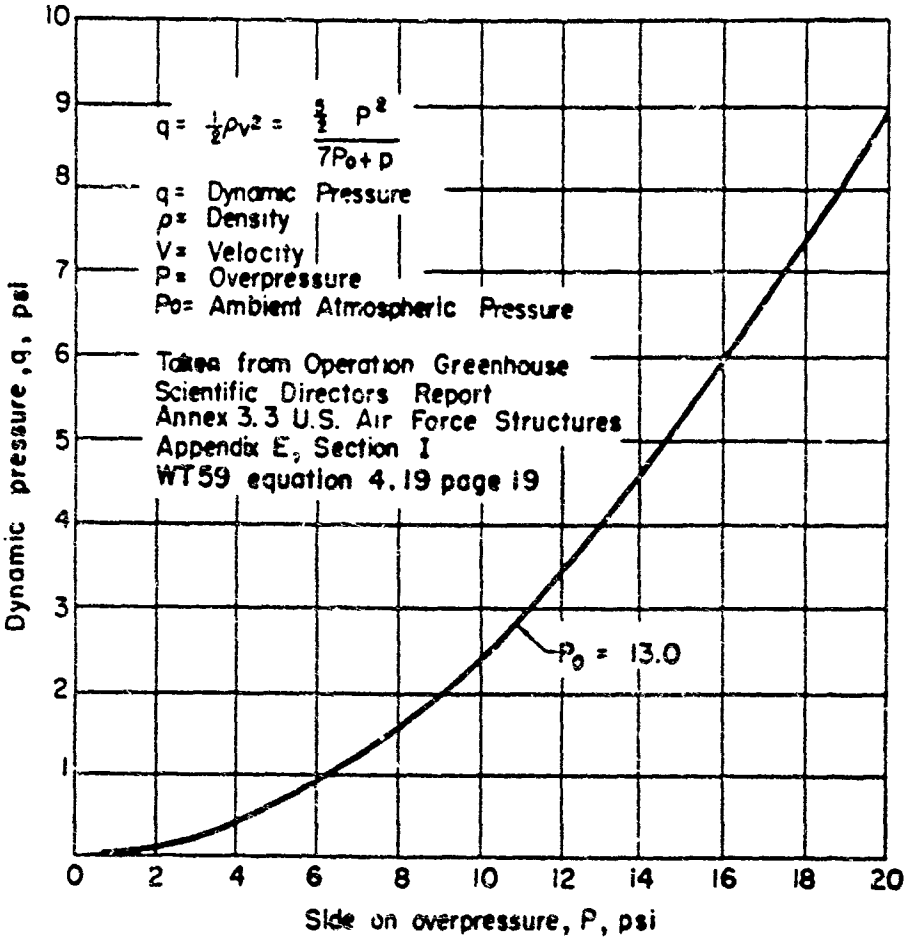

Fig. 1.3 Dynamic Pressure vs Side on Overpressure

The dynamic pressure vs time curve may be interpreted in terms of a force-time curve by application of Equation 1.3. This is plotted in Fig. 1.4 with the assumption that C_d is a constant and does not depend upon q. In calculations, it is convenient to approximate this relation--at least, over the positive phase region--by a simple, expressible analytic function. Two possible functions are the following:

$$F_d(t) = F_{do}\epsilon^{-\frac{4t}{t_1}} \tag{1.6}$$

$$F_d(t) = F_{do}\epsilon^{-\frac{4t}{t_1}}\cos 90\frac{t}{t_1} \tag{1.7}$$

where: F_{do} = peak value of drag force
The relative unimportance of the negative phase is apparent in Fig. 1.4.

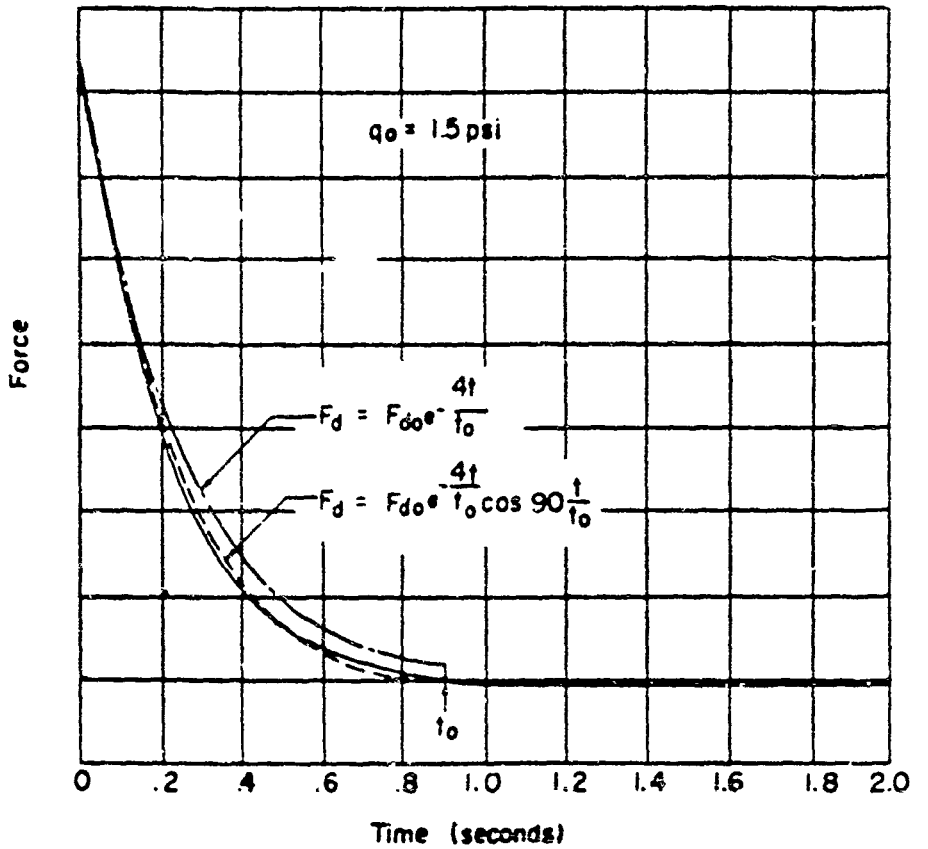

Fig. 1.4 Drag Force vs Time

CHAPTER 2

PREFABRICATED FIXED BRIDGING

2.1 GENERAL

The term "prefabricated" applies to bridges which are assembled "erector set" fashion from preformed structural components or bridging material. The word "fixed" is used to distinguish this class of bridging from floating or ponton bridges.

The present standard prefabricated fixed bridge in major use by the Army is the panel bridge, Bailey type, M2 (Ref 3, TM 5-277), or the "Bailey," as it is called. Several alternate types of fixed bridging are in various stages of development. The most promising of these now appears to be the Bridge, Fixed, Panel, Single Lane, Aluminum, T6, or simply the "T6," as it is referred to hereinafter. It was thus deemed desirable that the major effort of Project 3.22 should be directed toward a test of Bailey bridging. A lesser part of the work was to deal with a comparison test between T6 and Bailey bridging.

2.2 THE BAILEY, M2, BRIDGE

Bailey components are such that lengths of bridge in multiples of 10 ft up to a maximum of 210 ft and capacities up to 80 tons are possible. The major load-carrying components are the panels, transoms, stringers, and decking; and a description of these parts follows.

2.2.1 Panel

The Bailey panel is 10 ft long and approximately 5 ft high and is fabricated primarily from 4 in. channel sections. The bridge trusses consist of several panels pinned end to end to provide the desired length and bolted side-by-side or one above the other to obtain the desired capacity. The type of truss construction is designated by a term such as double-truss, single-story, or simply double-single, by which is meant a truss section composed of two panels side-by-side and one panel high. Truss constructions up to triple-triple are possible. Figure 2.1 shows a single, isolated Bailey panel; and Fig. 2.2 illustrates double-single truss construction with a cutaway view.

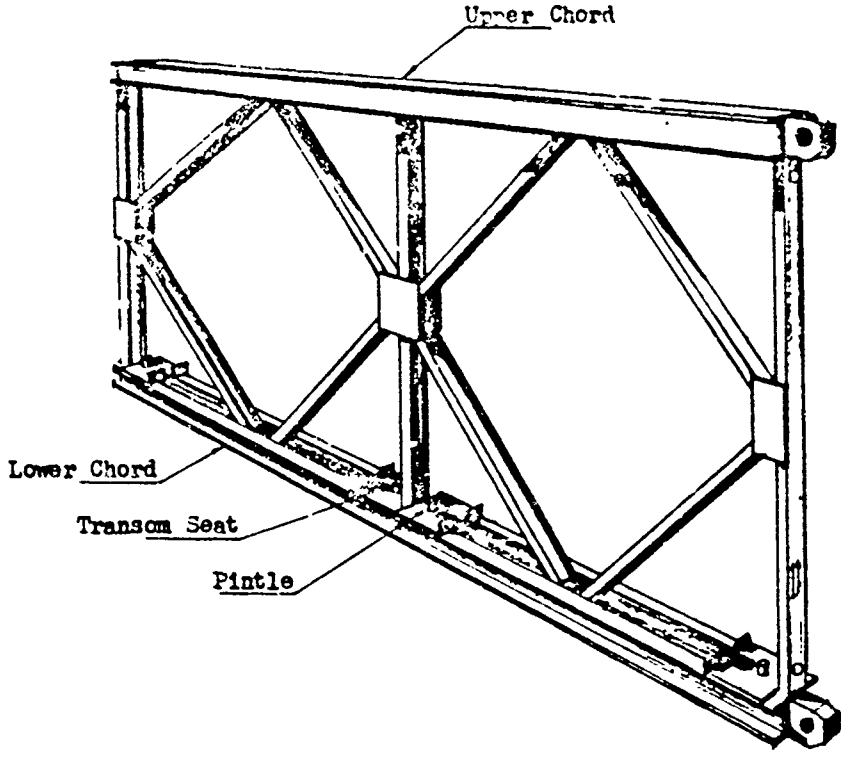

Fig. 2.1 Bailey Panel

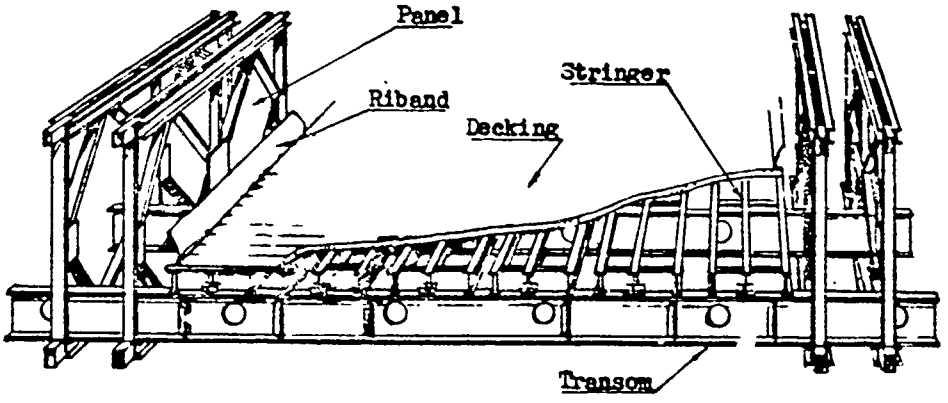

Fig. 2.2 Double-Truss Single-Story Bailey Construction

A 10-ft length of bridging is an integral unit attached to adjacent lengths only by the pins connecting the panels. Such a section is called a "bay" of bridging.

2.2.2 Transom

The transom is an I-beam approximately 20 ft long which crosses underneath the flooring and stringers and which rests on the transom seat (see Fig. 2.1) of the lower chord members of the panels. It serves to transmit load from the deck and stringers to the trusses and to tie the two trusses together. An isolated transom is illustrated in Fig. 2.3. Figure 2.2 shows the incorporation of the transom in the overall structure.

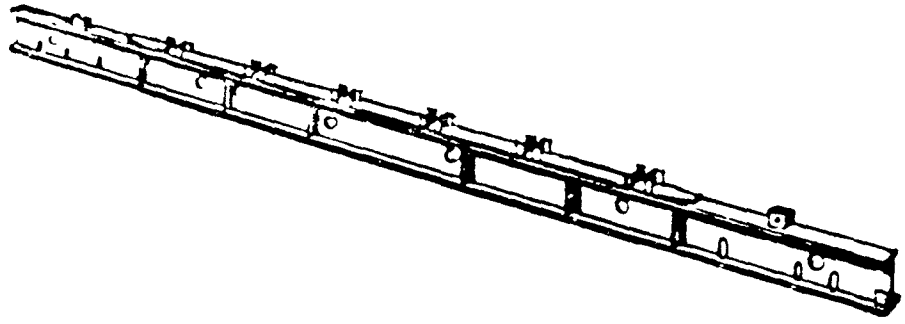

Fig. 2.3 Bailey Transom

2.2.3 Stringers and Decking

The stringers support the deck with its load and transmit this load to the transoms. They are composed primarily of 4-in. I-beam members 10 ft long. Three such members are attached together by means of lateral spacing members, and thus form a stringer unit. Six stringer units are placed side-by-side across the transoms as in Fig. 2.2 to provide complete decking support for one bay of bridge.

Stringers are of two types--button and plain. The button stringers have notches to receive the ends of the floor planks. Two of the six stringers in each bay of the bridge are of this type.

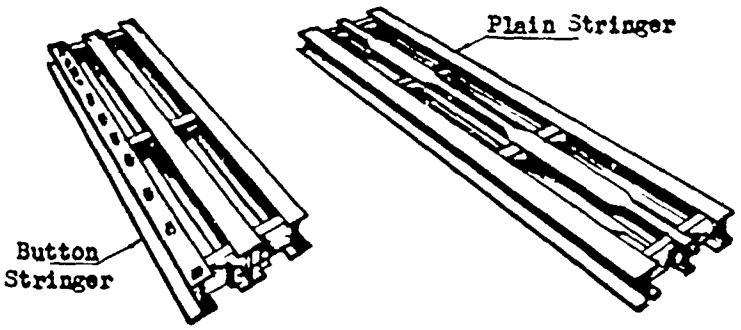

Fig. 2.4 Bailey Stringers

Three-in. thick by 9-in. wide planks (or chess, as they are called) provide a solid deck. A chess is illustrated in Fig. 2.5.

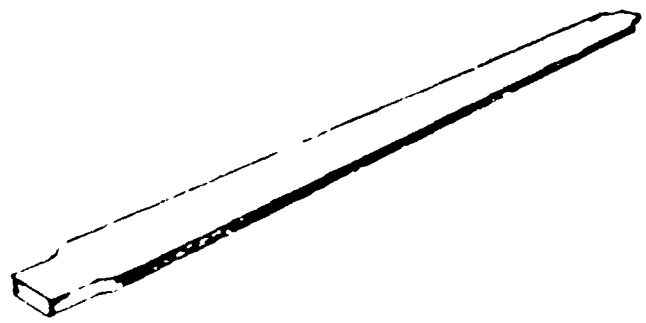

Fig. 2.5 Bailey Chess

The completed bridge with chess and minor non-load-carrying components appears in Fig. 2.6. These additional components are rakers, bracing frames, end posts, riband, transom clamps, and sway braces.

2.2.4 Rakers

The rakers provide lateral support for the inner truss panels. They run diagonally from the top of the panel down to the transom.

2.2.5 Bracing Frames

The bracing frames serve to rigidly brace the outer panels to the inner panels, thus making the truss a rigid unit.

2.2.6 End Posts

The end posts attach to the panels at the end of the bridge, thus providing a link between the trusses and the bridge bearings.

2.2.7 Riband

The riband or curb rail acts both in the capacity of a curb and in the capacity of a clamp to clamp the plank deck to the stringers of the bridge.

2.2.8 Transom Clamp

The transom clamp rigidly clamps the transom to the panel as indicated in Fig. 2.7. The lower part of the clamp fits into the slot in the transom seat, and the upper part fits into a slot in the upright member of the panel.

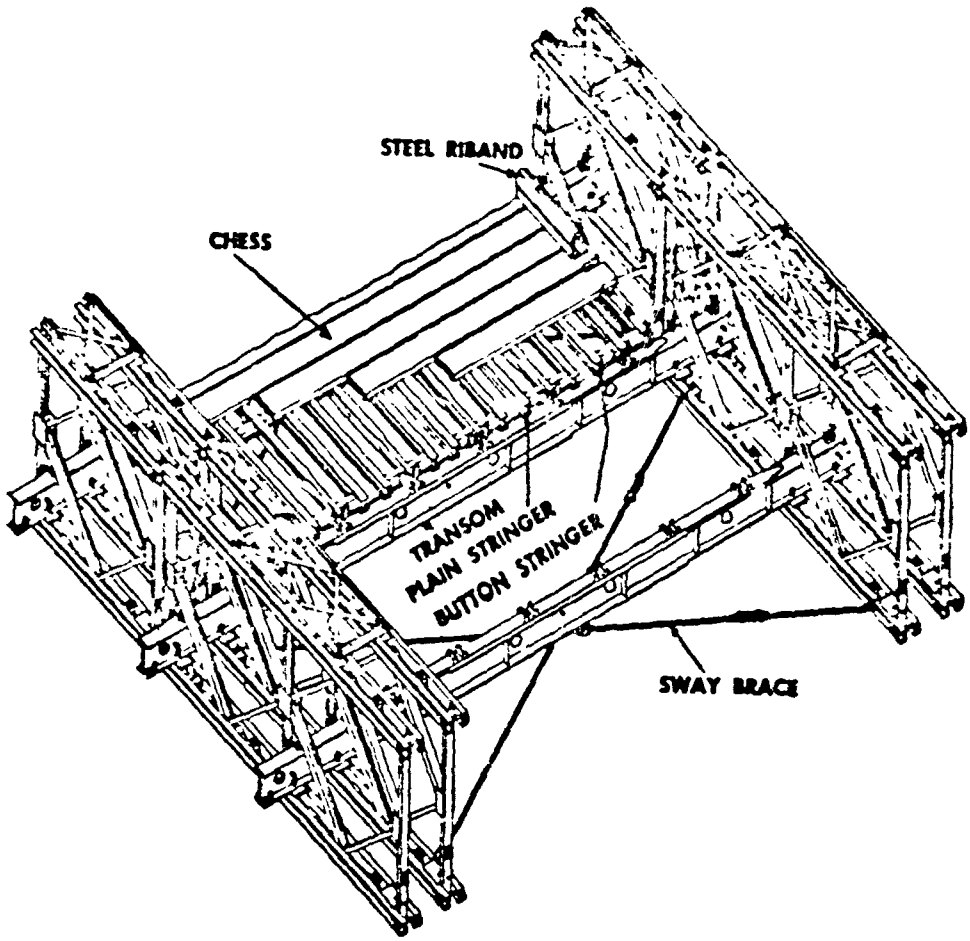

Fig. 2.6 Location of Bridge Parts in Decking of Double-Single Bridge

Fig. 2.7 Transom Clamp in Place

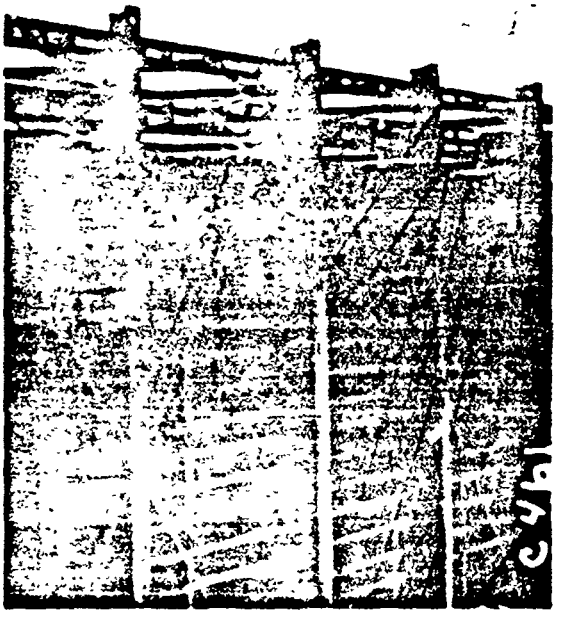

Fig. 2.8 View of Underside of Bailey Showing Sway Bracing

2.2.9 Sway Bracing

The underside of the bridge as seen in Fig. 2.8 shows the sway brace connections. The sway bracing (or lateral bracing) provides lateral strength and rigidity to the structure as a whole when subjected to horizontal loads; and the sway bracing, as we shall see later, is very important in blast loading calculations.

2.3 THE T-6 BRIDGE

The T-6 has in general the same components as the Bailey, the main differences being in its size, weight, and carrying capacity. For instance, a T-6 bay is 15 ft long. The part of the T-6 corresponding to the transom in the Bailey is called a floor beam, and the part corresponding to a Bailey's raker is called a truss brace. A solid aluminum deck is used on the T-6. A bay of T-6 is shown in Fig. 2.9.

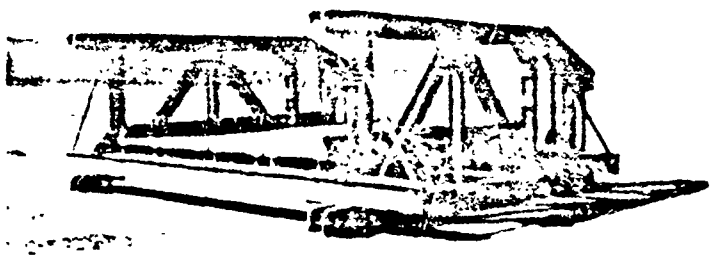

Fig. 2.9 The T-6 Bridge

CHAPTER 3

EXPERIMENT DESIGN

3.1 GENERAL

The test work accomplished under Project 3.22 involved two atomic detonations over the same ground zero and three test structure sites referred to herein as sites A, B, and C. The two atomic shots were Shots 9 and 10 of the test series. The Project 3.22 test sites were laid out at distances from the intended ground zero such that the blast conditions were anticipated to be as indicated in Table 3.1.

TABLE 3.1 - Anticipated Blast Conditions

Site	Shot 9			Shot 10		
	P_{so} (psi)	q_o (psi)	t_1 (sec)	P_{so} (psi)	q_o (psi)	t_1 (sec)
A	13.0		0.76	12.0	3.5	0.60
B	8.0	1.6	0.80	3.5	0.3	0.75
C	16.8		0.74	19.0	8.2	0.50

The anticipated q_o values were calculated from the expected maximum pressures based on the relationships which apply to idealized or non-precursor type blast waves in the Mach region.

3.2 TEST STRUCTURES

The structure chosen for the major part of the test effort was a 100-ft double-single Bailey bridge, and two of these were tested. One was subjected to Shot 9, and both were subjected to Shot 10. This particular bridge was chosen for two reasons: first, sufficient bridging material for two such bridges was readily available; and second, the bridge is of intermediate length and capacity and therefore permits extrapolation of results to both shorter and longer bridges.

3.2.1 Shot 9

A 100-ft double-single Bailey bridge was erected at Site B prior to the shot. The bridge was positioned on piers as shown diagrammatically in Fig. 3.1 such that its lower chord was approximately 22 ft above ground level and its centerline was perpendicular to the anticipated direction of blast propagation. This particular elevation was chosen to facilitate non-dust-obscured motion picture coverage of bridge response. The perpendicular orientation was chosen in consideration of the results of the M. I. T. wind tunnel tests, where it was shown that maximum loading severity occurs for blast loading almost directly from the side of the bridge. The completed bridge is illustrated in Fig. 3.2.

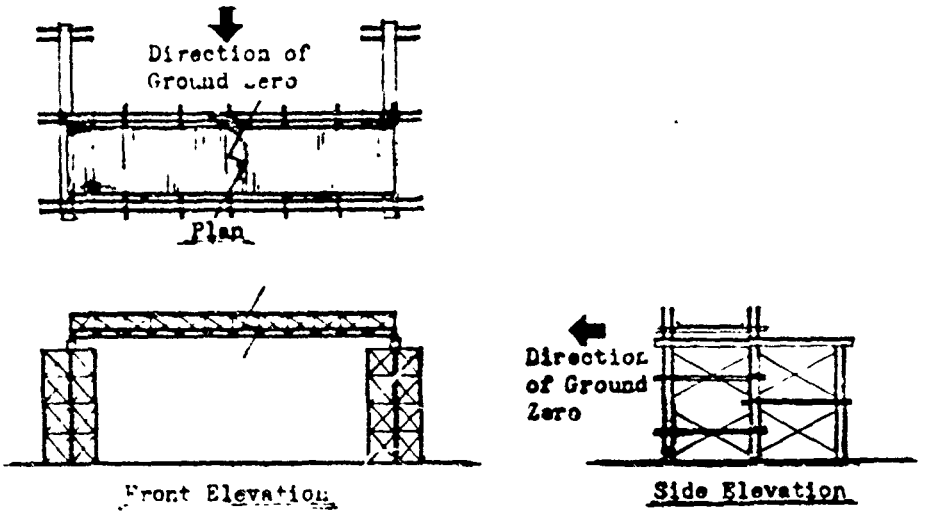

Fig. 3.1 Bailey Bridge Test Structure

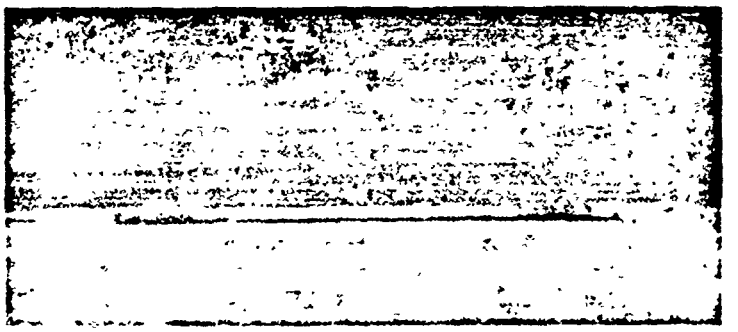

Fig. 3.2 Completed Test Structure at Site B

Site B was located such that the anticipated shock and wind forces would be essentially horizontal.

Each of the bridge end posts was fitted at its lower end with a short piece of cylindrical bar attached in such a manner that the centerline of the bar was horizontal and perpendicular to the centerline of the bridge, as in Fig. 3.3. These bars in turn rested in channel irons which were bolted to the top of the piers. The entire weight of the bridge was therefore transmitted to the channels through eight such bars (four end posts at either end of the bridge) and was free to slide in the channels.

Piers similar to those at Site B were erected at Site A in preparation for an identical bridge. The bridge at A was not placed, however, until just prior to Shot 10. Figure 3.4 illustrates the piers.

At Site C, there were two structures--a single bay of Bailey single-single without deck and stringers, and a single bay of T6 with decking.

Again, the orientation was chosen perpendicular to the direction of blast propagation.

3.2.2 Shot 10

A bridge identical to that at Site B was erected at Site A for participation in the Shot 10 test, as has previously been mentioned.

It was realized that the blast conditions at Site B would not be as severe for Shot 10 as they had been for Shot 9, so the bridge was welded solidly in place to increase the severity of the loading. In every other respect, the structures were arranged as for Shot 9.

3.3 INSTRUMENTATION

Data for Project 3.22 was provided by three means: basic instrumentation, project instrumentation, and before-and-after inspection.

3.3.1 Basic Instrumentation

Basic data used in this report consist of overpressure-time and dynamic pressure-time measurements made at stations along the blast line and at different heights above ground level at each station. Instrumentation for these measurements was provided by the Naval Ordnance Laboratory and by the Stanford Research Institute.

Certain assumptions had to be made concerning these data. Since the bridge structures were not placed along the blast line, it was necessary to assume a symmetrical blast wave about ground zero; i.e., that the blast intensity and duration along any line extending from ground zero was the same as the intensity and duration along the blast line for equal distances from ground zero. Also, since measurements were not made at the exact ground range of the bridge or the exact height above ground level of the bridge, it was necessary to interpolate data both as to height and range.

The coordinates of the true ground zero with respect to the intended ground zero (the aiming point) were also supplied as basic data.

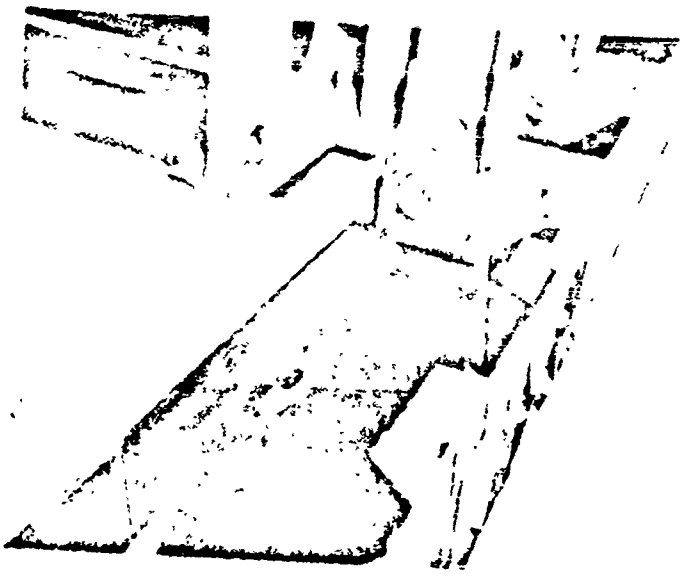

Fig. 3.3 Bridge Mounting, Site B

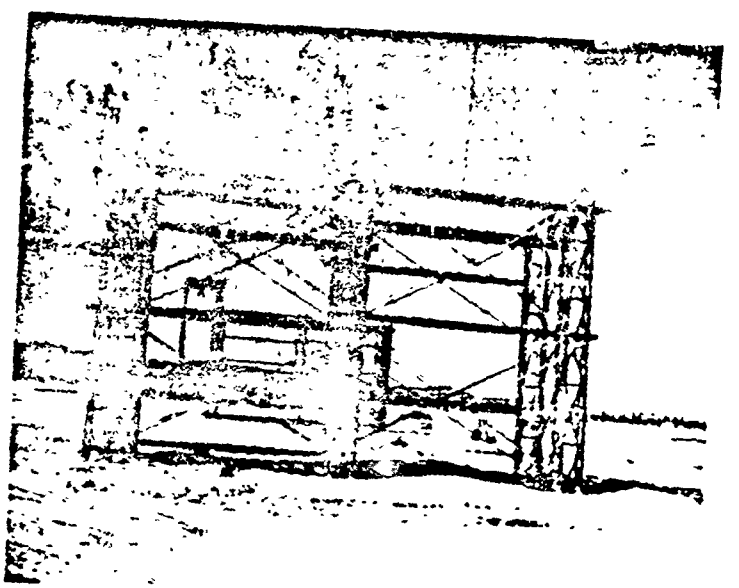

Fig. 3.4 Piers, Site A

3.3.2 Project Instrumentation

The instrumentation which was accomplished in direct support of Project 3.22 consisted of acceleration measurements (carried out by personnel of the Ballistic Research Laboratories) and motion picture coverage of bridge response (by AFSWP, Program 9).

Each of the bridges at Sites A and B had one accelerometer of the remote recording type, backed up by one self-contained recording accelerometer. The remote recording and self-contained accelerometers were both attached to the bridge two bays from one end (two-tenths of the length of the bridge from one end) in such a manner as to measure acceleration in a horizontal plane in a direction toward and away from the intended ground zero. Figure 3.5 illustrates the placement of the gages.

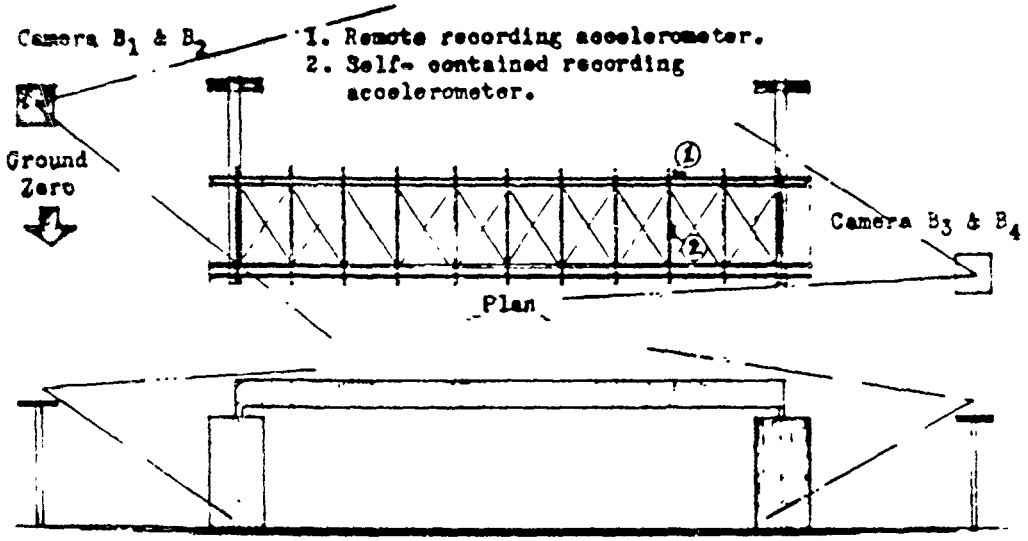

Fig. 3.5 Accelerometer and Camera Locations at Site B

Motion pictures were to provide a visual record of the bridge response at Site B for Shot 9 and at Site A for Shot 10. Four cameras were located off the ends of the bridge on towers at Site B as shown in Fig. 3.5. At Site A, two cameras were used, located at approximately the same relative position as cameras B_1 and B_2 at Site B.

Vertical, evenly spaced stripes were painted on the side of the channel irons on the piers. So, by choosing any point of reference on the bridge, the time displacement history of the bridge may be shown merely by plotting the position of this point with reference to the

scale versus time. It was planned that enlargements of selected motion picture frames would be made to accomplish this.

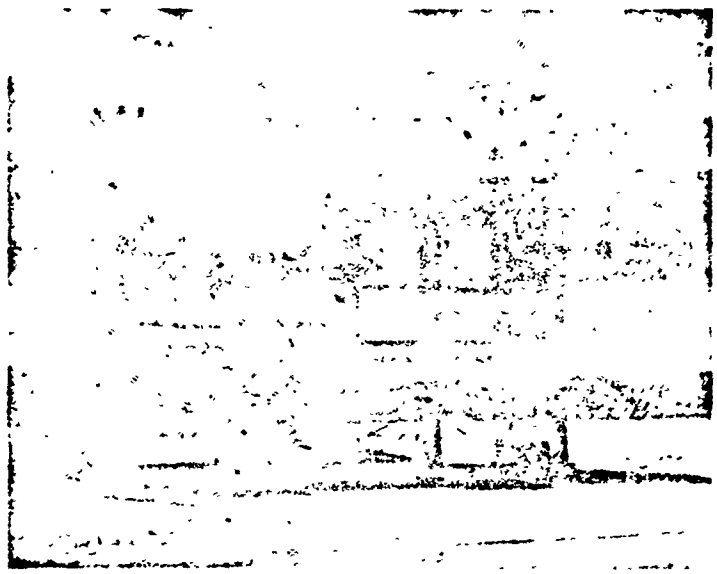

Fig. 3.6 View of Pier and End of Bridge, Site B

CHAPTER 4

RESULTS

4.1 SHOT 9

4.1.1 Site A

As has been stated in Chapter 3, the bridge at Site A was not erected for participation in Shot 9; however, it is of interest to note the effect of the blast on the piers at that site, since these piers were made of standard Bailey components. We shall introduce, at this point, an angle of yaw which is the angle between the bridge centerline and the blast front (further defined in Fig. 4.1). Due to bombing error, this angle was not zero as was planned. The basic data are presented in Table 4.1.

TABLE 4.1 - Basic Data, Shot 9, Site A

	P_{so} (psi)	q_o (psi)	t_1 (sec)	θ (deg)
Actual	11.0	2.45	0.81	18.4
Predicted	13.0	4.0	0.76	0

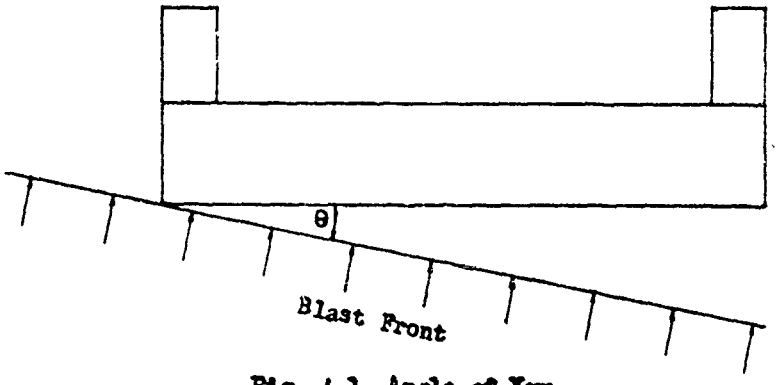

Fig. 4.1 Angle of Yaw

Figure 4.2 is a reproduction of a pressure-time record from a gage station located at approximately the same range as Site A and at an elevation of 10 ft.

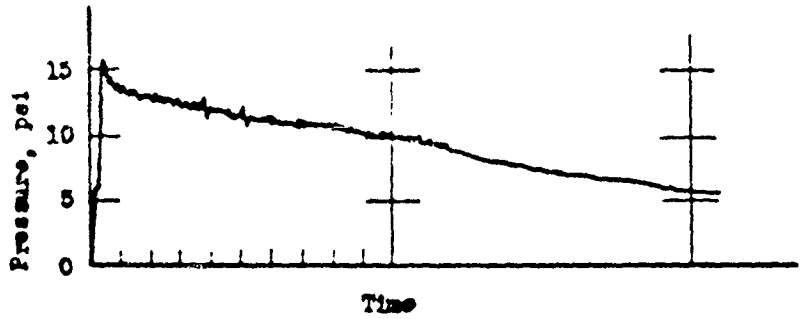

Fig. 4.2 Shot 9 Overpressure Record at the Approximate Range of Site A

Figure 4.3 shows portions of the piers after Shot 9. Examination of these photographs reveals bending in the panel chords at the point of juncture with the sway braces. It will be noticed that the sway braces that were anticipated would be in tension had been doubled to increase the overall strength of the pier. This is not standard Bailey construction.

4.1.2 Site B

Table 4.2 shows the basic data relative to Site B for Shot 9. The peak overpressure and positive phase duration were obtained by extrapolating data obtained at gage stations as shown in Appendix B. The vertical component of thermal intensity is also included as being of importance in the ignition of the wooden deck.

TABLE 4.2 - Basic Data, Shot 9, Site B

	P_{so} (psi)	q_o (psi)	t_1 (sec)	Q_v (cal/cm)	θ (deg)
Actual	7.75	1.52	0.94	19.5	11.0
Predicted	8.00	1.62	0.80		0

Figure 4.4 is a reproduction of a pressure-time record taken from a gage station located at approximately the same range as Site B and at an elevation of 10 ft.

At the range of the bridge, the Mach stem reached a height of 28.5 ft (Ref 5, WT-711); and the bridge was presumably entirely within the Mach reflection region, since its overall height above ground level was 27.0 ft.

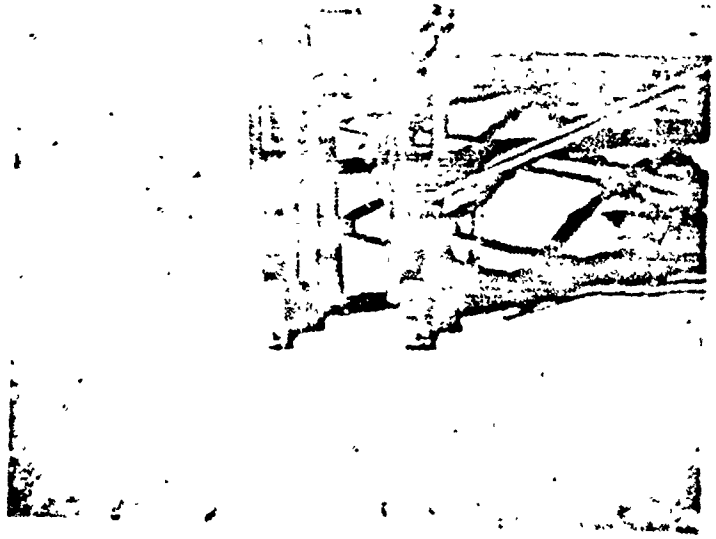

a. North Pier

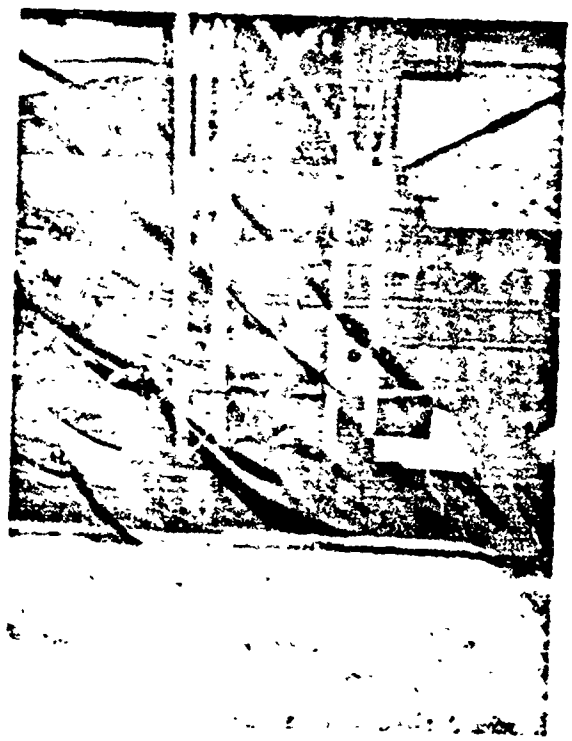

b. South Pier

Fig. 4.3 Damage Portion of Site A Piers After Shot 9

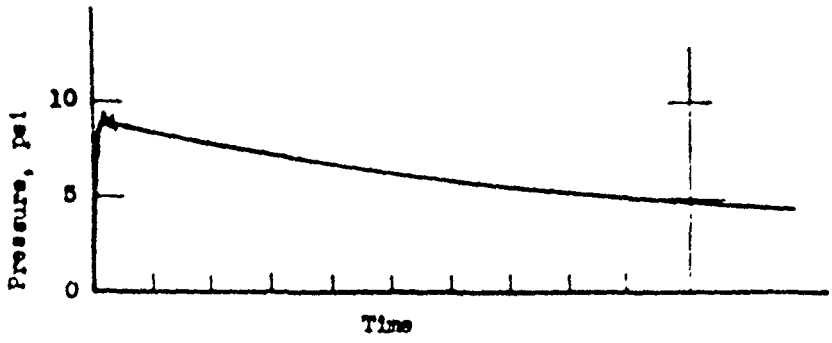

Fig. 4.4 Shot 9 Overpressure Record at the Approximate Range of Site B

The response of the bridge may be followed in the series of photographs in Fig. 4.5. These photos are merely enlarged prints of 16 mm moving picture frames. Figure 4.5a shows the bridge 0.30 sec after detonation time. The incident thermal energy has ignited the deck, and the deck is smoldering. Figures 4.5a through 4.5d present the thermal phase of the response. At H + 3.05 sec (Fig. 4.5e), the blast wave has arrived. Figure 4.5f shows the bridge after passage of the blast wave. A postshot inspection of the deck revealed that the net effect of the burning was to char only slightly the surface of the paint.

Figure 4.6 presents the displacement of the two ends of the bridge as a function of time as determined from the motion pictures of each end (Appendix C). It will be noted that the total distance slid was 30 in. on one end of the bridge, and 57 in. on the other end. Therefore, the center of gravity moved $\frac{30 + 57}{2}$ in., or 43.5 in.

Inspection of the skid marks in the channel showed that the bridge came to a stop at its maximum displacement and did not thereafter slide back toward ground zero during the negative phase. The skid marks showed evidence that the bridge had slid sideways slightly, such that the lower part of the end posts were binding against one edge of the channel over part of the bridge travel. This is shown in Fig. 4.7.

The acceleration record obtained from the ERA gage is given in Fig. 4.8. The record obtained from the Wiancko acceleration measurements appeared extremely erratic and indicated frequencies in excess of the natural frequency of the gage (100 cps). Since the instrumenting agency encountered trouble with the recording apparatus, those records are only presented in part. Figure 4.9 is taken directly from the records.

No permanent deformation of bridge or pier components was detectable. Other than sliding of the bridge as a unit and slight charring of the painted surfaces, the only damage occurred in the slight lifting of the floor sections of two bays. It required less than 5 min for one man to jostle them into place with a bar.

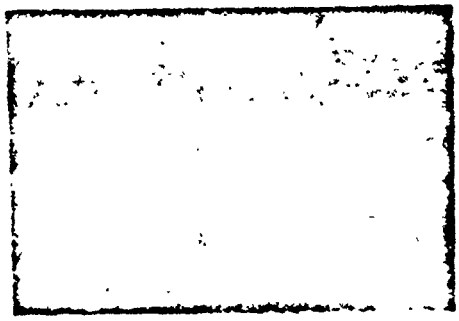

a. H 0.30 sec

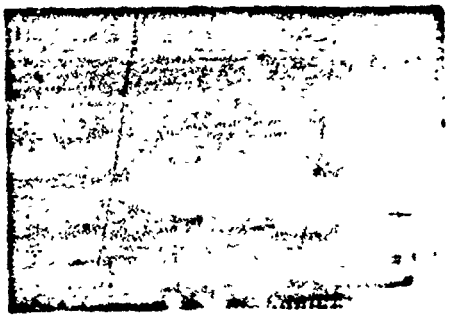

b. H 0.68 sec

c. H 1.70 sec

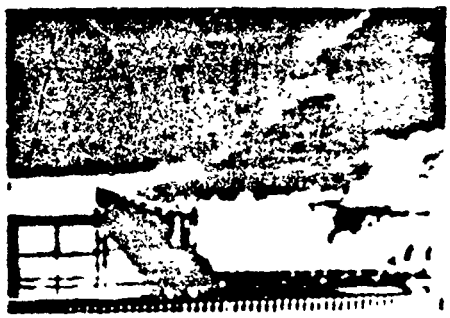

d. H 3.01 sec

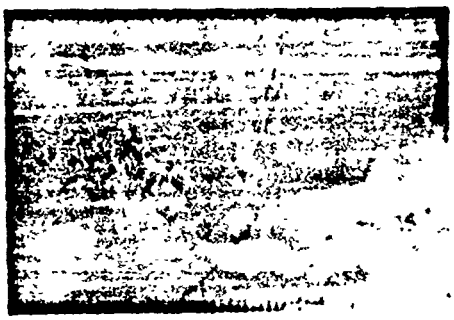

e. H 3.05 sec.

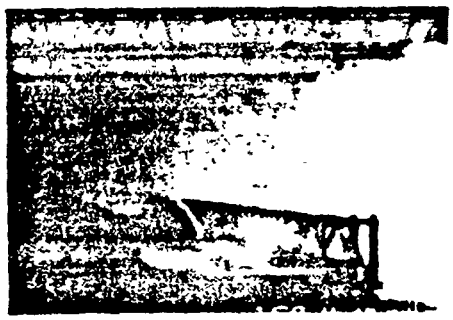

f. H 5.85 sec

Fig. 4.5 Ignition and Burning of Bridge Deck at Site B Subsequent to Detonation of Shot 9

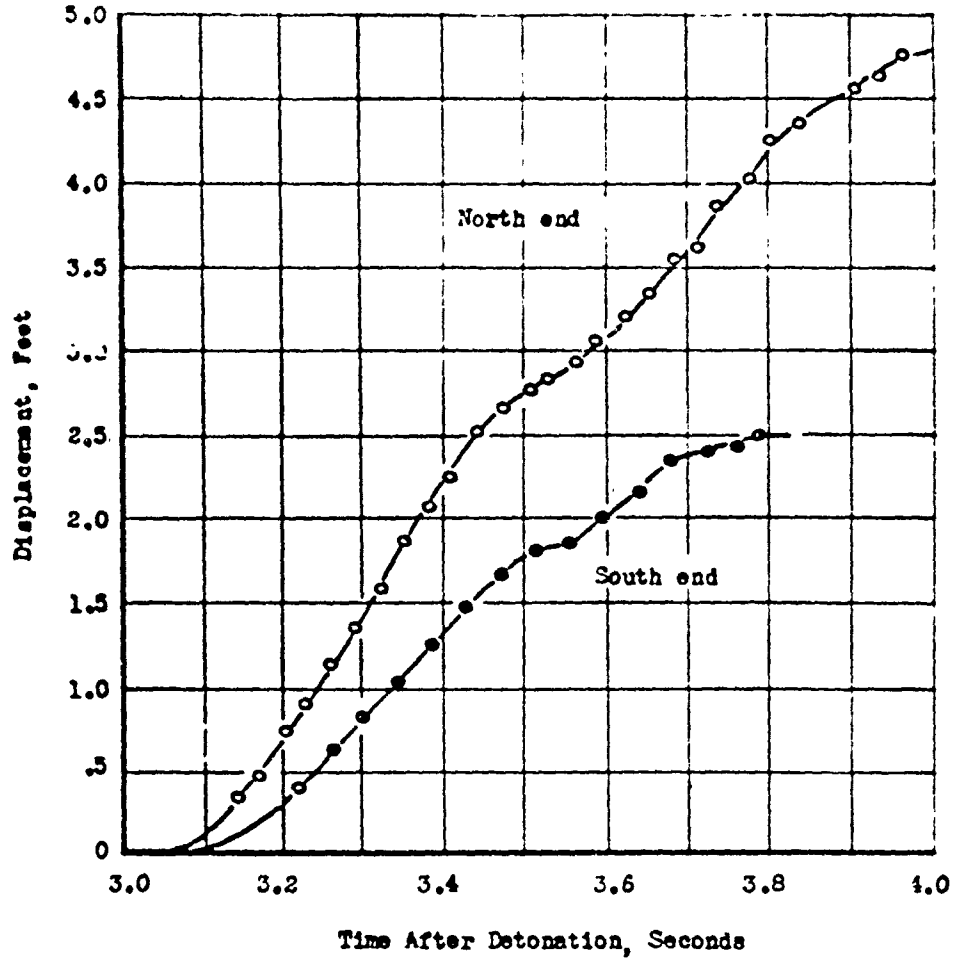

Fig.4.6 Displacement vs Time of Two Ends of Bridge, Site B, Shot 9

Fig. 4.7 Binding of End Post on Channel

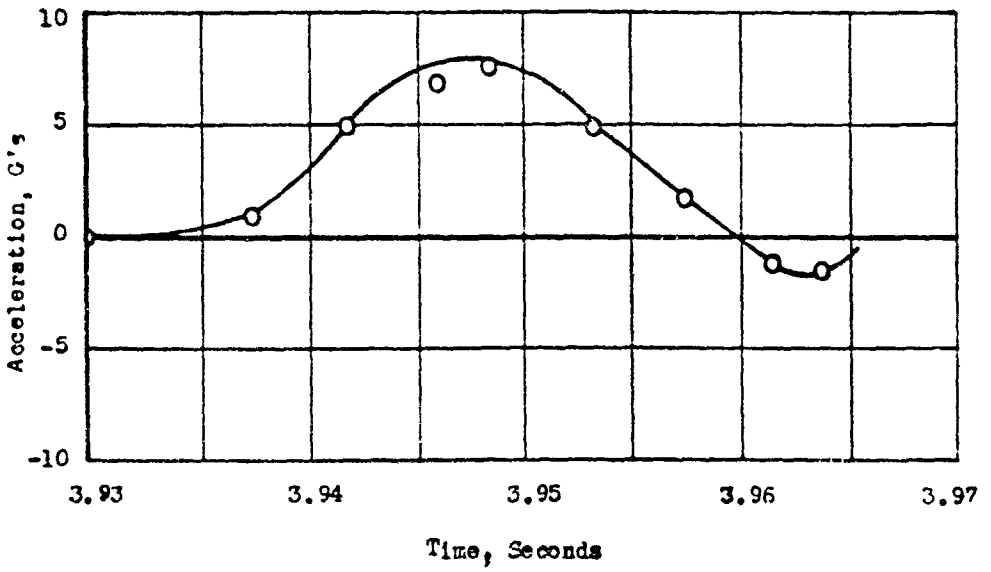

Fig. 4.8 ERA Acceleration of Structure, Site B, Shot 9

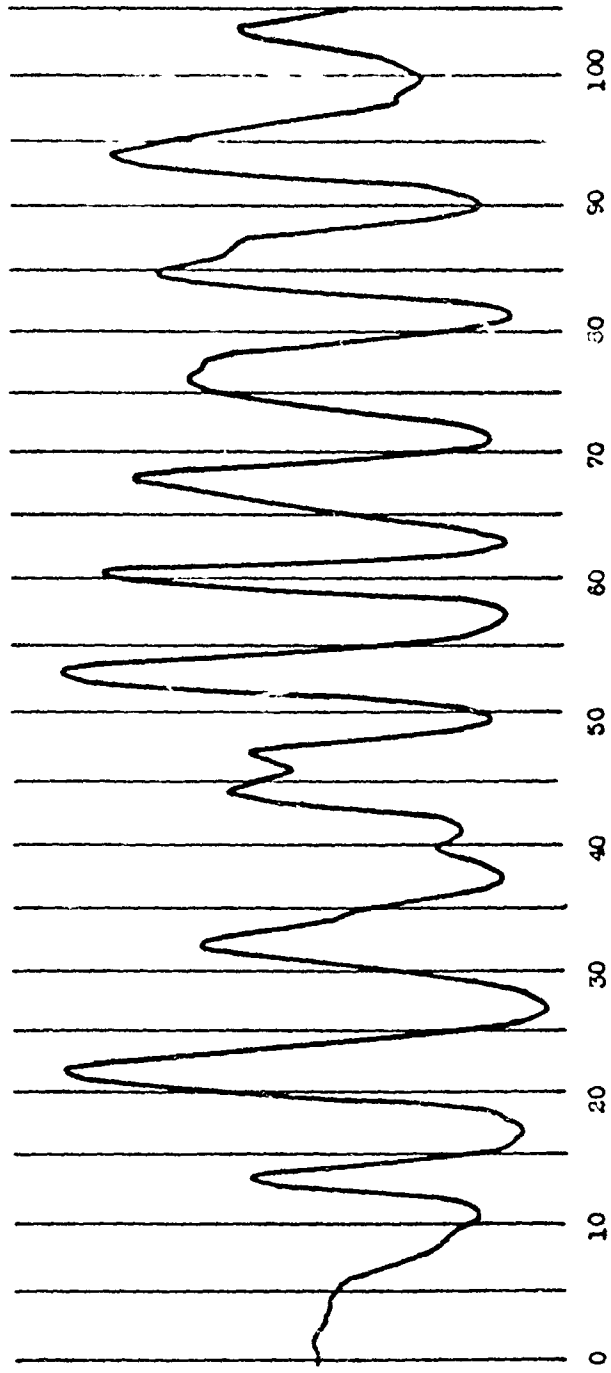

Calibration Equals Approximately 5.2 G/in.

Fig 4.9 Wianoko Acceleration, Site B, Shot 9

4.1.3 Site C

The basic data relative to the test structures at Site C are presented in Table 4.3.

TABLE 4.3 - Basic Data, Shot 9, Site C

	P_{so} (psi)	q_o (psi)	t_1 (sec)	θ (deg)
Actual	19.0	1.10	0.65	3.15
Predicted	16.8		0.74	0

The effect of the bombing error was to cause an exceedingly high angle of yaw for the structure at Site C; and, while this decreases the value of this portion of the test, the observations are worth noting. Both bridges slid along the ground without any damage whatever. Because the blast front struck them at an angle, they were both turned somewhat. The Bailey bridge slid about twice as far as did the T6.

4.2 SHOT 10

4.2.1 Site A

Blast pressure, duration, etc., are listed in Table 4.4.

TABLE 4.4 - Basic Data, Shot 10, Site A

	P_{so} (psi)	q_o (psi)	t_1 (sec)	Q_v (cal/cm)	θ (deg)
Actual	10.6	6	0.60	22.4	5
Predicted	12.0	3.5	0.66		0

In Fig. 4.10, dynamic pressure records at two heights above ground level at the approximate range of Site A are presented along with their corresponding overpressure records. The dotted curves are the dynamic pressures which would be expected on the basis of the corresponding overpressures. Caution should be used in the interpretation of the dynamic pressure records, as the information obtained from Sandia Corporation indicates that these gages were non-linear in the higher pressure regions and had saturated. The pressures may have been much higher than the 6 psi indicated by the records.

An intense precursor wave was observed at Sites A and C.

Shot 10 was detonated much more closely over the aiming point than was Shot 9; consequently, angles of yaw were much less at all structure sites. However, other factors contrived to produce results of limited value for the bridge at Site A. The bridge slid more than 20 ft (completely off the piers) and landed on the ground behind the

piers. Major damage was sustained by most bridge components, but it is impossible to separate this damage into that which occurred during the transit of the bridge and that which occurred due to impact forces when the bridge landed.

Motion picture photography of the response was not obtained, as the camera head was severed from the tower and was later located several feet behind the tower. The tower, itself, was also damaged, as evidenced in Fig. 4.11.

Acceleration as obtained by the EPA gage is reproduced in Fig. 4.12, and the corresponding Wianko record is given in Fig. 4.13.

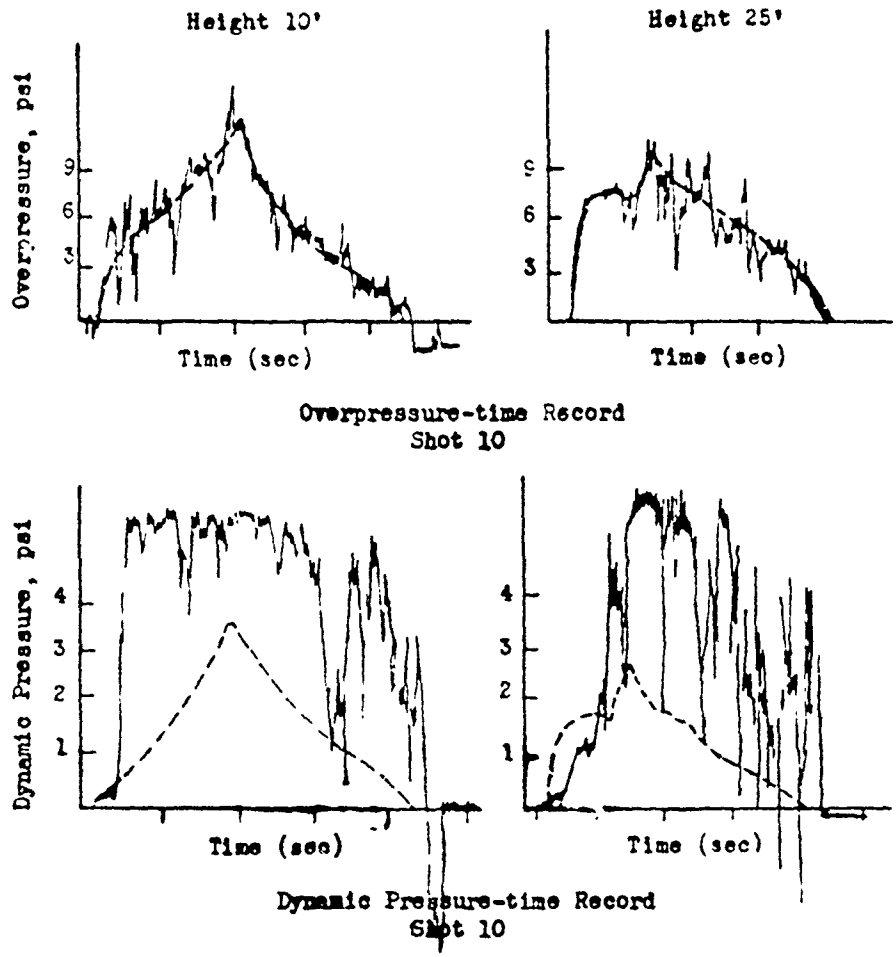

Fig. 4.10 Pressure Records at the Approximate Range of Site A

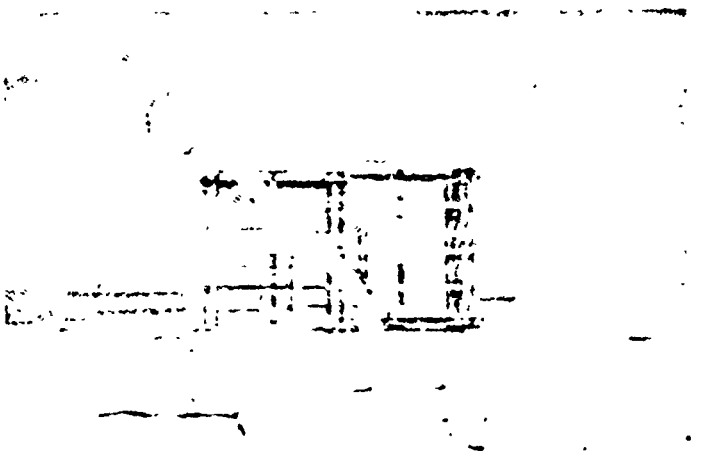

Fig. 4.11 Damage to Camera Tower, Site A, Shot 10

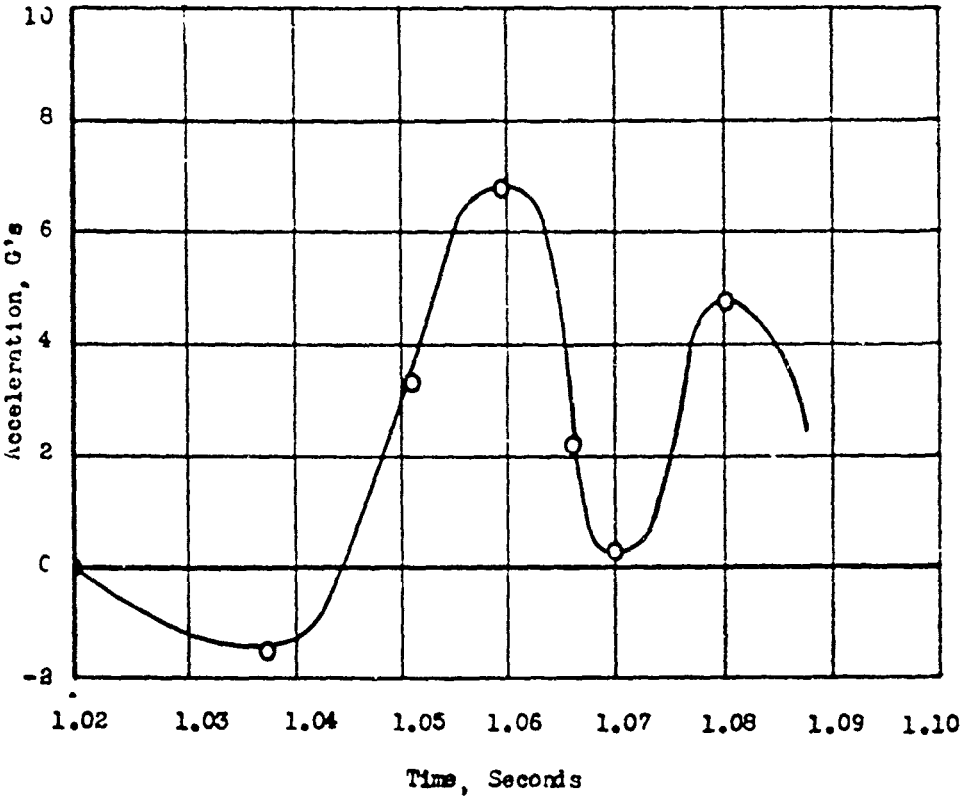

Fig. 4.12 ERA Accelerations of Structure, Site A, Shot 10

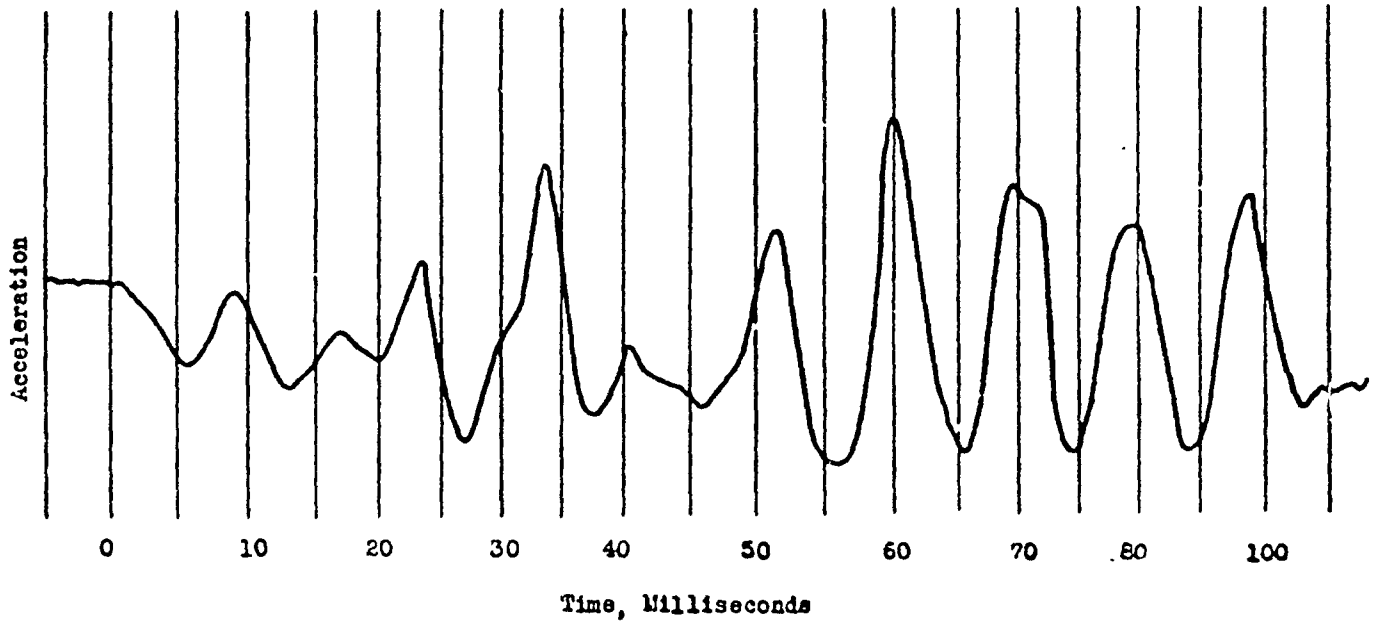

Calibration Equals Approximately 5.2 G/in.

Fig. 4.13 Wiancko Acceleration, Site A, Shot 10

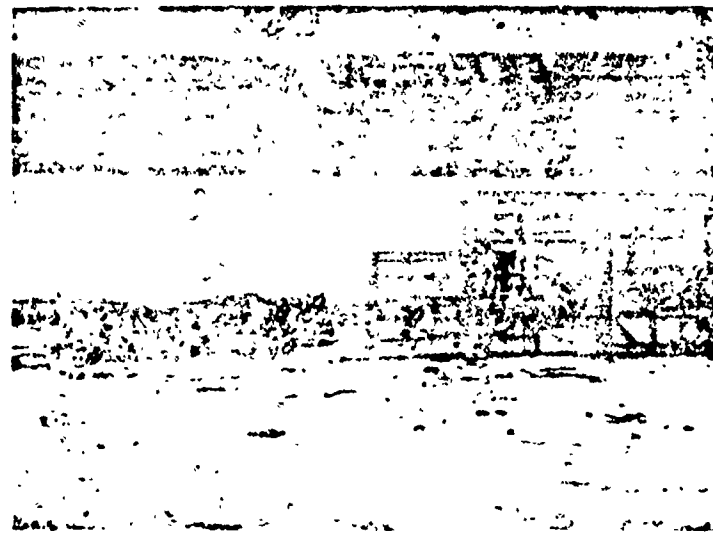

a.

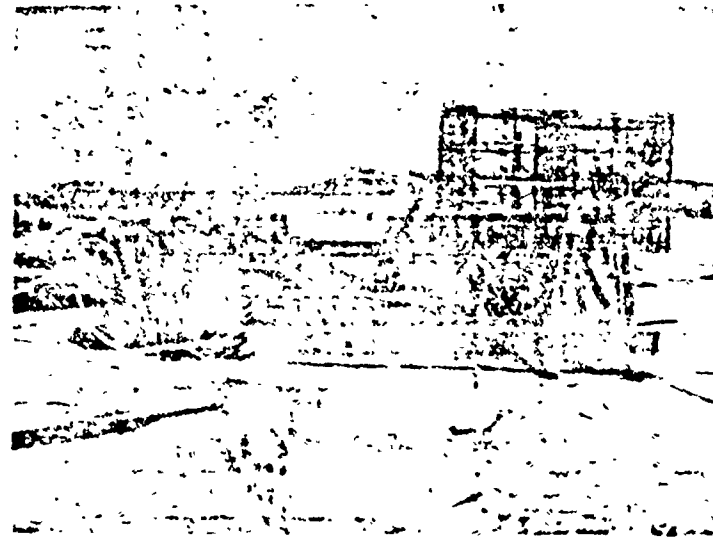

b.

Fig. 4.14 General View of Damage, Site A, Shot 10

To give an idea of the extent of the damage, a per cent usability figure has been attached to each Bailey component. By per cent usability is meant the per cent of the total number of a particular component of the bridge at Site A that remained usable. For example, of the 20 button stringers in the bridge, 14 were damaged beyond use and 6 (or 30 per cent) remained usable. Table 4.5 lists the numbers and the per cent of each item remaining usable.

TABLE 4.5 - Percentage Usability of Bridge Parts, Site A

Part	Total No.	No. Usable	Per Cent Usable
Panels	40	25	62.5
End Posts	8	8	100
Transoms	21	17	81
Button Stringers	20	6	30
Plain Stringers	40	20	50
Rakers	22	1	5
Bracing Frames	20	0	0
Chess	130	7	5.4
Riband	20	8	40

The panels on the leeward side of the bridge were generally damaged by bending of the lower chord (Fig. 4.15). Other panels were warped excessively.

Transom clamps had all been yanked loose by the transoms and, in every case, had bent the transom seats as shown in Fig. 4.16. The panels which were damaged only in this manner, however, were considered entirely usable, as the double-single construction makes use of only half of the available transom seats. The transom clamps were, for the most part, undamaged.

The end posts were judged to be in good condition. There was no detectable set in them. The damaged transoms were merely warped. Many of the button and plain stringers were thrown several feet beyond the bridge and were generally damaged by impact. Rakers were bent and twisted, bracing frames were warped and buckled, chess were broken and splintered, and riband were warped. Debris from the bridge was found scattered over an area extending 200 to 300 ft beyond the bridge. Those parts that were scattered so far were, for the most part, components associated with the deck; i.e., chess, riband, and stringers.

Examination of the skid marks in the channels revealed that the windward side of the bridge lifted with the incidence of the blast wave,

Fig. 4.15 Damaged Lower Chord of Bailey, Site A, Shot 10

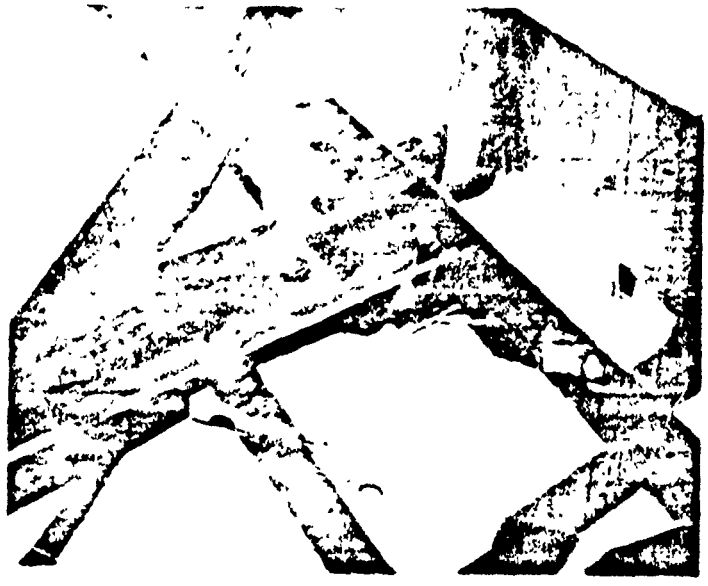

Fig. 4.16 Typical Damaged Transom Seat, Bailey, Site A, Shot 10

and the bridge slid along on its two leeward corners. This was evident in that no skid marks proceeded along the channel from the points where the windward end post rested. There were such skid marks at the leeward supports. During the latter part of the sliding, the skid marks in the channel of one pier disappeared, indicating that that end of the bridge had lifted completely off the pier. Shortly beyond the point where the skid mark disappeared, the edge of the channel was torn. This can be seen in Fig. 4.17.

In this shot, the piers suffered further damage of the same nature as they had for Shot 9. Figure 4.18 shows the bending in the chord members of the pier panels.

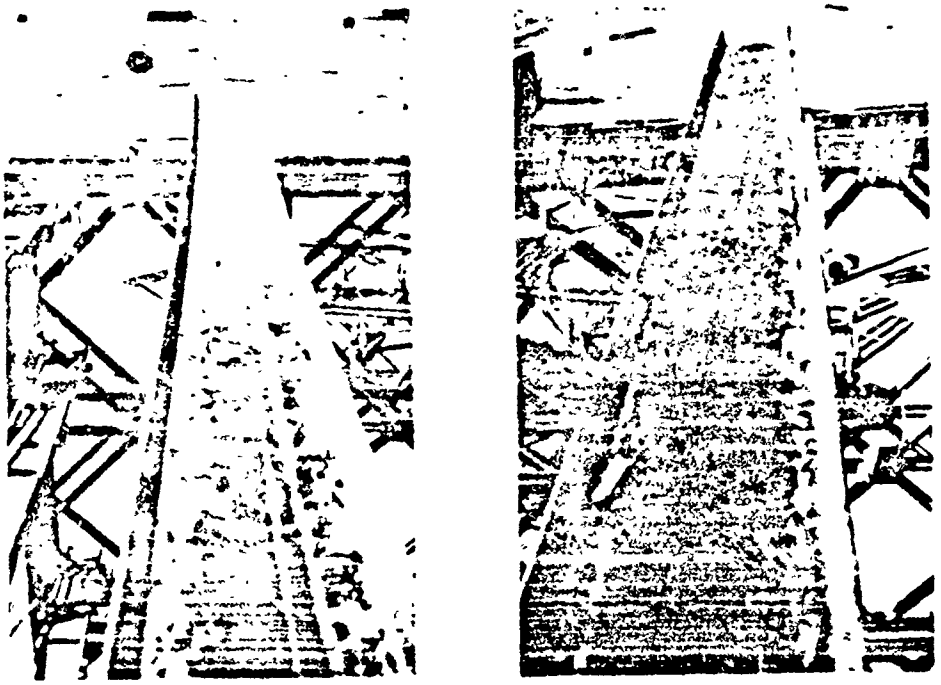

a. South Pier b. North Pier

Fig. 4.17 Channel Markings Resulting From Sliding of Bailey, Site A, Shot 10

4.2.2 Site B

As was stated in the previous chapter, the bridge at Site B was welded in place to prevent sliding and thereby increase the severity of the load. The blast parameters are given in Table 4.6.

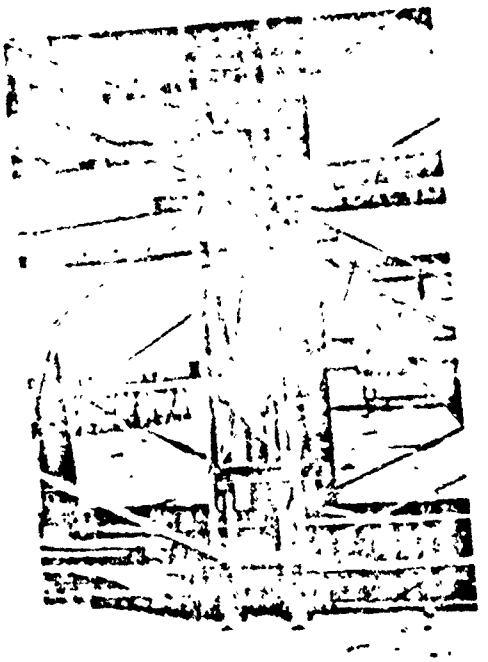

a.

b.

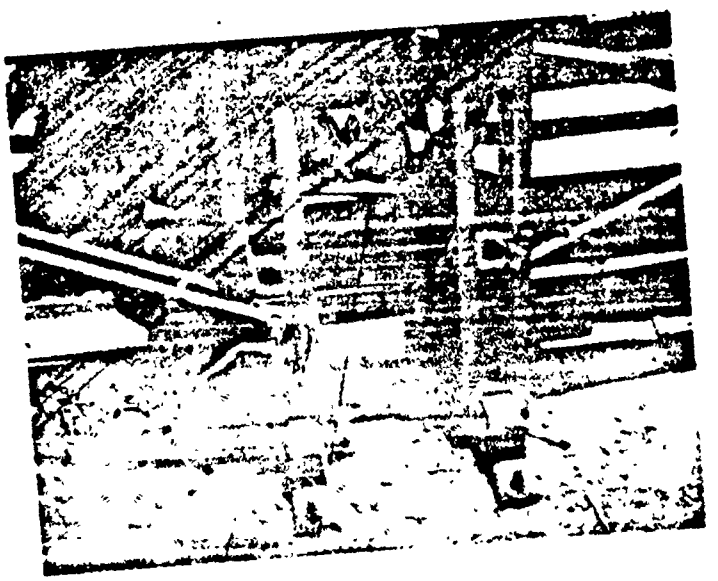

c.

Fig. 4.18 Bending of Pier Panels, Site A, Shot 10

TABLE 4.6 - Basic Data, Shot 10, Site B

	P_{so} (psi)	q_o (psi)	t_1 (sec)	θ (deg)
Actual	4.1		0.81	1.5
Predicted	3.5	0.3	0.75	0

No damage resulted. Motion pictures of bridge response were not made.

4.2.3 Site C

TABLE 4.7 - Basic Data, Shot 10, Site C

	P_{so} (psi)	q_o (psi)	t_1 (sec)	θ (deg)
Actual	14.0		0.50	6.2
Predicted	19.0	8.2	0.50	0

The single bay sections of Bailey and T6 slid approximately 20 and 10 ft, respectively. The Bailey was completely destroyed, as shown in the before-and-after photos, Fig. 4.19; whereas, the T6 was only slightly damaged.

Both of the truss braces on the windward side of the T6 were torn loose from their pin connections; the pins, however, were undamaged. On the leeward side, both truss braces had bent in compression. One corner of the deck had lifted, and one end of one sway brace had pulled out. The eye on the end of the sway brace was undamaged; therefore, it is supposed that the pin which holds the end of the sway brace must have sheared, although the pin could not be found.

Figure 4.20 shows damage to T6 Truss Braces, Site C, Shot 10, and Fig. 4.21 shows lifting of T6 Deck, Site C, Shot 10.

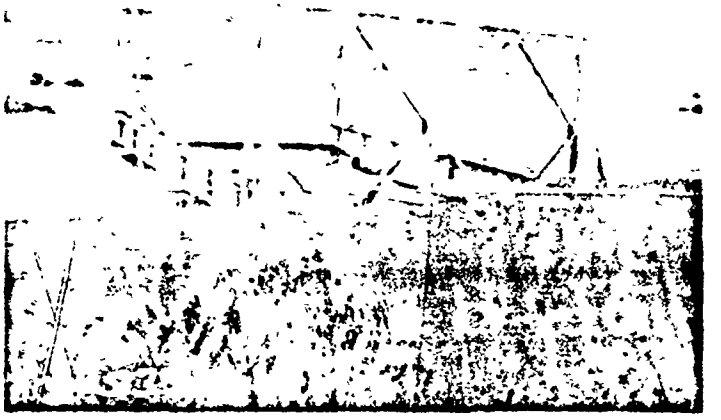

a. Before

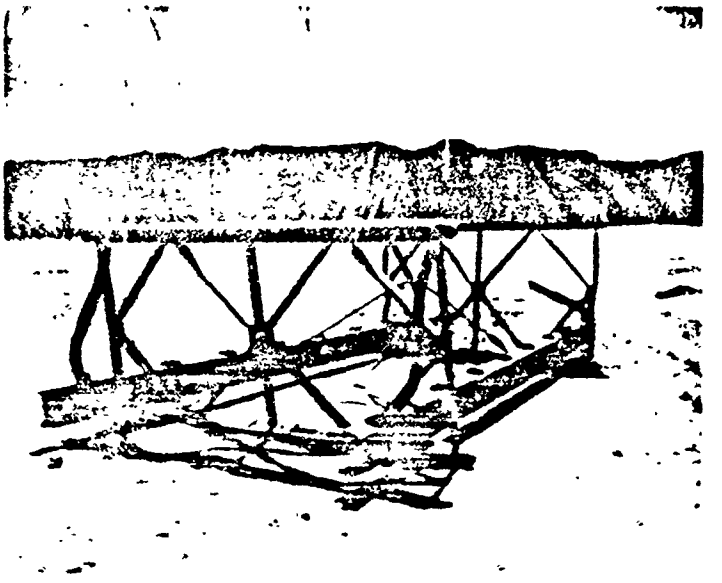

b. After

Fig. 4.19 Damage to Bailey, Site C, Shot 10

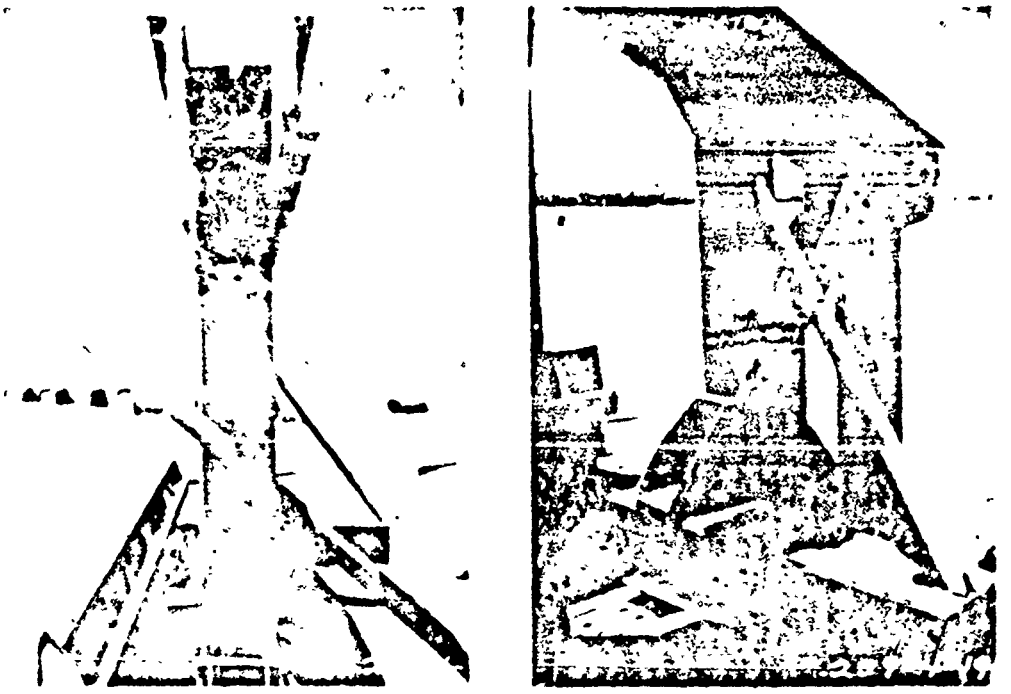

a. b.

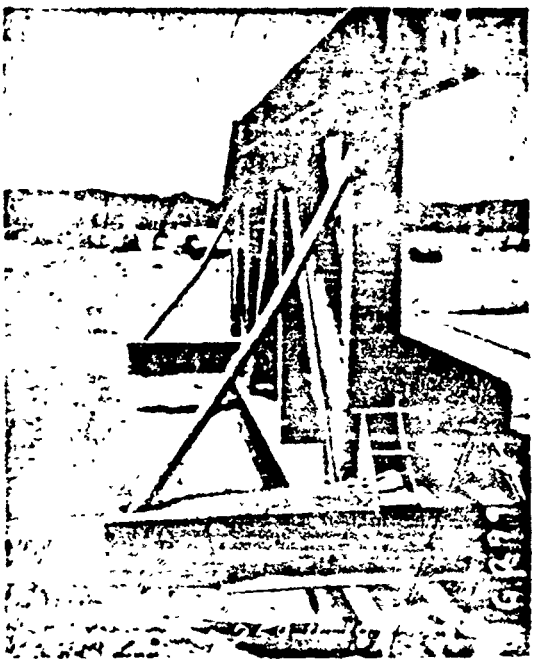

c.

Fig. 4.20 Damage to T6 Truss Braces, Site C, Shot 10

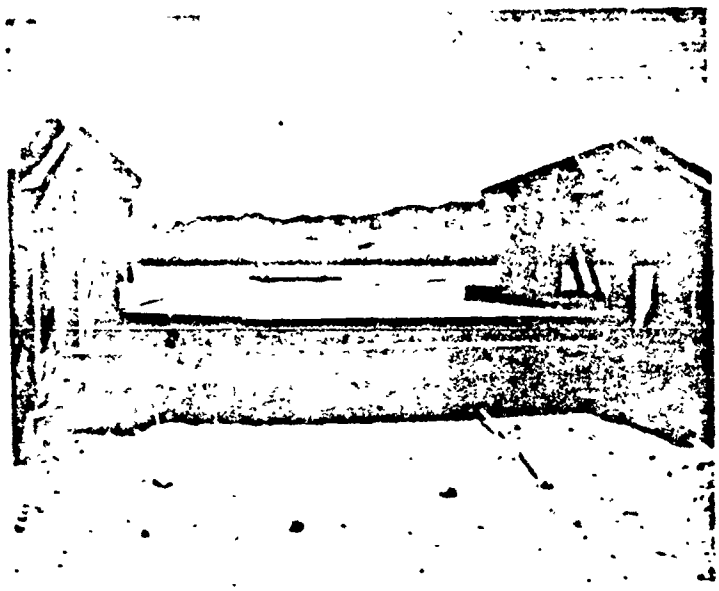

Fig. 4.21 Lifting of T6 Deck, Site C, Shot 10

CHAPTER 5

BRIDGE RESPONSE

5.1 GENERAL

The response of a bridge to any blast intensity depends very much on the anchorage strength--that is, on the force-resisting lateral movement of the bridge. Normally, a Bailey bridge will have end ramps, the effects of which may be highly indeterminate. However, for the purpose of analysis, it will be considered that the effects of the ramps are negligible. This condition may actually be very nearly realized in practice, inasmuch as a slight lifting of the ramp will unhook it from the bridge.

Assuming horizontal blast loading uniformly distributed over the bridge length, the motion of the bridge may be described as a lateral movement of the center of gravity plus a vibration in a horizontal plane about the center of gravity. Loadings on the bridge at any instant of time are shown in Fig. 5.1, where the bridge is represented in plan view by its centerline. The reaction loading is shown divided equally between the two ends of the bridge. The blast loading is uniformly distributed over the length of the bridge; and the inertia loading is broken down into two components, a uniformly distributed inertia load due to the acceleration of the center of gravity and an inertia load varying along the length of the bridge due to vibration about the center of gravity. Note that this latter load must exert a net force of zero over the length of the bridge.

Consider the bridge as a whole:

$$F(t) = M\ddot{x}_{cg} + R(t)$$

where: $F(t)$ = blast force as a function of time
M = mass of bridge
$\ddot{x}_{cg}$ = acceleration of the center of gravity
$R(t)$ = force-resisting lateral motion as a function of time

and the net uniform load acting along the length of the bridge is $F(t)-M\ddot{x}_{cg}=R(t)$. From the point of view of vibrations and internal stresses, the bridge may be considered to have a net uniform load of $R(t)$ suddenly applied at $t=0$. Thus, it can be seen that, for this case, the vibration depends only on the resisting force, $R(t)$, and not on the blast load, $F(t)$. If $R(t)$ is a frictional force and may be

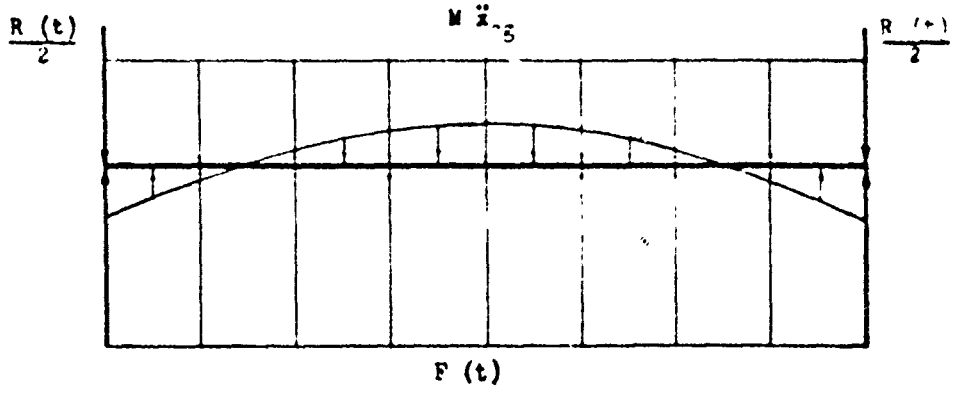

Fig. 5.1 Lateral Blast Forces Acting on Bridge

considered time invariant, the vibration of the bridge is as though a step force, $R(t) = F_f$ were applied to the bridge. Damage to the bridge may occur by internal failure if F_f is too large, or by excessive sliding if F_f is too small.

5.2 BRIDGE SLIDING ANALYSIS

The sliding of the bridge against a constant frictional force may be demonstrated quantitatively by rendering a solution of the equation $F = ma$, where F is the sum of all forces acting on the bridge as a function of time, m is the mass of the bridge, and a is the acceleration of the bridge as a function of time.

5.2.1 Assumptions

In this section, as in the following, several assumptions are required to provide an academic problem capable of solution which represents to a fair degree of accuracy the actual physical situation. These assumptions are mentioned here with a few remarks concerning each.

1. The blast overpressure may be represented by the equation $P(t) = P_{so}(1 - t/t_1)e^{-Kt/t_1}$ This equation, as was mentioned in Chapter 1, is an empirical representation of the blast pressure as a function of time. It represents the blast wave fairly accurately except in cases where there is a so-called precursor wave. In those cases, the overpressure is a very irregular, unpredictable function of time; and, although the precursor phenomenon may be present in important cases, it is not possible to include this effect in the present solution.

2. The dynamic pressure is a unique function of blast pressure as given in Chapter 1. Again, this is a good approximation, except in the presence of a precursor wave. In this latter case, dynamic pressures seem to be much higher than would be indicated by measured overpressure. This fact was illustrated in Chapter 4.

3. The diffraction or shock loading may be considered an impulse (an infinite force acting for an infinitesimal period of time).

The impulse is given by Fig. 1.2. This seems to be a good assumption, in view of the fact that the effect of the shock force on a drag-type structure such as a truss bridge is much less than the effect of drag forces (this will be demonstrated in the analysis which follows); therefore, a given per cent error in the shock force will result in a much lesser error in the overall effect.

4. The drag forcing function is given by Equation 1.6, which is: $F_d = F_{do}\epsilon^{-4t/t_1}$ where $F_{do} = C_d A_{eff} q_o$. This appears to be a good approximation within the limits of assumption No. 2. Of course, if the dynamic pressure does not conform to conventional waveshape, the drag force will be correspondingly in error. The error in assuming C_d is constant can be seen by inspection of Fig. 5.2, where C_d is shown to be a function of Reynold's number (of wind velocity, when only prototype test structures are considered) for a cylindrical member.

5. The coefficient of friction between the sliding surfaces of the bridge bearing is constant. Tests in which a bridge section was towed by a truck winch and tension in the towline was measured indicated a required pull to start a 36,000 lb bridge sliding of 18,000 to 23,000 lb and a pull of 9,000--11,000 lb required to maintain a rate of pull of 1 ft/sec. The same Bailey end posts and the same channels were used in this test as were used in the full-scale atomic test at Site B. It was impossible to obtain other rates of pull without having the winch jerk so the coefficient of friction was not accurately established as a function of pull velocity.

6. The ends of the bridge move in a direction away from ground zero at all times during the sliding phase, so that the friction force may be considered to be constant in one direction. Calculations show that this is so for bridge lengths considered. For very much longer bridges, calculations would show the tendency of the bridge ends to move toward ground zero during the first vibrational swing if the friction force were assumed to act toward ground zero at all times.

5.2.2 Analysis

The equation of motion of the bridge is:

$$F_s + F_d - F_f = M\ddot{x}_{cg}$$

where

F_s = shock force
F_d = drag force
F_f = friction force
M = mass of bridge
$\ddot{x}_{cg}$ = acceleration of center of gravity of bridge

Each component force imparts a component velocity to the bridge such that $V(t) = V_s + V_d - V_f$, where

$$V_s = \frac{1}{M}\int_0^t F_s\,dt$$

$$V_d = \frac{1}{M}\int_0^t F_d\,dt$$

$$V_f = \frac{1}{M}\int_0^t F_f\,dt$$

and, in turn, there are three component displacements such that $x(t) = x_s + x_d - x_f$ where

$$x_s = \int_0^t V_s dt$$

$$x_d = \int_0^t V_d dt$$

$$x_f = \int_0^t V_f dt$$

One of the initial assumptions was that the shock force may be considered as an impulse, occurring in zero time, so the shock force imparts a finite velocity to the bridge at $t=0$. This component velocity is constant thereafter.

$$V_s = \frac{1}{M}\int_0^t F_s dt = \frac{I_s}{M} = \text{constant} \qquad (5.1)$$

where I_s = shock impulse

$$F_d = F_{do}\epsilon^{-4t/t_1} \qquad t > t_1$$

$$F_d = 0 \qquad t < t_1$$

where F_{do} = peak value of F_d, determined from q_o, peak value of q

t_1 = positive phase duration

substitute

$$V_d = \frac{1}{M}\int_0^t F_{do}\epsilon^{-4t/t_1} \qquad t < t_1$$

$$= \frac{F_{do}t_1}{4M}(1-\epsilon^{-4t/t_1}) \qquad t < t_1 \qquad (5.2a)$$

$$= \frac{F_{do}t_1}{4M}(1-\epsilon^{-4}) \qquad t > t_1 \qquad (5.2b)$$

$$F_f = \mu Mg$$

substitute

$$V_f = \frac{1}{M}\int_0^t \mu M g dt = \mu g t \qquad (5.3)$$

when $X(t)$ reaches maximum displacement, the velocity will be zero. The time that this occurs may be solved for by summing the component velocities and setting them equal to 0.

$$V(t_o) = V_s(t_o) + V_d(t_o) - V_f(t_o) = 0$$

where t_o = time at which bridge comes to a stop

$$\frac{I_s}{M} + \frac{F_{do}t_1}{4M}(1-\epsilon^{-4t_o/t_1}) - \mu g t_o = 0 \qquad (5.4a)$$

$$\frac{I_s}{M} + \frac{F_{do} t_1}{4M}(1-\epsilon^{-4}) - \mu g t_o = 0 \qquad t_o > t_1 \tag{5.4b}$$

for solutions of $t_o < t_1$, the equation is transcendental and must be solved by approximate methods.

By integrating velocities

$$x_s = \frac{I_s}{M} t \tag{5.5}$$

$$x_d = \frac{F_{do} t_1}{4M} \int_0^t (1-\epsilon^{-4t/t_1}) dt \qquad t < t_1$$

$$= \frac{F_{do} t_1}{4M} \left(t + \frac{t_1}{4} \epsilon^{-4t/t_1} - \frac{t_1}{4}\right) \tag{5.6a}$$

$$x_d = F_{do} t_1 \left[\frac{t_1}{4} - \frac{t_1}{4}(1-\epsilon^{-4})\right] + \int_{t_1}^{t} \frac{F_{do} t_1}{4M} (1-\epsilon^{-4}) dt \qquad t > t_1$$

$$= \frac{F_{do} t_1}{4M} \left[t(1-\epsilon^{-4}) - \frac{t_1}{4}(1-5\epsilon^{-4})\right] \tag{5.6b}$$

$$x_f = \frac{1}{2} \mu g t^2 \tag{5.7}$$

the sum of these is the lateral displacement of the bridge. By substituting the value t_o, given by Equation 5.4, the final displacement may be calculated.

5.2.3 Example

As a sample case, the sliding of the bridge at Site B for Shot 9 will be calculated.

The shock impulse will be determined in the following manner: The impulse on any member is equal to the product of the unit impulse, (I_o/P_{so}), for that member, the overpressure, and the area of the member exposed to blast. For the Bailey bridge, a shock wave approaching from the side will be assumed to act over the entire area of the windward truss and the edge of the floor and to recover full strength in traversing the bridge and act over the leeward truss area. Thus, in shock impulse calculations, the projected elevation area of one truss will be doubled to account for both trusses. It was seen in Chapter 1 that the unit impulse also depends on the depth of the member. Considering the two panels in each truss, the depth is taken as shown in Fig. 5.3. The depth of the floor is taken as one quarter the width and the width (dimension perpendicular to blast propagation) as taken from the top edge of the riband to the bottom edge of the stringer. Thus, a unit impulse is determined for the truss and for the flooring. The shock impulse is, therefore, for a 10-bay bridge:

$$I_s = 10\left[\,2\left(\frac{I_o}{P_{so}}\right)_T A_T + \left(\frac{I_o}{P_{so}}\right)_F A_F\,\right] P_{so} \qquad (5\,8)$$

where

$\left(\frac{I_o}{P_{so}}\right)_T$ = impulse per unit overpressure per unit area for the truss members

$\left(\frac{I_o}{P_{so}}\right)_F$ = same quantity for floor

A_T = projected area of truss of one bay in elevation view

A_F = projected area of edge of floor of one bay in elevation view

These quantities are parameters of the bridge and are independent of the blast intensity.

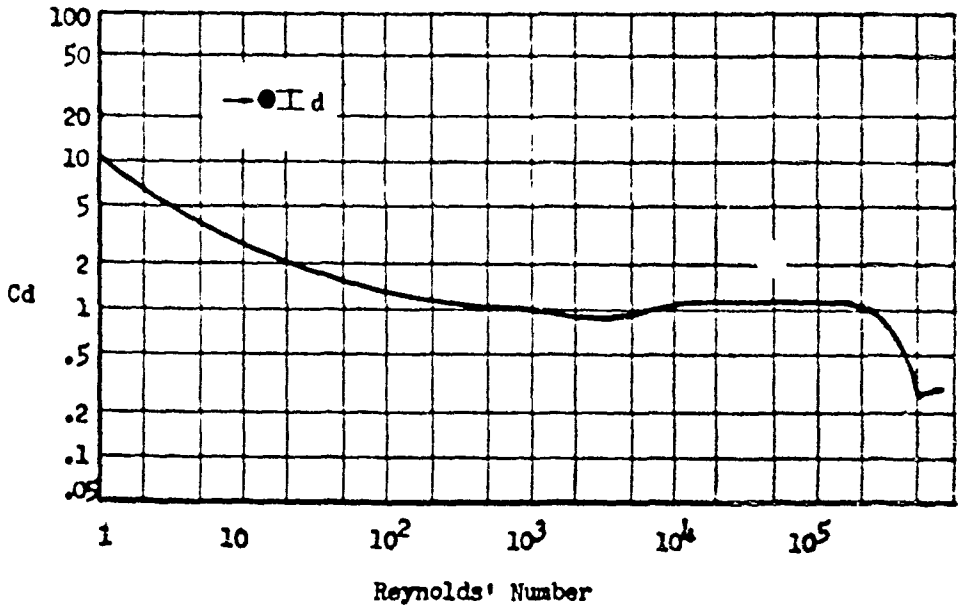

Fig. 5.2 Coefficient of Drag C_d, vs Reynolds Number

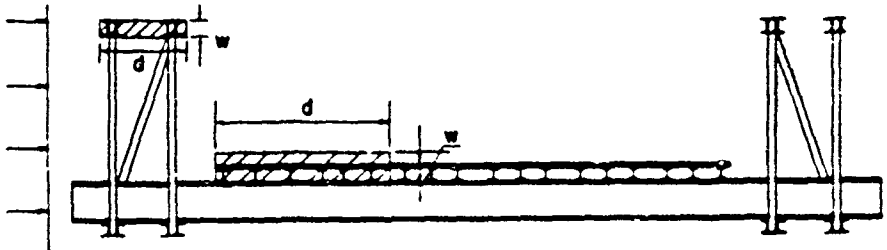

Fig. 5.3 Sections Chosen for Shock Impulse Calculations

Evaluation of the above quantities for the 100-ft bridge yields:

$$\left(\frac{I_Q}{P_{SO}}\right)_T = 1.8 \times 10^{-3} \text{ sec}$$

$$\left(\frac{I_Q}{P_{SO}}\right)_F = 5.0 \times 10^{-3} \text{ sec}$$

$$A_T = 1684 \text{ in}^2$$

$$A_F = 1680 \text{ in}^2$$

These values are substituted in Equation 5.8 to obtain $I_s = 144.6\, P_{SO}$. Since the blast overpressure at Site B for Shot 9 was 7.75 psi (Appendix B), the impulse is 144.6 x 7.75 = 1,120 lb sec.

In the calculation of the drag force, a constant coefficient of drag, C_d, of 1.63 is assumed. This value is taken directly from that value determined by wind tunnel tests of a model of a truss section (Ref 8). It is realized that the model tested represented a truss of fewer but larger members than in a Bailey truss. It is expected, therefore, that the value 1.63 may be low.

To determine the effective area upon which the dynamic pressure acts, shielding of the leeward truss by the windward truss must be considered. This effect was investigated in the M. I. T. wind tunnel tests. By varying the spacing between two model trusses, there was determined a curve of a shielding factor versus spacing, where the shielding factor is defined as the amount by which the force acting on the windward truss must be multiplied to account for the leeward or shielded truss. This curve is reproduced in Fig. 5.4.

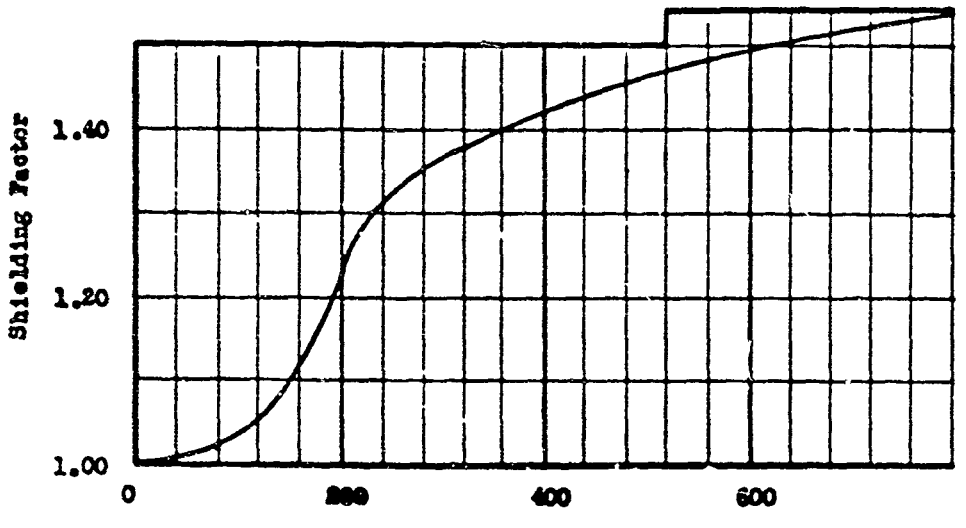

Fig. 5.4 Shielding Factor Versus Spacing of Two Trusses

For the Bailey bridge, the shielding factor is seen to be 1.28; thus, the area of the windward truss is multiplied by 1.28 to account for both trusses. The edge of the floor is considered unshielded by the windward truss, and its area is unmodified. Thus, the total effective area is

$A_{eff} = 1.28\ A_T + A_F = (1.28)(1684) + 1680 = 3840\ in^2$ per bay

From the basic data, $q_o = 1.52$ psi: therefore,

$F_{do} = 10(1.63)(3840)(1.52)$

$= 95{,}200$ lb

$$F_d(t) = 95000\epsilon^{-4t/t_1} \qquad t < t_1$$
$$= 0 \qquad t > t_1$$

$F_f = \mu W = 0.3W$

It was found in the M. I. T. wind tunnel tests that with increases in the angle of yaw from zero the normal force increased until an angle of about 20 degrees was reached. Further increases in angle of yaw resulted in a decrease in normal force. An experimentally determined curve is reproduced from Ref 5 in Fig. 5.5. Thus, the calculated drag force must be adjusted correspondingly.

For the case considered, this is 6 per cent; thus,

$F_{do} = (1.06)(95{,}200) = 101{,}000$ lb

$$F_d(t) = 101{,}000\,\epsilon^{-4t/t_1} \qquad t < t_1$$
$$= 0 \qquad t > t_1$$

$F_f = \mu W$

$= (0.3)(72{,}000)$

$= 21{,}600$ lb

The component velocities may now be calculated as follows:

$$V_s = I_s/M = \frac{1120\ \text{lb sec}}{2240\ \text{lb sec}^2/\text{ft}} = 0.5\ \text{fps}$$

$$V_d = \frac{(101{,}000)(0.938}{4 \times 2240}(1-\epsilon^{-4t/t_1})$$

$$= 10.6\,(1-\epsilon^{-4t/t_1}) \qquad t < 0.938$$

$$= 10.6\,(1-\epsilon^{-4}) \qquad t > 0.938$$

$V_f = (0.3)(32.2)t = 9.66\,t$

The displacements are:

$X_s = 0.5\,t$

$$X_d = 10.6\left[t + 0.234\,(\epsilon^{-4t/0.938} - 1)\right] \qquad t < 0.938$$
$$= 10.6\left[t\,(1-\epsilon^{-4}) - 0.234\,(1-5\epsilon^{-4})\right] \qquad t > 0.938$$

$X_f = 1/2\,(0.3)(52.2)\,t^2 = 4.83\,t^2$

In Fig. 5.6, the calculated displacement is compared with the displacements obtained from the moving pictures. Calculated velocity vs time is presented in Fig. 5.7.

Calculations are made in Appendix D for other conditions of blast loading and other frictional restraints. These results are plotted in Fig. 5.8.

For lengths of double-single bridge other than 100 ft, the mass curves apply. Doubling the bridge length doubles the total force (by doubling the area exposed to blast) and doubles the mass.

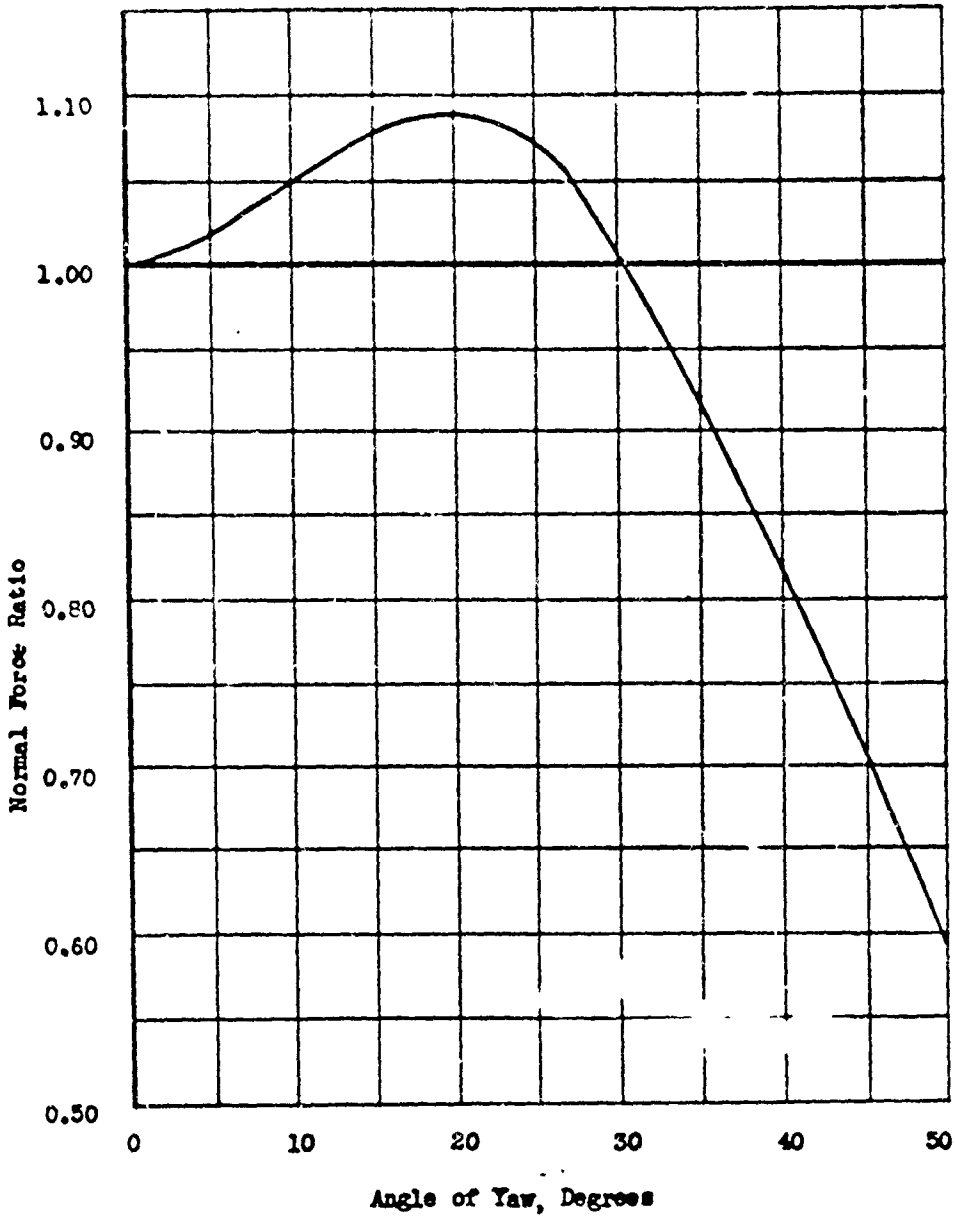

Fig. 5.5 Normal Force Ratio Versus Angle of Yaw

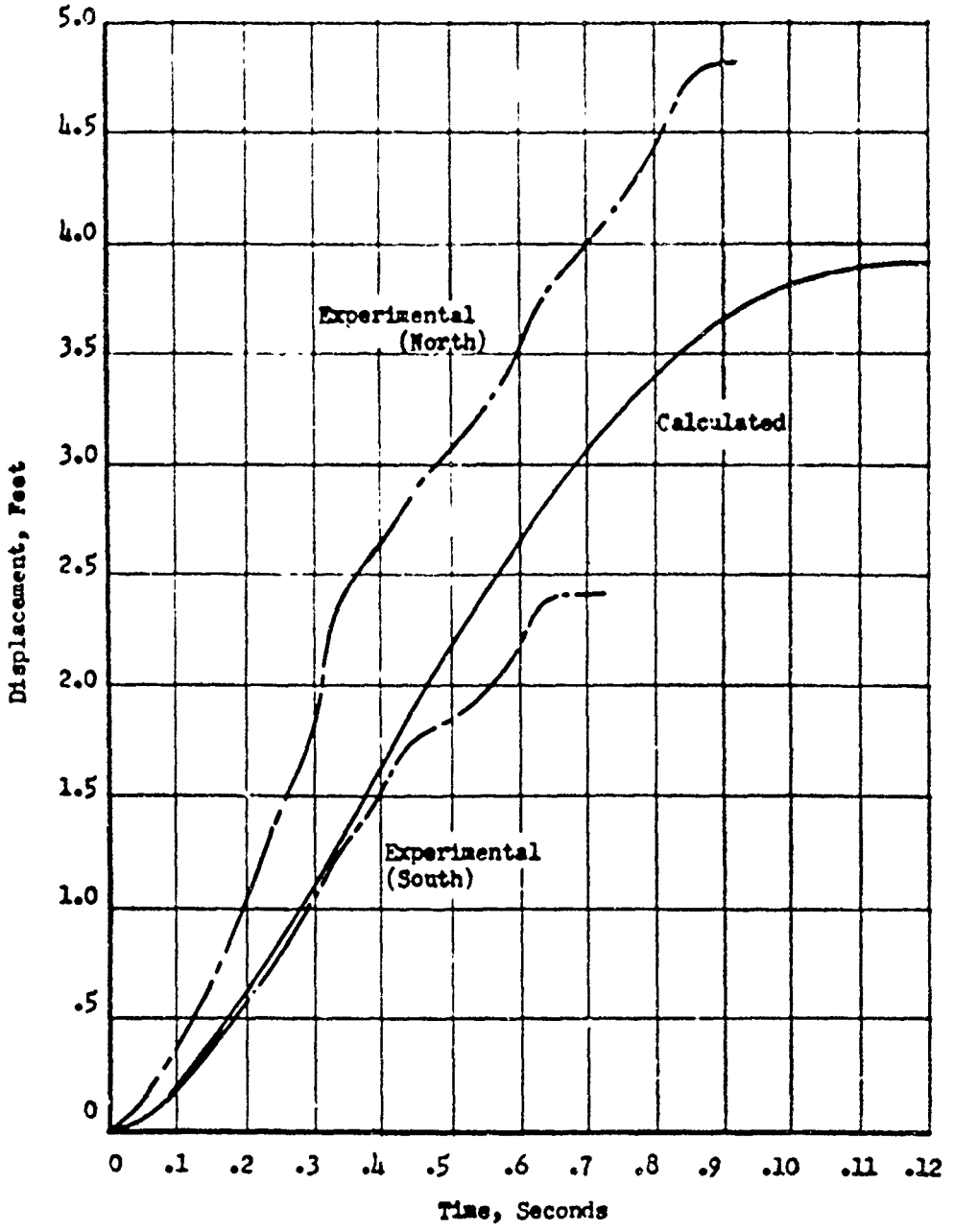

Fig. 5.6 Displacement Versus Time of Bailey Bridge, Site B, Shot 9

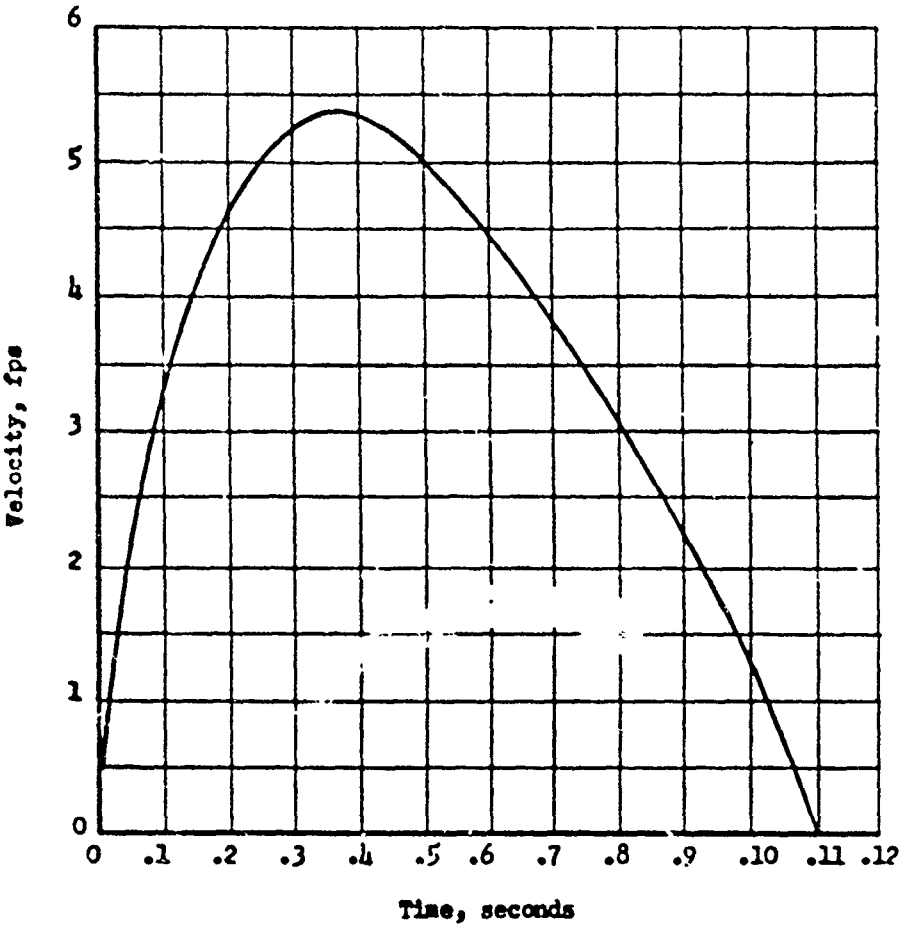

Fig. 5.7 Velocity Versus Time of Bailey Bridge, Site B, Shot 9

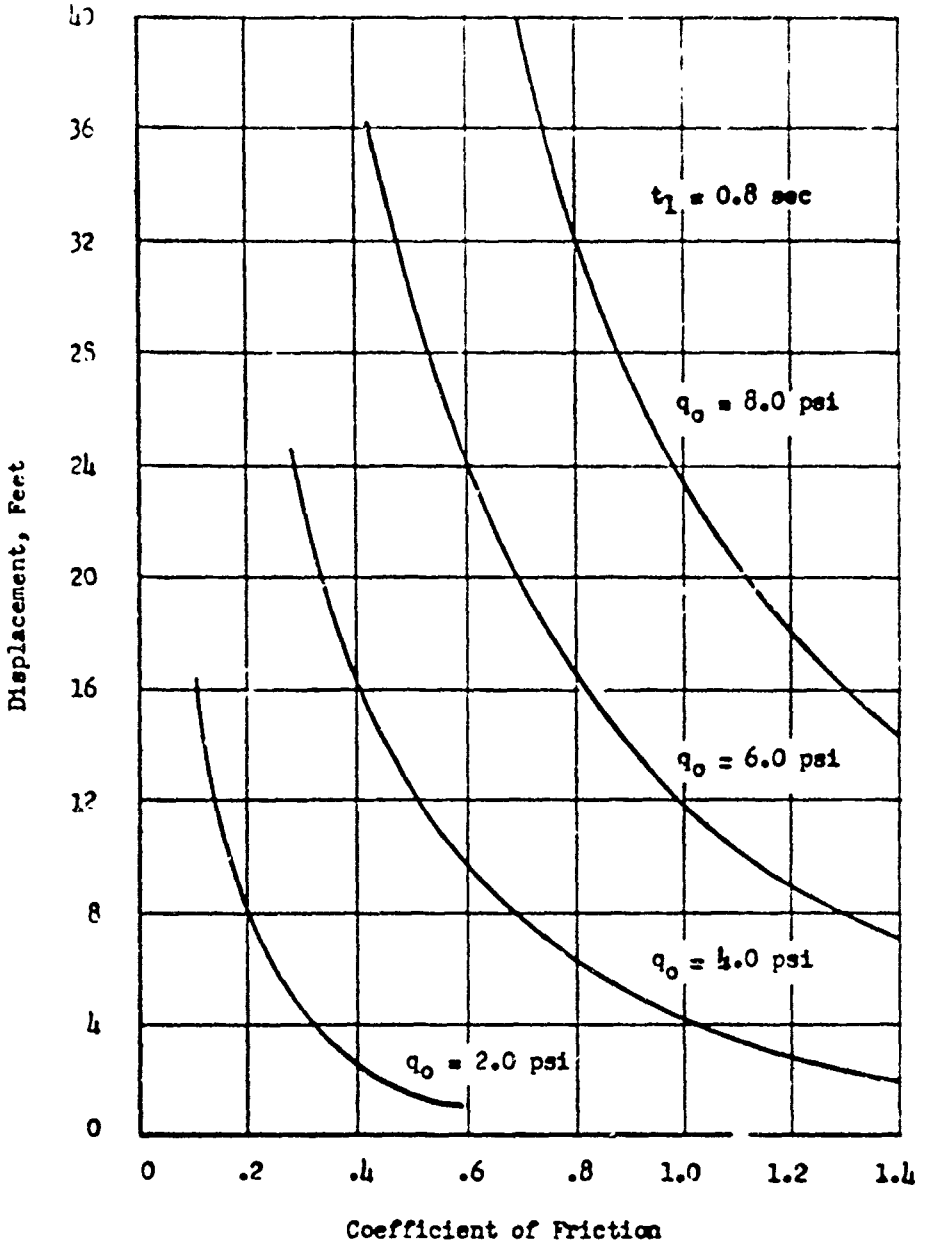

Fig. 5.8 Maximum Displacement of Double Single Bailey Bridge Exposed to Blast Versus Coefficient of Friction of Mounting

5.3 BRIDGE VIBRATION

5.3.1 Assumptions

For the purpose of determining the vibrational response of the bridge, the following assumptions are made:

1. The only bridge components which suffer deformation are the sway braces. The transoms and panels are considered perfectly rigid and are considered hinged at their pin joints. This is perhaps the most important restriction placed upon the analysis. However, the fact that this kind of deformation takes place to some extent is demonstrated in Fig. 5.9. The photo of the collapsed bridge illustrates that a great amount of articulation has occurred at the pin connections between panels. Bending of the panels themselves appears, by comparison, to be negligible.

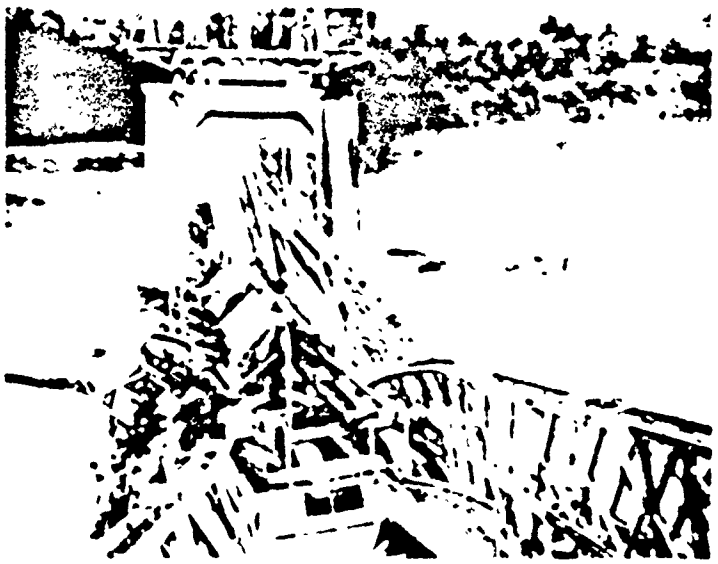

Fig. 5.9 A Collapsed Bailey Bridge

2. There is no damping of the motion. This assumption will cause the calculated natural frequencies of vibration to be high and the magnitude of the calculated response to be greater.

3. The stress-strain relationship for the elongation of the sway braces may be approximated by a curve consisting of two straight lines. Over the range of the first portion of the curve, the sway brace obeys Hooke's law perfectly. After the yield point is reached, the bar continues to elongate without increase in tension.

4. The loading of the bridge is perfectly symmetrical, as shown in Fig. 5.1. Since the bridge itself is considered symmetrical, only the symmetric mode of vibration can be set up; and the assymetric

frequencies will not be present. This makes possible the consideration of only half of the bridge in the calculations.

5.3.2 Elastic Response

Figure 5.10 is a schematic diagram of half of the bridge in plan view. This diagram shows how the deflection of the bridge brings about an elongation of the sway braces. Those sway braces which are shown dotted are not considered in this analysis; since they are unable to withstand compressive stresses and are, therefore, inactive. With the bridge at rest, the panels and transoms of one bay form a right angle parallelogram. A measure of the deflection will be called the incremental displacement, defined here as the difference in lateral displacement of the ends of the bay in question. It will be shown that the incremental displacement is directly proportional to the elongation of the sway brace for small deflections.

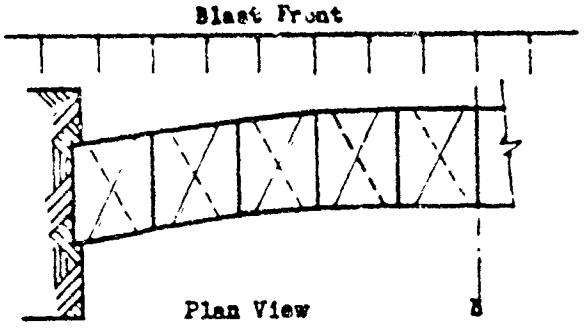

Fig. 5.10 Bridge Deflection

One bay is isolated in Fig. 5.11. From this diagram, it may be seen:

$$a = \frac{\Delta \ell}{\cos\theta} \tag{5.9}$$

$$\Delta X = a \frac{L}{d} \frac{\Delta \ell L}{\cos\theta} \tag{5.10}$$

The static force on the bay necessary to cause a displacement, Δ_x, will be considered. A force, P, will be taken to act at the right end of the bay and moments taken about the left end:

$$PL = Td \cos\theta \tag{5.11}$$

where T = tension in sway brace

$$T = \frac{PL}{d \cos\theta} \tag{5.12}$$

$T = \frac{EA}{\ell} \Delta \ell$; this is merely Hooke's law for the sway brace (5.13)

where E = Young's modulus for the sway brace

A = cross sectional area of sway brace

eliminating T from Equations 5.12 and 5.13 and substituting the resulting expression for $\Delta \ell$ into Equation 5.11 gives the following:

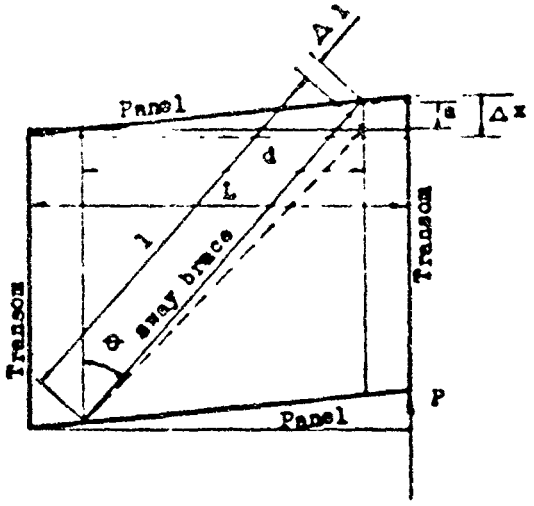

Fig. 5.11 Incremental Displacement of One Bay

$$\Delta X = \frac{L}{d\cos\theta}\,\frac{PL\ell}{EAd\cos\theta} \tag{5.14}$$

$$P = \frac{EA(d\cos\theta)^2\Delta X}{\ell L^2} \tag{5.15}$$

which is of the form

$$P = K\Delta X \quad \text{, where}$$

$$K = \frac{EA(d\cos\theta)^2}{\ell L^2} \tag{5.16}$$

Under the symmetrical loading, only those vibrations which are symmetrical with respect to the center of gravity of the bridge are excited. An equivalent mathematical model is shown in Fig. 5.12a and 5.12b. The longitudinal frequencies and displacements of the model correspond to the transverse frequencies and displacements of the prototype. Each bay is represented by two equal masses connected by a spring of stiffness given by Equation 5.16. The masses are each equal to one-half the mass of the bay. The half bridge is represented by the equivalent mechanical system of Fig. 5.12a and 5.12b.

It has been shown that, from the point of view of vibrations, the bridge may be considered to be acted upon by a uniformly distributed load, $F(t) - M\ddot{x}_{CG} = R(t)$. Let $10F = R(t) = F_t$ and F becomes the force per bay. Consider $\frac{1}{2}F$ as acting on each end of each bay. These conditions are depicted in Fig. 12b.

The equations describing the behavior of the system are:

$$\tfrac{1}{2}m\ddot{x}_0 + Kx_0 - Kx_1 = -\frac{9}{2}F$$

$$\ddot{x}_0 + 2\frac{K}{m}x_0 - 2\frac{K}{m}x_1 = \frac{9}{m}F \tag{5.17}$$

$$-\frac{K}{m}x_0 + \ddot{x}_1 + 2\frac{K}{m}x_1 - \frac{K}{m}x_2 = \frac{F}{m} \tag{5.18}$$

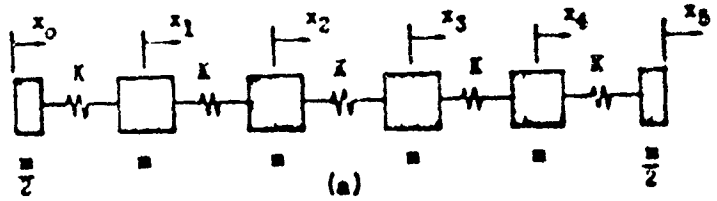

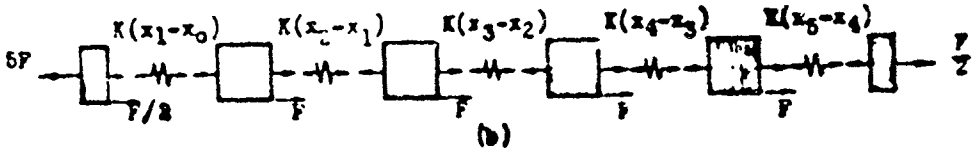

Fig. 5.12 Spring-Mass Equivalent of Bridge

$$-\frac{k}{m}x_1+\ddot{x}_2+2\frac{k}{m}x_2-\frac{k}{m}x_3=\frac{F}{m} \qquad (5.19)$$

$$-\frac{k}{m}x_2+\ddot{x}_3+2\frac{k}{m}x_3-\frac{k}{m}x_4=\frac{F}{m} \qquad (5.20)$$

$$-\frac{k}{m}x_3+\ddot{x}_4+2\frac{k}{m}x_4-\frac{k}{m}x_5=\frac{F}{m} \qquad (5.21)$$

$$-2\frac{k}{m}x_4+\ddot{x}_5+2\frac{k}{m}x_5=\frac{F}{m} \qquad (5.22)$$

Let $\frac{k}{m}=\omega_0^2$ and simplify the equations by writing equivalent Laplace equations (see Ref 9). With all initial conditions zero, these are:

$$(S^2+2\omega_0^2)X(s)-2\omega_0^2X_1(s)=-\frac{9}{m}F(s) \qquad (5.23)$$

$$-\omega_0^2X_0(s)+(s^2+2\omega_0^2)X_1(s)-\omega_0^2X_2(s)=\frac{1}{m}F(s) \qquad (5.24)$$

$$-\omega_0^2X_1(s)+(s^2+2\omega_0^2)X_2(s)-\omega_0^2X_3(s)=\frac{1}{m}F(s) \qquad (5.25)$$

$$-\omega_0^2X_2(s)+(s^2+2\omega_0^2)X_3(s)-\omega_0^2X_4(s)=\frac{1}{m}F(s) \qquad (5.26)$$

$$-\omega_0^2X_3(s)+(s^2+2\omega_0^2)X_4(s)-\omega_0^2X(s)=\frac{1}{m}F(s) \qquad (5.27)$$

$$-2\omega_0^2X_4(s)+(s^2+2\omega_0^2)X_5(s)=\frac{2}{m}F(s) \qquad (5.28)$$

These equations yield a sixth order determinant which, when solved, gives the Laplacians of the displacements. The absence of certain terms greatly simplifies the work, and the solution may be accomplished without setting up a determinant. This is accomplished and the inverse transforms are solved for in Appendix E.

The incremental displacements ($\Delta x_1 = x - x_0$, $\Delta x_2 = x_2 - x_1$ etc.) are thus found and are presented below.

$$\Delta x_1 = [4.50 - 1.00 \cos 0.618 W_0 t - 1.00 \cos 1.18 W_0 t - 1.00 \cos 1.62 W_0 t - 1.00 \cos 1.90 W_0 t - 0.50 \cos 2.00 W_0 t] \frac{F}{W_0^2 m}$$

$$\Delta x_2 = [3.50 - 2.62 \cos 0.618 W_0 t - 1.62 \cos 1.18 W_0 t - 0.38 \cos 1.62 W_0 t + .62 \cos 1.90 W_0 t + 0.50 \cos 2.00 W_0 t] \frac{F}{W_0^2 m}$$

$$\Delta x_3 = [2.50 - 3.24 \cos 0.618 W_0 t + 1.24 \cos 1.62 W_0 t - .005 \cos 200 W_0 t] \frac{F}{W_0^2 m}$$

$$\Delta x_4 = [1.50 - 2.62 \cos 0.618 W_0 t + 1.62 \cos 1.18 W_0 t - 0.38 \cos 1.62 W_0 t - .062 \cos 1.90 W_0 t + 0.50 \cos 2.0 W_0 t] \frac{F}{W_0^2 m}$$

$$\Delta x_5 = [0.50 - 1.00 \cos 0.618 W_0 t + 1.00 \cos 1.18 W_0 t - 1.00 \cos 1.62 W_0 t + 1.00 \cos 1.62 W_0 t + 1.00 \cos 1.90 W_0 t - 0.50 \cos 2.00 W_0 t]$$

The greatest incremental displacement is seen to occur in the end bay; thus, the end bay sway brace will be stressed the most and may be the limiting factor.

Figure 5.13 is a normalized curve of $\Delta x_1 W_0^2 m/F$ vs $W_0 t$. If undamped oscillations continue, the maximum displacement, Δx_{1m} will be $9.0 F/W_0^2 m$ and will occur when all the cosine terms are simultaneously negative maximums. The curve shows the first maximum to be only $7.2F/W_0^2 m$, since in the first oscillation the cosine terms do not reach negative maximums at the same time. The theoretical maximum of $9.0 F/W_0^2 m$ will never be reached due to the presence of damping; and the first swing may, therefore, be considered the largest.

Specific values of displacement may be obtained by specializing the constants in the equations.

$F = \mu mg$, as was shown at the outset, the net uniformly distributed load over the entire bridge is equal to the frictional resisting force. The force per bay is one tenth of the total force.

$$\frac{F}{W_0^2 m} = \frac{\mu g}{W_0^2} = \frac{\mu g m}{K}$$

Equation 5.16 is repeated here for convenience:

$$K = \frac{EA(d \cos\theta)^2}{\ell L^2}$$

lb per in *

$E = 30 \times 10^6$

$A = 10$ in^2

$d = 95$ in

$\ell = 202$ in

$L = 120$ in

*See Appendix F

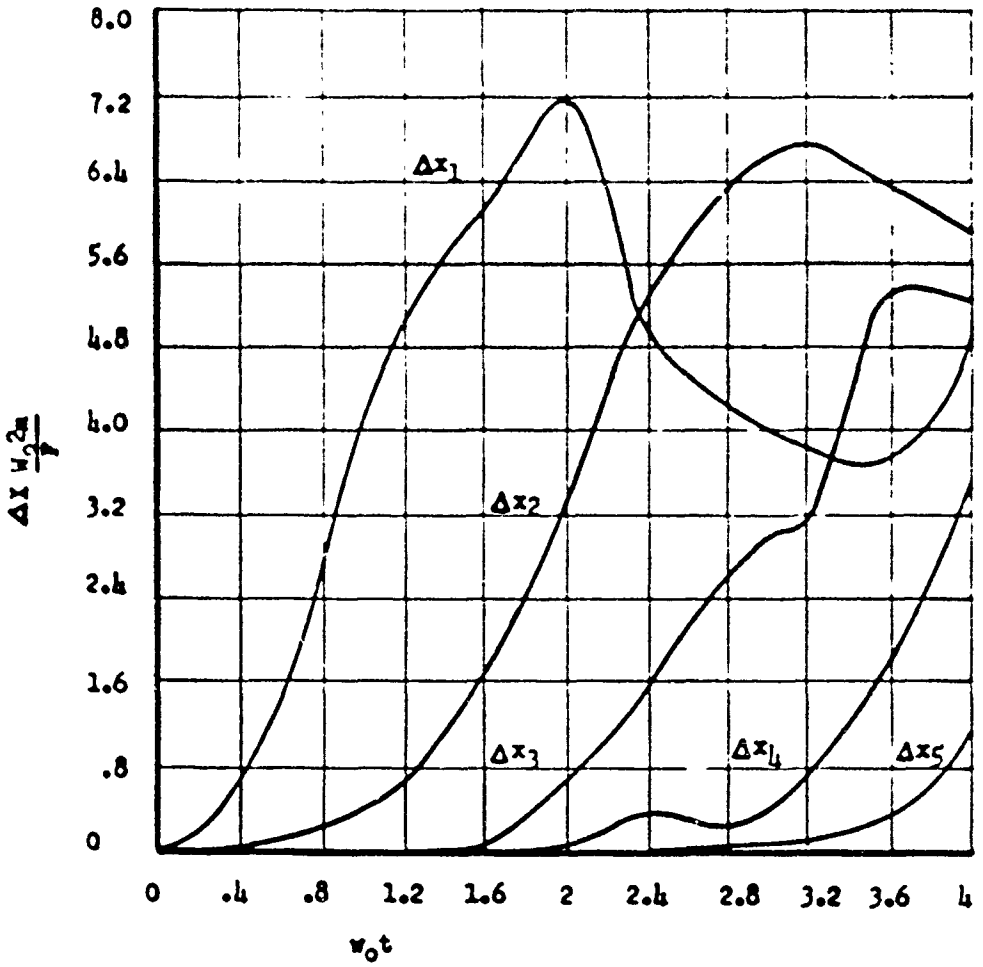

Fig. 5.13 Non-dimensional Plot of Incremental Displacement, 100-ft Bailey Bridge

$$\text{Cos}\,\Theta = \sqrt{\frac{\ell^2 - d^2}{\ell^2}} = \sqrt{1 - \left(\frac{d}{\ell}\right)^2}$$

$$K = \frac{(30 \times 10^6)(952)}{(202)(120)^2}\left[1 - \frac{95^2}{202^2}\right] \text{ lb/in.}$$

$$= 7.3 \times 10^4 \text{ lb/ in.} = 87 \times 10^4 \text{ lb/ ft.}$$

$m = 224$ slugs

$$\frac{\mu g m}{K} = 82.8 \times 10^4 \text{ ft.}$$

To obtain specific values of displacement in feet from Fig. 5.13, the numerical ordinates must be multiplied by $82.8 \times 10^{-4}\mu$ ft or, for $\mu = 0.3$, by 24.84×10^{-4} ft.

$$\omega_o = \sqrt{\frac{k}{m}} = 10^2 \times \frac{87}{224}$$

$$= 62.2 \text{ radians/sec.}$$

To obtain specific values of time in seconds from Fig. 5.13, the abscissas must be multiplied by 1/62.2. Thus, the maximum displacement is $7.2 \times 24.8 \times 10^{-4} = 0.0179$ ft. By substituting Equation 5.11 in Equation 5.14, we obtain

$$T = \frac{EA}{\ell} \frac{d}{L} \cos\theta \, \Delta X \qquad (5.29)$$

or, for the case above, T = 19,700 lb.

5.3.3 Plastic Response

By rearranging Equation 5.25,

$\Delta X = \frac{\ell L}{EA d \cos\theta}$, the value of displacement at which yield occurs is

$$\Delta X_y = \frac{(202)(120)}{(30 \times 10^6)(95)(12)(0.779)} (5 \times 10^4)$$

$= 45.5 \times 10^{-3}$ ft, considering 50,000 lb as the yield tension.

where ΔX_y = incremental displacement at which yield occurs.

The maximum value of displacement reached in the elastic region is:

$$(10^{-4})(7.2)(82.4)\,\mu \text{ ft.}$$

$$= 5.96 \times 10^{-2}\mu \text{ ft.}$$

The plastic yield point, therefore, will just be reached when

$$\mu = \frac{4.55}{5.96} = 0.76$$

When μ exceeds this value, the displacement goes into the plastic region and the following analysis applies. If t_y is the time that it takes for the plastic yield point to be reached, the elastic analysis applies for $0 < t < t_y$; and at t_y, ΔX_o and V_o are evaluated and these values become initial conditions for the plastic analysis which follows.

The plastic analysis may consider elastic forces throughout the mechanical system of Fig. 5.12, with the exception that the $K(X_1 - X_o)$ is replaced by a constant force, $K\Delta X_y$.

As before, the incremental displacement, Δx_1, is of interest.

$$\Delta X_1 = X_1 - X_o$$

is large in magnitude in comparison to ΔX_1 for the cases of primary interest, since X_1 is limited by elastic deformations. Therefore, the problem of plastic response may be tremendously simplified if we consider X_1 negligible in the above equation. The following approximation is made:

$$\Delta X_1 \approx -X_o$$

Referring again to Fig. 5.12b, one may see that the forces acting on the mass on the left end of the system will be constant during the plastic response. The end reaction force, 5F, and the step load $\frac{F}{2}$, of course, are constant as they were in the elastic response. In

addition, the spring force, $K(x_1 - x_0)$, is constant (equal to $K\Delta xy$), and the net force is therefore constant. If a new origin of time is chosen so that $t = 0$ at the instant plastic yield occurs, and if initial conditions are considered, the following equations result:

$$\ddot{x} = 2\frac{K}{m}\Delta xy - 9\frac{F}{m}$$

$$X_0 = \frac{K}{m}\Delta Xy\, t^2 - \frac{9}{2}\frac{F}{m}t^2 + V_0(0)t + X_0(0)$$

$$\Delta Xy = (\frac{9}{2}\frac{F}{m} - \omega_0^2 \Delta Xy)\, t^2 - V_0(0)t + 45.5 \times 10^{-3}$$

$$= (145\mu - 176)\, t^2 - V_0(0)t + 45.5 \times 10^{-3} \qquad (5.30)$$

by differentiating the expression for X_0 (Appendix E) and setting $t = ty$, the initial velocity is obtained.

$$V_0(0) = 82.8 \times 10^{-3}\mu\omega_0 [3.24 \text{ Sin } 0.618\,\omega_0 ty$$

$$+1.71 \text{ Sin } 1.18\,\omega_0 ty + 1.23 \text{ Sin } 1.62\,\omega_0 ty$$

$$+1.05 \text{ Sin } 1.90\,\omega_0 ty + 0.50 \text{ Sin } 2.00\,\omega_0 ty]$$

For elastic vibrations, the incremental displacement reaches a maximum of 5.96×10^{-2} ft in 0.0322 sec. For oscillations into the plastic region, the displacement will reach the elastic limit in a time less than 0.0322 sec. By choosing a value of ty (less than 0.0322 sec), the cosine terms in the expression for ty (Appendix E) may be solved for. The result is an expression for X_0 in terms of a constant multiplied by μ. This may be equated to the known yield value of ΔX_0 and may be solved for. The resulting value of μ will, of course, be greater than 0.76 and will be the value which will cause yield to be reached in the chosen ty. The expression for X_0 may be differentiated and the chosen ty substituted for t. This gives $V_0(0)$, the initial velocity of the plastic analysis. μ and $V_0(0)$ may be substituted into Equation 5.30 and ΔXy, as a function of time determined. The maximum displacement attained will, of course, be of interest.

Such a calculation was made with $\omega_0 ty = 1.8$ or $ty = 0.029$ sec. The value of μ for this case is 0.79, or just above the elastic limit value. The resulting maximum displacement is 1.22 ft. Higher values of μ will cause correspondingly higher maximum values of plastic deformation. From this analysis, it appears that 0.76 is a threshold value of μ, beyond which the maximum displacement increases rapidly with small increments of μ. $\mu = 0.75$ will be chosen as the maximum allowable value, therefore, since going above this value requires that μ be controlled within closer limits than is practicable in order to limit plastic displacement.

It should be borne in mind that the frequencies of response calculated are high due to the assumptions of no damping and perfect hinging at the pin joints. The magnitude of the response in the plastic region depends very much upon the initial vibrational velocity of the end of the bridge, $V_0(ty)$, upon entering the plastic region. Since the calculated value of ω_0 is high, the calculated V_0 is correspondingly high and the elastic response is undoubtedly high.

5.4 BRIDGE OVERTURN

Two modes of overturn appear to be possible--one in which the bridge overturns as a whole, and the second in which the windward truss overturns or collapses. The first mode was seen to occur at Site A, where it was noticed that there were no skid marks produced by the windward runners over the initial portion of the sliding path. However, the bridge did not completely turn over but settled upright when it landed on the ground. It is possible that the amount of overturn experienced by the bridge caused a lift force on the bridge as a whole by tilting the front edge of the deck upward and thus, in effect, presenting an airfoil. In turn, the lift reduced the frictional retarding force and undoubtedly contributed to the excessive sliding. The latter type of overturn is treated by Mr. Norman G. Hansen, of the Bridge and Marine Test Branch, ERDL, in Appendix G.

5.5 DISCUSSION

Perhaps the most outstanding feature of the results is the large discrepancy between acceleration records obtained by the various means. The ERA records indicate accelerations in excess of anticipated values but of much shorter duration than anticipated. It is also notable that these records start some time after the time of arrival of the blast wave. As an example, the ERA measurement on the bridge at Site B for Shot 9 indicates the acceleration begins to rise from zero at approximately H = 3.05 sec and lasts until H = 3.97 sec. The actual time of arrival of the blast wave at the range of Site B is presented as H = 3.05 sec in the reports dealing with basic data (Ref 4 and 5). This is in close agreement with the time of arrival, as indicated by the motion pictures at Site B. The actual transit time of the bridge, again as determined from the motion pictures, was of the order of 0.9 sec as compared to the 0.05 sec duration of the ERA record.

The Wianko acceleration record, on the other hand, evidenced frequencies of approximately 200 cps which may have been actual or may have originated in the recording apparatus. If the frequencies measured were real frequencies of vibration of the local member to which the gage was attached, the gage may have acted more as a velocity gage rather than an acceleration gage, since accelerations are measured accurately only for frequencies much less than the natural frequency of the gage (100 cps).

The reliability of the results obtained from the two types of acceleration gages does not warrant quantitative conclusions.

The two experimentally determined displacement curves are seen to compare favorably with the calculated displacement curve. This is especially true over the initial region of the displacement of the south end of the bridge. As was noted in the chapter on results, however, the ends of the bridge gouged the edges of the channels; and it is probably the retarding force resulting from this effect that causes the displacement curve of the south end of the bridge to suddenly fall below the calculated curve. The displacement curve of the north end of the bridge lies above the calculated curve. This may be in part because the binding force against the edge of the channel on that end of the

bridge was negligible compared to the retarding action on the other end, with the result that part of the kinetic energy of the south end was transferred to the north end. The experimental curves show a large negative second derivative toward the end compared with the calculated curve. This is probably due to an increase in the coefficient of friction, approaching static coefficient of friction, as the bridge velocity decreased. The result was a higher negative acceleration than would be indicated by a coefficient of friction of 0.3.

Because the dynamic vibration analysis presented in this report depends upon many assumptions, and because experimental evidence is not present to bear out the calculated results, it should not be relied upon for quantitative information. However, the following indications are present: The magnitude of elongation of the end bay sway braces is somewhat proportional to the length of the bridge; the end bay (or possibly the second bay) will be the most stressed; the limiting distributed force to which a 100-ft double-single bridge may be subjected without rupture of the sway braces is in the order of 75 per cent of its weight. If the bridge is allowed to slide, the inertia force may be subtracted from the blast force to determine the net uniform force; the force a bridge may be subjected to is inversely proportional to the length, or for any given length is inversely proportional to the mass per bay (deflection is proportional to $\mu mg/K$; therefore, triple-single would suffer greater deflection than double-single subjected to the same force).

There is nothing in the results to indicate that significant lift forces can be attributed to the precursor. All bridges experiencedlift; however, there are several possible reasons for this--perhaps that, due to the aerodynamic profile of the bridge, a coefficient of lift may be ascribed to the bridge. The lifting of the bridge flooring at Site B for Shot 9 (in a region where no precursor was detected) is evidence of this. Lift was most evident on the bridge at Site A for Shot 10. It may be remembered that only the windward edge of that bridge lifted at first and, initially, the bridge slid along on its leeward supports. The lifting may have been a result of an overturning moment on the bridge caused by the horizontal wind forces, it may have been caused by a coefficient of lift as mentioned above, it may have been caused by the precursor, or it may have been caused by a combination of these.

That the bridge at Site A (Shot 10) slid much in excess of what was anticipated, considering so-called "ideal" conditions, is an indication of excessive drag at that range. That this excessive sliding may be correlated to measurements of excessive drag pressure at the same range is an indication that the bridge is a drag structure. Actual data for Shot 9, Site B, bears out the methods used in calculating the sliding response of the bridge; and it may be concluded that the sliding response of any similar bridge may be predicted to the same degree of accuracy within the limitations imposed upon the prediction of the drag pressure.

CHAPTER 6

CONCLUSIONS AND RECOMMENDATIONS

6.1 CONCLUSIONS

1. The Bailey bridge (and, in fact, all truss-type bridges) may be classified among the so-called "drag" type of structures, in that its response to an atomic blast depends mainly on the dynamic pressure associated with the blast and only slightly on the peak overpressure. Predictions of response (or damage), therefore, can be stated in terms of a peak overpressure only insofar as the dynamic pressure may be considered a single-valued function of peak overpressure. In general, this will not be true.

2. Burning or charring of the Bailey deck will not be critical for detonations of the size used in this test series. It is possible that for much larger detonations the blast wave, being weaker and arriving later at a point of equivalent thermal flux, might actually aid the burning.

3. In the presence of lift forces, the full weight of the Bailey is not effective in causing a frictional retarding force. The results at Site A, Shot 10, indicate that lift forces may be significant. A frictional restraint anchorage by itself is, therefore, considered an unsatisfactory solution. An anchor cable that will "give" after a certain tension is reached appears to be a more satisfactory answer and has the additional advantage that it can be connected to the bridge out several feet from the end, thus reducing the effective span.

4. The loading is primarily drag; and, with the assumptions chosen as in Chapter 5, the drag coefficient, C_d, of 1.63 is slightly low. This is illustrated in Fig. 5.6, which shows the calculated displacement to be less than the average of the two experimental curves. Since the experiment does not merit three significant figures for the drag coefficient, a value of 1.7 may be chosen with fair accuracy.

5. The analysis indicates that the end bay sway braces will be damaged before other components for single story bridges of moderate or great spans. Transom clamp seats and rakers may be limiting factors in considerations of double or triple story bridges.

6. Rupture of the end bay sway braces will, in general, result in the progressive collapse of the bridge by allowing the bridge to

accelerate and imposing excessive bending moments at the truss pin joint between the end bays and adjacent bay. For bridges above single story height, failure of rakers and transom seats will allow the windward truss to lay over and reduce the vertical rigidity of the structure. Collapse will probably ensue.

7. The analytical methods of Chapter 5 may be used with sufficient accuracy to calculate the sliding response of a bridge with the reservation that the drag coefficient be chosen as in conclusion 4.

8. Sufficient knowledge is not available to enable accurate predictions of overpressures and dynamic pressures near detonations of relatively low altitude.

6.2 RECOMMENDATIONS

It is recommended that:

1. Response of prefabricated fixed bridging be correlated with drag pressures and not with overpressures.

2. Anchor cables be used in the field as a means of limiting the response of a bridge to blast when attack is imminent. The earth anchor should have some "give" to it. As an interim guide, Table 6.1 and Fig. 6.1 are presented to indicate the arrangement of such anchor cables.

3. The drag coefficient for Bailey bridges be chosen as 1.7 until additional tests indicate a more accurate value.

4. Model Bailey bridges and T6 bridges of different constructions be tested in a wind tunnel to more accurately establish drag coefficients and load distribution.

5. The "give" characteristics of earth anchors be investigated.

6. Consideration be given to upturning the ends of the sway braces prior to threading, in order to increase the effective section area in that region. At present, it is the reduced diameter of the braces in this region that limits the strength of the sway braces.

7. The transom seats of Bailey panels be strengthened.

8. Static deflection tests be made on the Bailey and T6 bridges to determine accurately their horizontal deflection characteristics. Strain gage measurements should be made.

9. In the light of static tests, wind tunnel tests, and anchor cable considerations, an analysis of Bailey and T6 bridging be made which will result in useful tabular data of response versus dynamic pressure for various truss constructions and bridge lengths.

10. In future full-scale atomic tests in which precursor phenomena are anticipated, particular attention should be paid to obtaining dynamic pressure data.

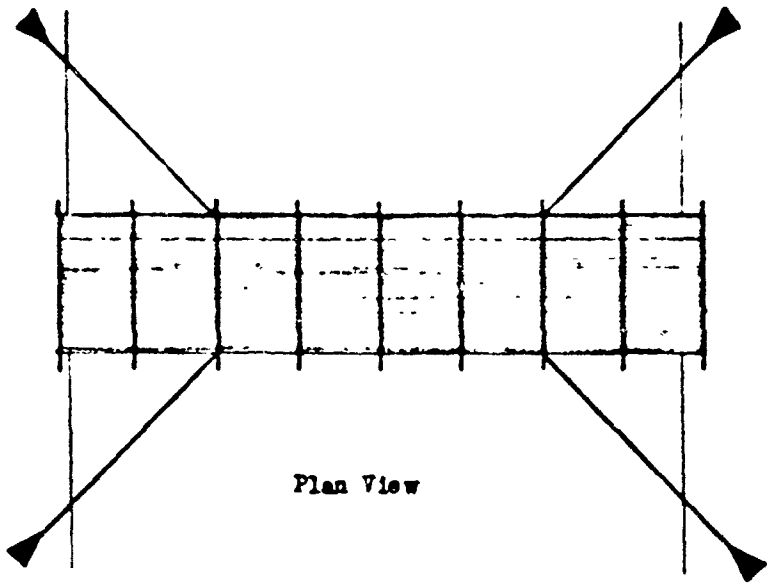

Fig. 6.1 Bailey Bridge Showing Attachment of Anchor Cables

TABLE 6.1 - Attachment of Anchor Cables

Attachment of Anchor Cables			
l = Length of Bridge in Bays n = Distance From End of Bridge to point where anchor cable is is fastened in bays			
l	n	l	n
6	2	13	4
7	2	14	4
8	2	15	5
9	3	16	5
10	3	17	5
11	3	18	6
12	4	19	6

APPENDIX A

SYMBOLS

p = Free stream side-on overpressure
p_{so} = Peak side on overpressure
t_+ = Positive phase duration
I_s = Shock impulse delivered to a structure by the blast wave during its initial or diffraction phase
I_o = Shock impulse delivered to the structure per unit of exposed area
F_s = Shock force
F_d = Drag force (force of the high velocity winds)
F_{do} = Peak drag force
C_d = Drag coefficient
A_{eff} = Area effective in drag loading
q = Dynamic pressure
q_o = Peak dynamic pressure
ρ = Density of air behind shock front
v = Particle velocity behind shock front
p_o = Atmospheric pressure
θ = Angle of yaw
Q_v = Vertical component of thermal intensity
W = Weight of 100-ft double-single Bailey bridge
M = Mass of 100-ft double-single Bailey bridge
x_{cg} = Displacement of center of gravity of bridge
F_f = Friction force resisting lateral sliding of bridge
μ = Coefficient of friction
v_d = Component of bridge velocity due to drag force
v_f = Component of bridge velocity due to friction force
x_s = Component of bridge displacement due to shock force
x_d = Component of bridge displacement due to drag force
x_f = Component of bridge displacement due to friction force
t_c = Time of transit of sliding bridge
A_T = Elevation area of Bailey bridge truss per bay
A_F = Elevation area of Bailey bridge flooring per bay
Δx = Incremental displacement of one bay of Bailey bridge
ℓ = Length of Bailey sway brace
$\Delta \ell$ = Elongation of Bailey sway brace
L = Length of one bay of Bailey bridging

d = Distance between sway brace pin connections along Bailey panel
T = Tension in Bailey sway brace
E = Young's modulus for sway brace
K = Spring constant
m = Mass of one bay of double-single Bailey bridge

APPENDIX B

BLAST DATA

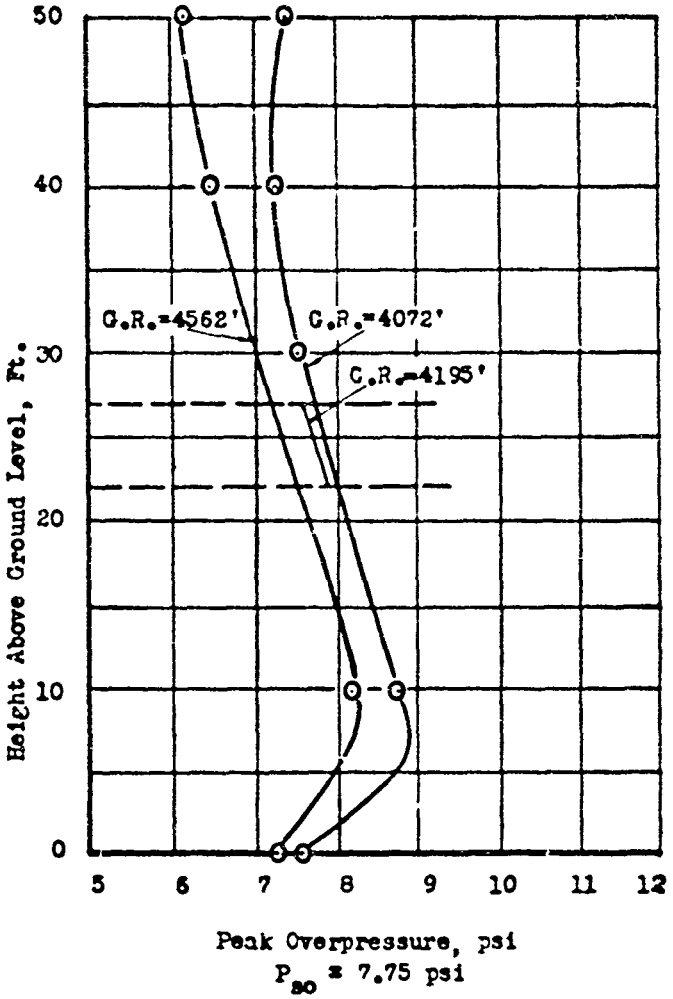

Fig. B.1 Graphical Interpolation to Determine Peak Overpressure at Height and Range of Bridge, Shot 9, Site B

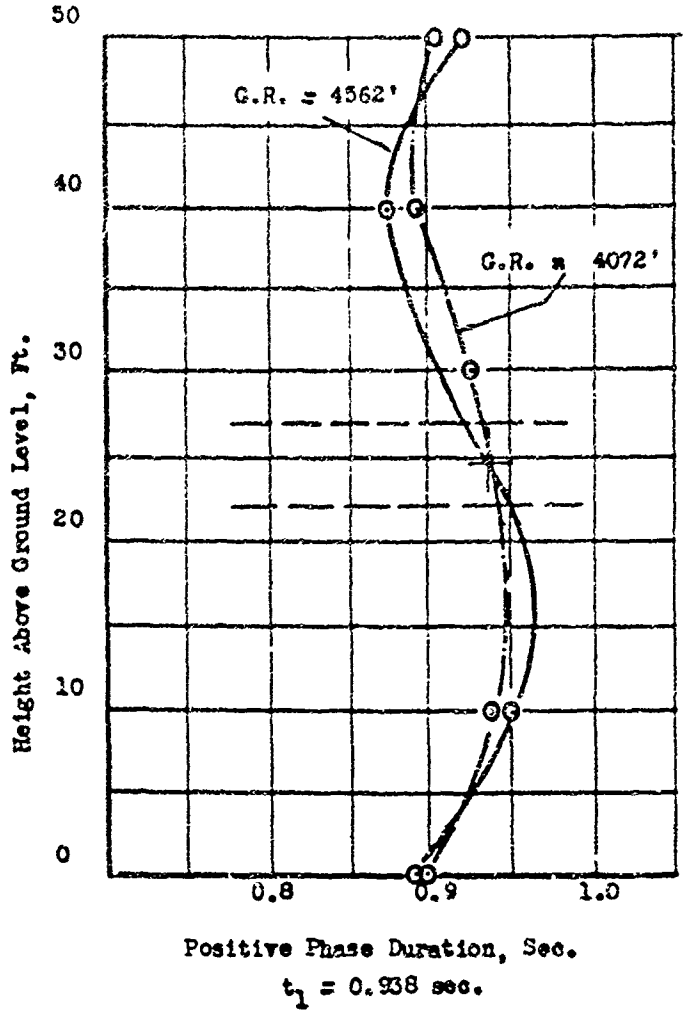

Fig. B.2 Graphical Interpolation to Determine Positive Phase Duration at Height and Range of Bridge, Shot 9, Site B

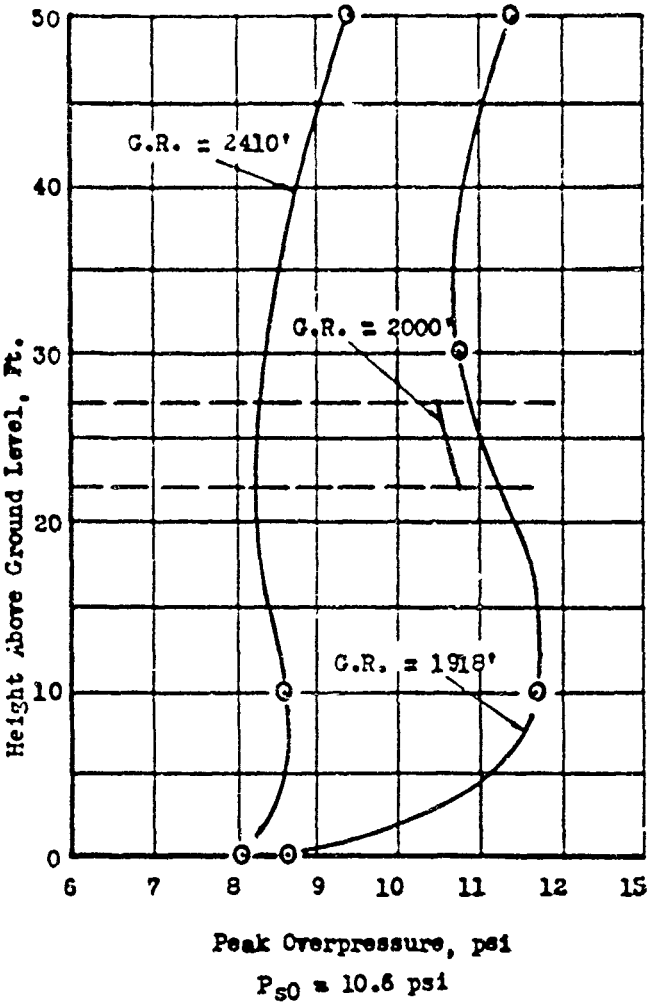

Fig. B. 3 Graphical Interpolation to Determine Peak Overpressure at Height and Range of Bridge, Shot 10, Site A

APPENDIX C

DISPLACEMENT DATA

The displacement of the bridge at Site B as a function of time was determined as follows:

The displacement of the south end of the bridge was determined by making enlargements of the successive moving picture frames taken of that end of the bridge during its sliding phase. The speed of the camera during the time of interest was 23.6 frames per second; thus, successive frames show the position of the bridge at intervals of time of 42.4 msec. The time-displacement history of the north end of the same bridge was determined in like manner. Displacement in centimeters was measured from the enlargements with the aid of an optical viewer with crosshairs, and the centimeter dimensions were converted to prototype dimensions in inches.

TABLE C.1 - Bridge Displacement, Shot 9, Site B, South End of Bridge

Frame No.	Time (sec)	(Displacement (cm)	Prototype Displacement (in.)
	3.05	0	0
1	3.092	Record	
2	3.135	Obscured	
3	3.177		
4	3.220	0.110	5.33
5	3.262	0.155	7.51
6	3.304	0.205	9.9
7	3.347	0.250	12.1
8	3.389	0.310	15.0
9	3.432	0.370	17.9
10	3.474	0.410	19.9
11	3.516	0.445	21.6
12	3.559	0.451	22.1
13	3.601	0.495	24.0
14	3.644	0.535	25.9
15	3.686	0.590	28.6
16	3.729	0.595	28.8
17	3.771	0.600	29.1
		0.619	30.0

Camera speed = 23.6 frames per sec
Interval between frames = 0.0424 sec
Final displacement, photo enlargement = 0.619 cm
Final displacement, prototype = 30 in.
Conversion factor 48.6 in./cm
Time of arrival of blast wave = 3.05 sec

TABLE C.2 - Bridge Displacement, Shot 9, Site B, North End of Bridge

Frame No.	Time (sec)	Displacement (cm)	Prototype Displacement (in.)
	3.050	0	0
1	3.080	Record	
2	3.110	Obscured	
3	3.140	0.095	4.2
4	3.171	0.135	5.9
5	3.201	0.202	8.9
6	3.231	0.247	10.8
7	3.261	0.312	13.7
8	3.291	0.367	16.1
9	3.322	0.435	19.1
10	3.352	0.505	22.1
11	3.382	0.570	25.0
12	3.412	0.637	27.9
13	3.442	0.690	30.2
14	3.473	0.707	31.0
15	3.503	0.750	32.8
16	3.533	0.790	34.6
17	3.563	0.830	36.3
18	3.593	0.877	38.4
19	3.624	0.920	40.3
20	3.654	0.977	42.8
21	3.684	1.012	44.4
22	3.714	1.067	46.8
23	3.744	1.082	47.5
24	3.775	1.102	48.4
25	3.805	1.160	50.9
26	3.845	1.197	52.5
27	3.875	1.240	54.4
28	3.905	1.240	54.4
29	3.936	1.260	55.3
30	3.966	1.300	57.0

Camera speed = 33.1 frames per sec
Interval between frames = 0.0302 sec
Final displacement, photo enlargement = 1.300 cm
Final displacement, prototype = 57 in.
Conversion factor = 43.8 in./cm
Time of arrival of blast wave = 3.05 sec

APPENDIX D

DISPLACEMENT CALCULATIONS

D.1 SHOT 9, SITE B

D.1.1 Force and Acceleration Calculations

$F(t) = F_s + F_d - F_f \qquad \ddot{x}(t) = F(t)/M$

M = mass of 100 ft DS bridge = 2240 slugs

$F_s = \infty$ at $t = 0$ and $= 0$ thereafter

$F_d = 101{,}000\,\varepsilon^{-4t/t_1}$ lb

$t_1 = 0.938$ sec

$F_f = 21{,}600$ lb

TABLE D.1 - Force and Acceleration Calculations, Shot 9, Site B

t	$4t/t_1$	ε^{-4t/t_1}	F_s(lbs)	F_d(lbs)	$F(t)$(lbs)	$\ddot{x}(t)$(ft/sec^2)
0	0	1	∞	101,000		
0+	0	1	0	101,000	79,400	35.5
0.1	0.427	0.653	0	65,900	44,300	19.8
0.2	0.854	0.426	0	43,000	21,400	9.55
0.3	1.282	0.278	0	28,000	6,400	2.88
0.4	1.709	0.181	0	18,300	-3,300	-1.47
0.5	2.136	0.118	0	11,900	-9,700	-4.33
0.6	2.563	0.077	0	7,800	-13,800	-6.16
0.7	2.990	0.051	0	5,200	-16,400	-7.32
0.8	3.418	0.033	0	3,300	-18,300	-8.17
0.9	3.845	0.021	0	2,200	-19,400	-8.66
1.0					-21,600	

D.1.2 Velocity Calculations

$V(t) = V_s + V_d - V_f$

$V_s = 0.5$ fps

$V_d = 10.6(1-\varepsilon^{-4t/t_1})$ fps $\quad t < t_1$

$= 10.6(1-\varepsilon^{-4}) = 10.4$ fps $\quad t > t_1$

$V_f = 9.66\,t$ fps

$t_1 = 0.938$ sec

TABLE D.2 - Velocity Calculations, Shot 9, Site B

t	$4t/t_1$	ε^{-4t/t_1}	$1-\varepsilon^{-4t/t_1}$	V_d(fps)	V_f(fps)	$V(t)$(fps)
0	0	1	0	0	0	.5
0.1	0.427	0.653	0.347	3.68	0.97	3.21
0.2	0.854	0.426	0.574	6.08	1.93	4.65
0.3	1.282	0.278	0.722	7.65	2.90	5.25
0.4	1.709	0.181	0.819	8.68	3.86	5.32
0.5	2.136	0.118	0.882	9.35	4.83	5.03
0.6	2.563	0.077	0.923	9.78	5.80	4.48
0.7	2.990	0.051	0.949	10.05	6.76	3.79
0.8	3.418	0.033	0.967	10.25	7.72	3.03
0.9	3.845	0.021	0.979	10.38	8.69	2.19
1.0				10.4	9.66	1.24
1.1				10.4	10.63	0
1.2				10.4	11.60	0

D.1.3 Displacement Calculations

$X(t) = X_s + X_d - X_f$

$X_s = 0.5\,t$ ft.

$X_d = 10.6\,t + 0.234(\varepsilon^{-4t_1/t} - 1)$ ft $\quad t < t_1$

$= 10.6\,t\,(1-\varepsilon^{-4}) - 0.234(1-5\varepsilon^{-4})$ ft $\quad t > t_1$

$X_f = 4.83\,t^2$ ft

$t = 0.938$ sec

TABLE D.3 - Displacement Calculations, Shot 9, Site B

t	ϵ^{-4t/t_1}	$c\,234(\frac{gc}{L}-1)$	$x_1(ft)$	$x_2(ft)$	$x_3(ft)$	$x(ft)$
0	1	0	0	0	0	0
0.1	0.653	-0.081	0.05	0.20	0.05	0.20
0.2	0.426	-0.134	0.10	0.70	0.19	0.61
0.3	0.278	-0.169	0.15	1.39	0.44	1.10
0.4	0.181	-0.192	0.20	2.20	0.77	1.63
0.5	0.118	-0.206	0.25	3.12	1.21	2.16
0.6	0.077	-0.216	0.30	4.07	1.74	2.63
0.7	0.051	-0.222	0.35	5.06	2.36	3.05
0.8	0.033	-0.226	0.40	6.08	3.09	3.39
0.9	0.021	-0.229	0.45	7.12	3.91	3.66
1.0			0.50	8.15	4.83	3.82
1.1			0.55	9.20	5.84	3.91
1.2			0.60	10.22	6.95	3.87

D.2 MAXIMUM DISPLACEMENTS

Maximum displacement is expressed in Chapter 5 as a function of the blast parameters, coefficient of friction, and time of transit, where time is a transcendental function of the blast parameters and the coefficient of friction. To facilitate calculations, time of transit and blast parameters have been chosen as independent variables and coefficient of friction calculated by application of Equation 5.4. This eliminates the necessity for a trial-and-error solution of a transcendental equation.

$$\mu = \frac{1}{g t_o}\left[\frac{I_s}{M} + \frac{F_{do} t_o}{4M}\left(1-\epsilon^{-4t_o/t_1}\right)\right] \qquad t_o < t_1$$

$$\mu = \frac{1}{g t_o}\left[\frac{I_s}{M} + \frac{F_{do} t_1}{4M}\left(1-\epsilon^{-4t_o/t_1}\right)\right] \qquad t_o > t_1$$

$g = 32.2$ fps

$M = 2240$ slugs

In general, t_1 is not a single valued function of P_{so} or q_o, but depends on the bomb yield as well. For the purpose of these calculations, t_1 = 0.8 sec had been chosen as a median value representing with reasonable accuracy positive phase durations of from 0.6 sec. to 1.0 sec. For shorter positive phase durations, the sliding displacement calculated by the use of t_1 = 0.8 sec. would tend to be too large. For bomb yields in the range of several hundreds of kilotons, a larger duration should be used to calculate response.

$$\mu = \frac{1}{t_o^{1.9}}\left[I_s + 0.20 F_{do}(1-\epsilon^{-5t_o})\right]10^{-5} \qquad t_o < 0.8$$

$$= \frac{1.39}{t_o}\left[I_s + 0.196 F_{do}\right]10^{-5} \qquad t_o > 0.8$$

$$x_s = 4.47 \times 10^{-4} I_s t_o$$

$$x_d = 0.893 F_{do}\left[t_o - 0.20(1-\epsilon^{-5t_o})\right]10^{-4} \qquad t_o < 0.8$$

$$= 0.816 F_{do}\left[t_o - 0.185\right]10^{-4} \qquad t_o > 0.8$$

$$x_f = 16.1 \mu t_o^2$$

$$x = x_s + x_d - x_f$$

$$P_{do} = 62.45 q_o$$

$$I_s = 144.6 P_{so}$$

TABLE D.4 - Maximum Displacement of Double-Single Bailey

$q_o = 20$ psi $P_{so} = 9.0$ psi $F_{do} = 124{,}000$ lb $I_s = 1300$ lb sec

$$\mu = \frac{1}{t_o}\left[.018 + .250(1-\epsilon^{-5t_o})\right] \qquad t_o < 0.8$$

$$= \frac{0.263}{t_o} \qquad t_o > 0.8$$

$$x_s = 0.58\, t_o$$

$$x_d = 111\left[t_o - 0.20(1-\epsilon^{-5t_o})\right] \qquad t_o < 0.8$$

$$= 10.9(t_o - 0.185) \qquad t_o > 0.8$$

$$x_f = 16.1 \mu t_o^2$$

t_o(sec)	μ	x_s(ft)	x_d(ft)	x_f(ft)	x(ft)
0.4	0.585	0.23	2.53	1.51	1.25
0.6	0.427	0.35	4.57	2.48	2.44
0.8	0.329	0.46	6.73	3.39	3.80
1.0	0.263	0.58	8.92	4.23	5.27
1.25	0.210	0.73	11.65	5.28	7.10
1.50	0.185	0.87	14.39	6.70	8.56
1.75	0.150	1.02	17.12	7.40	10.74
2.00	0.132	1.16	19.86	8.50	12.52
2.50	0.105	1.45	25.33	10.56	16.22

TABLE D.4.1 - Maximum Displacement of Double-Single Bailey

q_o = 80 psi P_{so} = 130 psi F_o = 261,000 lbs I_s = 2081 lb sec

$$\mu = \frac{1}{t_o}\left[0.14 + .674(1 - e^{-5t_o})\right] \qquad t_o < 0.8$$

$$= \frac{0.710}{t_o} \qquad t_o > 0.8$$

$$x_s = 0.942\, t_o$$

$$x_d = 223\left[t_o - 0.20(1 - e^{-5t_o})\right] \qquad t_o < 0.8$$

$$= 214(t_o - 0.185) \qquad t_o > 0.8$$

$$x_f = 16.1\, \mu t_o^2$$

t_o (sec)	μ	x_s (ft)	x_d (ft)	x_f (ft)	x (ft)
0.4	1.325	0.37	5.07	3.41	2.03
0.6	1.148	0.56	9.15	6.65	3.06
0.8	0.889	0.75	13.47	9.16	5.06
1.0	0.710	0.93	17.83	11.43	7.33
1.25	0.568	1.16	23.30	14.30	10.16
1.50	0.473	1.40	28.77	17.13	13.04
1.75	0.406	1.63	34.24	20.01	15.86
2.00	0.353	1.86	39.71	22.86	18.72
2.50	0.284	2.33	50.65	28.57	24.41

TABLE D.4.2 - Maximum Displacement of Double-Single Bailey

q_o = 60 psi P_{so} = 160 psi F_o = 374,700 lb I_s = 2315 lb sec

$$\mu = \frac{1053}{t_o} \qquad t_o > 0.8$$

$$x_s = 1035\, t_o$$

$$x_d = 328(t_o - 0.185) \qquad t_o > 0.8$$

$$x_f = 16.1\, \mu t_o^2$$

t_o (sec)	μ	x_s (ft)	x_d (ft)	x_f (ft)	x (ft)
0.80	1.316	0.83	20.17	13.56	7.44
1.00	1.053	1.04	26.73	16.95	10.82
1.25	0.843	1.29	34.93	21.21	15.01
1.50	0.702	1.55	43.13	25.43	19.25
1.75	0.602	1.82	51.33	29.68	23.47
2.00	0.527	2.07	59.53	33.94	27.66
2.50	0.421	2.59	75.93	42.36	36.16

TABLE D.4.3 - Maximum Displacement of Double-Single Bailey

$q_o = 50$ psi $P_{so} = 12.5$ psi $F_d = 444,000$ lb $I_s = 2120$ lb-sec

$$\mu = \frac{1.300}{t_o}$$

$$x_s = 1.216\, t_o$$

$$x_d = 438(t_o - 0.185)$$

$$x_f = 16.1 \mu t_o^2$$

t_o (sec)	μ	x_s (ft)	x_d (ft)	x_f (ft)	x (ft)
0.80	1.738	0.97	26.91	18.08	9.80
1.00	1.390	1.22	35.66	22.38	14.50
1.25	1.112	1.52	46.60	27.97	20.15
1.50	0.927	1.82	57.54	33.58	25.78
1.75	0.794	2.13	68.48	39.15	31.46
2.00	0.695	2.43	79.42	44.76	37.09
2.50	0.556	3.06	101.30	55.95	48.39

APPENDIX E

VIBRATION ANALYSIS

E.1 [illegible]-BAY (100') BRIDGE

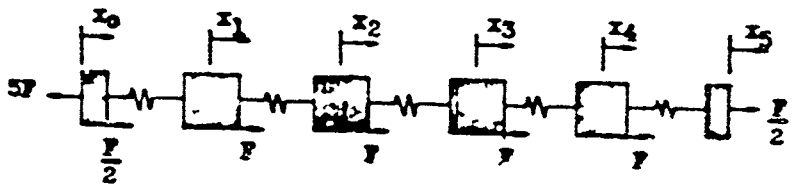

Equations of motion:

$$\ddot{x}_0 + 2\omega_0^2 x_0 - 2\omega_0^2 x_1 = -\frac{g}{m} F \qquad \text{(E.1)}$$

$$-\omega_0^2 x_0 + \ddot{x}_1 + 2\omega_0^2 x_1 - \omega_0^2 x_2 = F/m \qquad \text{(E.2)}$$

$$-\omega_0^2 x_1 + \ddot{x}_2 + 2\omega_0^2 x_2 - \omega_0^2 x_3 = F/m \qquad \text{(E.3)}$$

$$-\omega_0^2 x_2 + \ddot{x}_3 + 2\omega_0^2 x_3 - \omega_0^2 x_4 = F/m \qquad \text{(E.4)}$$

$$-\omega_0^2 x_3 + \ddot{x}_4 + 2\omega_0^2 x_4 - \omega_0^2 x_5 = F/m \qquad \text{(E.5)}$$

$$-2\omega_0^2 x_4 + \ddot{x}_5 + 2\omega_0^2 x_5 = F/m \qquad \text{(E.6)}$$

Equivalent Laplace equations:

$$(s^2 + 2\omega_0^2) X_0(s) - 2\omega_0^2 X_1(s) = -\frac{g}{m} F(s) \qquad \text{(E.7)}$$

$$-\omega_b^2 X_0(s) + (s^2 + 2\omega_b^2) X_1(s) - \omega_b^2 X_2(s) = 1/m\ F(s) \qquad (E.8)$$

$$-\omega_b^2 X_1(s) + (s^2 + 2\omega_b^2) X_2(s) - \omega_b^2 X_3(s) = 1/m\ F(s) \qquad (E.9)$$

$$-\omega_b^2 X_2(s) + (s^2 + 2\omega_b^2) X_3(s) - \omega_b^2 X_4(s) = 1/m\ F(s) \qquad (E.10)$$

$$-\omega_b^2 X_3(s) + (s^2 + 2\omega_b^2) X_4(s) - \omega_b^2 X_5(s) = 1/m\ F(s) \qquad (E.11)$$

$$-2\omega_b^2 X_4(s) + (s^2 + 2\omega_b^2) X_5(s) = 1/m\ F(s) \qquad (E.12)$$

solve equation E.12 for $X_5(s)$

$$X_5(s) = \frac{2\omega_b^2}{s^2+2\omega_b^2} X_4(s) + \frac{1}{s^2+2\omega_b^2} F(s)/m$$

substitute into equation E.11

$$-\omega_b^2 X_3(s) + \left(s^2 + 2\omega_b^2 - \frac{2\omega_b^4}{s^2+2\omega_b^2}\right) X_4(s) = \left(1 + \frac{\omega_b^2}{s^2+2\omega_b^2}\right) F(s)/m$$

$$-\omega_b^2 X_3(s) + \left(\frac{s^4+4s^2\omega_b^2+2\omega_b^4}{s^2+2\omega_b^2}\right) X_4(s) = \frac{s^2+3\omega_b^2}{s^2+2\omega_b^2} F(s)/m$$

solve for $X_4(s)$:

$$X_4(s) = \frac{(s^2+2\omega_b^2)\omega_b^2}{s^4+4s^2\omega_b^2+2\omega_b^4} X_3(s) + \frac{s^2+3\omega_b^2}{s^4+4s^2\omega_b^2+2\omega_b^4} F(s)/m$$

substitute into equation E.10.

$$-\omega_b^2 X_2(s) + \left[s^2 + 2\omega_b^2 + \frac{\omega_b^4(s^2+2\omega_b^2)}{s^4+4s^2\omega_b^2+2\omega_b^4}\right] X_3(s) = \left[1 + \frac{\omega_b^2(s^2+3\omega_b^2)}{s^4+4s^2\omega_b^2+2\omega_b^4}\right] F(s)/m$$

$$-\omega_b^2 X_2(s) + \frac{s^4+6s^2\omega_b^2+9\omega_b^4+2\omega_b^4}{s^4+4s^2\omega_b^2+2\omega_b^4} X_3(s) = \frac{s^4+3s^2\omega_b^2+s\omega_b^4}{s^4+4s^2\omega_b^2+2\omega_b^4} F(s)/m$$

solve for $X_3(s)$

$$X_3(s) = \frac{\omega_b^2(s^2+4s^2\omega_b^2+2\omega_b^4)}{s^4+6s^2\omega_b^2+9\omega_b^4+2\omega_b^4} X_2(s) + \frac{s^4+3s^2\omega_b^2+s\omega_b^4}{s^4+6s^2\omega_b^2+9\omega_b^4+2\omega_b^4} \frac{F(s)}{m}$$

substitute into equation E.9

$$-\omega_b^2 X_1(s) + \left[s^2 + 2\omega_b^2 - \frac{\omega_b^4(s^2+4s^2\omega_b^2+2\omega_b^4)}{s^4+6s^2\omega_b^2+9\omega_b^4+2\omega_b^4}\right] X_2(s) = \left[1 + \frac{\omega_b^2(s^2+5s^2\omega_b^2+5\omega_b^4)}{s^4+6s^2\omega_b^2+9\omega_b^4+2\omega_b^4}\right] \frac{F(s)}{m}$$

$$-\omega_0^2 X_1(s) + \frac{s^6+85\omega_0^2 s^4+205\omega_0^4 s^2+165\omega_0^6 s+2\omega_0^8}{s^5+63\omega_0^2 s^3+95\omega_0^4 s+2\omega_0^6} X_2(s) = \frac{s^6+75\omega_0^2 s^4+145\omega_0^4 s^2+70\omega_0^6}{s^5+63\omega_0^2 s^3+95\omega_0^4 s+2\omega_0^6} F(s)/m$$

solve for $X_2(s)$

$$X_2(s) = \frac{\omega_0^4(s^6+65\omega_0^2 s^4+95\omega_0^4 s^2+2\omega_0^6)}{s^8+85\omega_0^2 s^6+205\omega_0^4 s^4+165\omega_0^6 s^2+2\omega_0^8} X_1(s) + \frac{s^6+75\omega_0^2 s^4+145\omega_0^4 s^2+70\omega_0^6}{s^8+85\omega_0^2 s^6+205\omega_0^4 s^4+165\omega_0^6 s^2+2\omega_0^8} F(s)/m$$

substitute in equation E.8

$$-\omega_0^2 X_1(s) + \left[s^2+2\omega_0^2 - \frac{\omega_0^4(s^6+65\omega_0^2 s^4+95\omega_0^4 s^2+2\omega_0^6}{s^8+85\omega_0^2 s^6+205\omega_0^4 s^4+165\omega_0^6 s^2+2\omega_0^8}\right] X_1(s) = \left[1+\frac{\omega_0^2(s^6+75\omega_0^2 s^4+145\omega_0^4 s^2+2\omega_0^6}{s^8+85\omega_0^2 s^6+205\omega_0^4 s^4+165\omega_0^6 s^2+2\omega_0^8}\right] F(s)/m$$

$$-\omega_0^2 X_2(s) + \frac{s^{10}+105\omega_0^2 s^8+355\omega_0^4 s^6+505\omega_0^6 s^4+255\omega_0^8 s^2+2\omega_0^{10}}{s^8+85\omega_0^2 s^6+205\omega_0^4 s^4+165\omega_0^6 s^2+2\omega_0^8} X_1(s) = \frac{s^8+95\omega_0^2 s^6+275\omega_0^4 s^4+205\omega_0^6 s^2+9\omega_0^8}{s^8+85\omega_0^2 s^6+205\omega_0^4 s^4+165\omega_0^6 s^2+2\omega_0^8} F(s)/m$$

solve for $X_1(s)$

$$X_1(s) = \frac{\omega_0^2(s^8+85\omega_0^2 s^6+205\omega_0^4 s^4+165\omega_0^6 s^2+2\omega_0^8)}{s^{10}+105\omega_0^2 s^8+355\omega_0^4 s^6+505\omega_0^6 s^4+255\omega_0^8 s^2+2\omega_0^{10}} X_2(s) + \frac{s^8+95\omega_0^2 s^6+275\omega_0^4 s^4+205\omega_0^6 s^2+9\omega_0^8}{s^{10}+105\omega_0^2 s^8+355\omega_0^4 s^6+505\omega_0^6 s^4+255\omega_0^8 s^2+2\omega_0^{10}} F(s)/m$$

substitute in equation E.7:

$$\left[s^2+2\omega_0^2 - \frac{2\omega_0^4(s^8+85\omega_0^2 s^6+205\omega_0^4 s^4+165\omega_0^6 s^2+2\omega_0^8)}{s^{10}+105\omega_0^2 s^8+355\omega_0^4 s^6+505\omega_0^6 s^4+255\omega_0^8 s^2+2\omega_0^{10}}\right] X_2(s) = \left[-9+\frac{2\omega_0^2(s^8+95\omega_0^2 s^6+275\omega_0^4 s^4+205\omega_0^6 s^2+9\omega_0^8}{s^{10}+105\omega_0^2 s^8+355\omega_0^4 s^6+505\omega_0^6 s^4+255\omega_0^8 s^2+2\omega_0^{10}}\right] \frac{F(s)}{m}$$

solve for $X_0(s)$

$$X_2(s) = -\frac{s^8+88\omega_0^2 s^6+297\omega_0^4 s^4+376\omega_0^6 s^2+165\omega_0^8}{s^{10}+125\omega_0^2 s^8+535\omega_0^4 s^6+1045\omega_0^6 s^4+855\omega_0^8 s^2+20\omega_0^{10}} \frac{F(s)}{m} \quad (E8)$$

and so, the characteristic equation for the response is:

$$s^{10}+125\omega_0^2 s^8+535\omega_0^4 s^6+1045\omega_0^6 s^4+855\omega_0^8 s^2+20\omega_0^{10}=0$$

This is, in effect, a quintic equation, since it may be rewritten in the form,

$$r^5+125r^4+531r^3+1045r^2+855r+20=0$$

where $r=\left(\frac{s}{\omega_0}\right)^2$

By inspection, we see that this may be factored as follows:

$$r^5+4r^4+6r^3+2r^2+2r+5) = 0$$

and a quartic remains to be solved. This may be accomplished by plotting the value of the quartic as a function of r and choosing the roots as the values of r for which the function equals zero. This process yields the following roots:

$$r_1 = -.382$$
$$r_2 = -1.382$$
$$r_3 = -2.618$$
$$r_4 = -3.618$$

and the roots of the characteristic equation are:

$$S_1^2 = -0.382\,\omega_0^2 \qquad S_1 = \pm j0.618\,\omega_0$$
$$S_2^2 = -1.382\,\omega_0^2 \qquad S_2 = \pm j1.18\,\omega_0$$
$$S_3^2 = -2.618\,\omega_0^2 \qquad S_3 = \pm j1.62\,\omega_0$$
$$S_4^2 = -3.618\,\omega_0^2 \qquad S_4 = \pm j1.90\,\omega_0$$
$$S_5^2 = -4.000\,\omega_0^2 \qquad S_5 = \pm j2.00\,\omega_0$$

If the applied force, F, is a step function, being zero for $t < 0$ and F thereafter,

$$F(S) = \frac{F}{S}$$

and equation E.13 may be written as

$$X_1(S) = \frac{9S^8+88\omega_0^2S^6+297\omega_0^4S^4+396\omega_0^6S^2+165\omega_0^8}{S(S^2+0.382\omega_0^2)(S^2+1.382\omega_0^2)(S^2+2.618\omega_0^2)(S^2+3.618\omega_0^2)(S^2+4.00\omega_0^2)m}\,F$$

The quantity on the right-hand side of the equation may be expanded in terms of its partial fractions.

$$X_1(S) = \frac{A}{S} + \frac{BS}{S^2+.382\omega_0^2} + \frac{CS}{S^2+1.382\omega_0^2} + \frac{DS}{S^2+2.618\omega_0^2} + \frac{ES}{S^2+3.618\omega_0^2} + \frac{GS}{S^2+4.0\omega_0^2}$$

The constants are evaluated as follows:

$$A = -\frac{165\omega_0^8}{20\omega_0^{10}m}F = -8.25\frac{F}{\omega_0^2 m}$$

$$B = \frac{[9(0.382)^4-88(0.382)^3+297(0.382)^2-396(0.382)+165]\omega_0^8\,F}{(1-0.382)(-0.382+1.382)(-0.382+2.618)(-0.382+3.618)(-0.382+4.00)m}$$

$$= \frac{52.4}{10.0}\frac{F}{\omega_0^2 m} = 5.24\frac{F}{\omega_0^2 m}$$

$$C = \frac{[9(1.382)^4 - 88(1.382)^3 + 297(1.382)^2 - 396(1.382) + 165]\omega_0^8}{(1.382)(1.382+0.382)(1.382+2.618)[-1.382+3.618][-1.382+4.0]\omega_0^{10}m}\frac{F}{}$$

$$= \frac{19.5}{100}\frac{F}{\omega_0^2 m} = 1.45\frac{F}{\omega_0^2 m}$$

$$D = \frac{[9(2.618)^4 - 88(2.618)^3 + 297(2.618)^2 - 396(2.618) + 165]\omega_0^8}{(-2.618)(-2.618+.382)[-2.618+1.382][-2.618+3.618][-2.618+4.0]\omega_0^{10}m}\frac{F}{}$$

$$= \frac{76}{100}\frac{F}{\omega_0^2 m} = 0.76\frac{F}{\omega_0^2 m}$$

$$E = -\frac{[9(3.618)^4 - 88(3.618)^3 + 297(3.618)^2 - 396(3.618) + 165]\omega_0^8 F}{(-3.618)(-3.618+.382)[-3.618+1.382][-3.618+2.618][-3.618+4.0]\omega_0^{10}m}$$

$$= \frac{55}{100}\frac{F}{\omega_0^2 m} = 0.55\frac{F}{\omega_0^2 m}$$

$$G = -\frac{[9(4.0)^4 - 88(4.0)^3 + 297(4.0)^2 - 396(4.0) + 165]\omega_0^8}{(-4.0)(-4.0+.382)[-4.0+1.382][-4.0+2.618][-4.0+3.618]\omega_0^{10}m}\frac{F}{}$$

$$= \frac{2.5}{10}\frac{F}{\omega_0^2 m} = 0.25\frac{F}{\omega_0^2 m}$$

Thus, the inverse transform is:

$$x_2(t) = [5.24\cos 0.618\omega_0 t + 1.45\cos 1.18\omega_0 t + 0.76\cos 1.62\omega_0 t + 0.55\cos 1.90\omega_0 t + 0.25\cos 2.0\omega_0 t - 8.25]\frac{F}{\omega_0^2 m}$$

$$x_2(t) = (2\cos 0.618\omega_0 t + 2\cos 1.18\omega_0 t + 2\cos 1.62\omega_0 t + 2\cos 1.90\omega_0 t + 1\cos 2.0\omega_0 t)\frac{F}{m}$$

From equation E.1:

$$x_1(t) = \left[4.50\frac{F}{\omega_0^2 m} + x_0 + \ddot{x}_0\frac{1}{2\omega_0^2}\right]$$

$$x_1(t) = [4.24\cos 0.618\omega_0 t - 0.24\cos 1.62\omega_0 t + 0.45\cos 1.18\omega_0 t - 0.45\cos 1.90\omega_0 t - 0.25\cos 2\omega_0 t - 3.75]\frac{F}{\omega_0^2 m}$$

$$\ddot{x}_1 = [-1.62\cos 0.618\omega_0 t + 0.62\cos 1.18\omega_0 t - 0.62\cos 1.62\omega_0 t - 1.62\cos 1.90\omega_0 t - \cos 2\omega_0 t]\frac{F}{m}$$

From equation E.2:

$$x_2(t) = -x_0 + \frac{1}{\omega_0^2}\ddot{x}_1 + 2x_1 - \frac{F}{\omega_0^2 m}$$

$$= [-.25 + 1.62\cos 0.618\omega_0 t - 1.17\cos 1.18\omega_0 t - 0.62\cos 1.62\omega_0 t + 0.17\cos 1.90\omega_0 t - 0.25\cos 2.0\omega_0 t]\frac{F}{\omega_0^2 m}$$

$$\ddot{x}_2 = [-0.62\cos 0.618\omega_0 t + 1.62\cos 1.18\omega_0 t + 1.62\cos 1.62\omega_0 t - 0.62\cos 1.90\omega_0 t - 1.00\cos 2.0\omega_0 t]\frac{F}{m}$$

From Equation E.3:

$$x_3(t) = -x_1 + \frac{1}{\omega_0^2}\ddot{x}_2 + 2x_2 - F/m$$

$$\ddot{x}_3(t) = [-1.62\cos 0.618\omega_0 t - 1.17\cos 1.18\omega_0 t + 0.62\cos 1.62\omega_0 t + 0.17\cos 1.90\omega_0 t - 0.25\cos 2.0\omega_0 t + 2.25]\frac{F}{\omega_0^2 m}$$

$$\ddot{x}_3 = [0.62\cos 0.618\omega_0 t + 1.62\cos 1.18\omega_0 t - 1.62\cos 1.62\omega_0 t - 0.62\cos 1.90\omega_0 t + 1.00\cos 2\omega_0 t]\frac{F}{m}$$

From equation E.4:

$$x_4(t) = -x_3 + \frac{1}{\omega_0^2}\ddot{x}_3 + 2x_3 - F/m$$

$$= [-4.24\cos 0.618\omega_0 t + 0.45\cos 1.18\omega_0 t + 0.24\cos 1.62\omega_0 t - 0.45\cos 1.90\omega_0 t + 0.25\cos 2.0\omega_0 t + 3.75]\frac{F}{\omega_0^2 m}$$

$$\ddot{x}_4 = [1.62\cos 0.618\omega_0 t - 0.62\cos 1.18\omega_0 t - 0.62\cos 1.62\omega_0 t + 1.62\cos 1.90\omega_0 t - 1.00\cos 2.0\omega_0 t]\frac{F}{m}$$

From equation E.5:

$$x_5(t) = -x_3 - \frac{1}{\omega_0^2}\ddot{x}_4 + 2x_4 - F/m$$

$$= [-5.24\cos 0.618\omega_0 t + 1.45\cos 1.18\omega_0 t - 0.76\cos 1.62\omega_0 t + 0.55\cos 1.90\omega_0 t - 0.25\cos 2.0\omega_0 t + 4.25]\frac{F}{\omega_0^2 m}$$

$$\Delta x_1 = \dot{x}_1 - x_0$$

$$= [-1.00\cos 0.618\omega_0 t - 1.00\cos 1.18\omega_0 t - 1.00\cos 1.62\omega_0 t - 1.00\cos 1.90\omega_0 t - 0.50\cos 2.0\omega_0 t + 4.50]\frac{F}{\omega_0^2 m} \quad (E.14)$$

$$\Delta x_2 = x_2 - x_1$$

$$= [-2.62\cos 0.618\omega_0 t - 1.62\cos 1.18\omega_0 t - 0.38\cos 1.62\omega_0 t + 0.62\cos 1.90\omega_0 t + 0.50\cos 2.0\omega_0 t + 3.50]\frac{F}{\omega_0^2 m} \quad (E.15)$$

$$\Delta x_3 = x_3 - x_2$$

$$= [-3.24\cos 0.618\omega_0 t + 1.24\cos 1.62\omega_0 t - 0.50\cos 2.0\omega_0 t + 2.50]\frac{F}{\omega_0^2 m} \quad (E.16)$$

$$\Delta x_4 = x_4 - x_3$$

$$= [-2.62\cos 0.618\omega_0 t + 1.62\cos 1.18\omega_0 t - 0.38\cos 1.62\omega_0 t - 0.62\cos 1.90\omega_0 t + 0.50\cos 2.0\omega_0 t + 1.50]\frac{F}{\omega_0^2 m} \quad (E.17)$$

$$\Delta x_5 = x_5 - x_4$$

$$= [-1.00\cos 0.618\omega_0 t + 1.00\cos 1.18\omega_0 t - 1.00\cos 1.62\omega_0 t + 1.00\cos 1.90\omega_0 t - 0.50\cos 2.0\omega_0 t + 0.50]\frac{F}{\omega_0^2 m} \quad (E.18)$$

E.2 EIGHT-BAY (80') BRIDGE

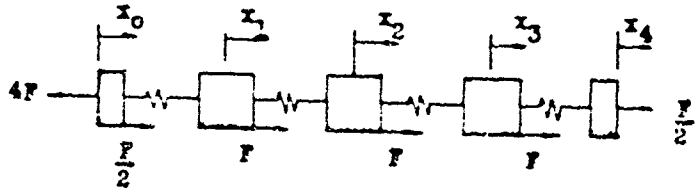

equations of motion:

$$\ddot{x}_0 + 2\omega_0^2 x_0 - 2\omega_0^2 x_1 = -F/m \quad (E.19)$$

$$-\omega_0^2 x_0 + \ddot{x}_1 + 2\omega_0^2 x_1 - \omega_0^2 x_2 = F/m \quad (E.20)$$

$$-\omega_0^2 x_1 + \ddot{x}_2 + 2\omega_0^2 x_2 - \omega_0^2 x_3 = F/m \quad (E.21)$$

$$-\omega_0^2 x_2 + \ddot{x}_3 + 2\omega_0^2 x_3 - \omega_0^2 x_4 = F/m \quad (E.22)$$

$$-2\omega_0^2 x_3 + \ddot{x}_4 + 2\omega_0^2 x_4 = F/m \quad (E.23)$$

equivalent Laplace equations:

$$(s^2 + 2\omega_0^2) X_0(s) - 2\omega_0^2 X_1(s) = -F/m\, F(s) \quad (E.24)$$

$$-\omega_0^2 X_0(s) + (s^2 + 2\omega_0^2) X_1(s) - \omega_0^2 X_2(s) = F(s)/m \quad (E.25)$$

$$-\omega_0^2 X_1(s) + (s^2 + 2\omega_0^2) X_2(s) - \omega_0^2 X_3(s) = F(s)/m \quad (E.26)$$

$$-\omega_0^2 X_2(s) + (s^2 + 2\omega_0^2) X_3(s) - \omega_0^2 X_4(s) = F(s)/m \quad (E.27)$$

$$-2\omega_0^2 X_3(s) + (s^2 + 2\omega_0^2) X_4(s) = F(s)/m \quad (E.28)$$

solve equation E.28 for $X_4(s)$

$$X_4(s) = \frac{2\omega_0^2}{s^2 + 2\omega_0^2} X_3(s) + \frac{1}{s^2 + 2\omega_0^2} F(s)/m$$

substitute into equation E.27

$$-\omega_0^2 X_2(s) + \left[s^2 + 2\omega_0^2 - \frac{\omega_0^2 (2\omega_0^2)}{s^2 + 2\omega_0^2} \right] X_3(s) = \left[1 + \frac{\omega_0^2}{s^2 + 2\omega_0^2} \right] F(s)/m$$

$$-\omega_0^2 X_2(s) + \frac{s^4 + 4s^2\omega_0^2 + 2\omega_0^4}{s^2 + 2\omega_0^2} X_3(s) = \frac{s^2 + 3\omega_0^2}{s^2 + 2\omega_0^2} F(s)/m$$

solve for $X_3(s)$

$$X_3(s) = \frac{\omega_o^2(s^4+2\omega_o^2)}{s^6+4s^4\omega_o^2+2\omega_o^4} X_2(s) + \frac{s^4+3\omega_o^2}{s^4+4s^2\omega_o^2+2\omega_o^4} \text{ Ft}/\text{in}$$

substitute into equation E.26:

$$-\omega_o^2 X_1(s) + \left[s^2+2\omega_o^2 - \frac{\omega_o^4(s^4+2\omega_o^2)}{s^6+4s^4\omega_o^2+2\omega_o^4}\right] X_2(s) = \left[1 + \frac{\omega_o^2(s^4+3\omega_o^2)}{s^6+4s^4\omega_o^2+2\omega_o^4}\right] \text{Ft}/\text{in}$$

$$-\omega_o^2 X_1(s) + \frac{s^6+6s^4\omega_o^2+9s^2\omega_o^4+2\omega_o^6}{s^6+4s^4\omega_o^2+2\omega_o^4} X_2(s) = \frac{s^4+5s^2\omega_o^2+5\omega_o^4}{s^4+4s^2\omega_o^2+2\omega_o^4} \text{ Ft}/\text{in}$$

solve for $X_2(s)$

$$X_2(s) = \frac{\omega_o^2(s^4+4s^2\omega_o^2+7\omega_o^4)}{s^6+6s^4\omega_o^2+9s^2\omega_o^4+2\omega_o^6} X_1(s) + \frac{s^4+5s^2\omega_o^2+5\omega_o^4}{s^6+6s^4\omega_o^2+9s^2\omega_o^4+2\omega_o^6} \text{ Ft}/\text{in}$$

substitute into equation E.25

$$-\omega_o^2 X_0(s) + \left[s^2+2\omega_o^2 - \frac{\omega_o^4(s^4+4s^2\omega_o^2+7\omega_o^4)}{s^6+6s^4\omega_o^2+9s^2\omega_o^4+2\omega_o^6}\right] X_1(s) = \left[1 + \frac{\omega_o^2(s^4+5s^2\omega_o^2+5\omega_o^4)}{s^6+6s^4\omega_o^2+9s^2\omega_o^4+2\omega_o^6}\right] \text{Ft}/\text{in}$$

$$-\omega_o^2 X_0(s) + \frac{s^8+8s^6\omega_o^2+20s^4\omega_o^4+16s^2\omega_o^6+2\omega_o^8}{s^6+6s^4\omega_o^2+9s^2\omega_o^4+2\omega_o^6} X_1(s) = \frac{s^6+7s^4\omega_o^2+14s^2\omega_o^4+7\omega_o^6}{s^6+6s^4\omega_o^2+9s^2\omega_o^4+2\omega_o^6} \text{ Ft}/\text{in}$$

solve for $X_1(s)$

$$X_1(s) = \frac{\omega_o^2(s^6+6s^4\omega_o^2+9s^2\omega_o^4+2\omega_o^6)}{s^8+8s^6\omega_o^2+20s^4\omega_o^4+16s^2\omega_o^6+2\omega_o^8} X_0(s) + \frac{s^6+7s^4\omega_o^2+14s^2\omega_o^4+7\omega_o^6}{s^8+8s^6\omega_o^2+20s^4\omega_o^4+16s^2\omega_o^6+2\omega_o^8} \text{ Ft}/\text{in}$$

substitute into equation E.24

$$\left[s^2+2\omega_o^2 - \frac{2\omega_o^4(s^6+6s^4\omega_o^2+9s^2\omega_o^4+2\omega_o^6)}{s^8+8s^6\omega_o^2+20s^4\omega_o^4+16s^2\omega_o^6+2\omega_o^8}\right] X_0(s) = \left[-7 + \frac{2\omega_o^2(s^6+7s^4\omega_o^2+14s^2\omega_o^4+7\omega_o^6)}{s^8+8s^6\omega_o^2+20s^4\omega_o^4+16s^2\omega_o^6+2\omega_o^8}\right] \text{Ft}/\text{in}$$

$$\frac{s^{10}+10s^8\omega_o^2+34s^6\omega_o^4+44s^4\omega_o^6+16s^2\omega_o^8}{s^8+8s^6\omega_o^2+20s^4\omega_o^4+16s^2\omega_o^6+2\omega_o^8} X_0(s) = -\frac{7s^8+54s^6\omega_o^2+126s^4\omega_o^4+84s^2\omega_o^6}{s^8+8s^6\omega_o^2+20s^4\omega_o^4+16s^2\omega_o^6+2\omega_o^8} \text{ Ft}/\text{in}$$

$$X_0(s) = -\frac{7s^8+54s^6\omega_o^2+126s^4\omega_o^4+84s^2\omega_o^6}{s^{10}+10s^8\omega_o^2+34s^6\omega_o^4+44s^4\omega_o^6+16s^2\omega_o^8} \text{ Ft}/\text{in}$$

and the characteristic equation is:

$$s^8 + 10\omega_0^2 s^6 + 34\omega_0^4 s^4 + 44\omega_0^6 s^2 + 16\omega_0^8 = 0$$

by inspection, the equation may be factored as follows:

$$(s^2 + 2\omega_0^2)(s^2 + 4\omega_0^2)(s^4 + 4\omega_0^2 s^2 + 2\omega_0^4) = 0$$

solution of the remaining quadratic yields the following roots:

$s_1^2 = -(\sqrt{2}-2)\omega_0^2 = -0.586\omega_0^2$ $\quad s_1 = \pm j\,0.765\omega_0$

$s_2^2 = -2.0\omega_0^2$ $\quad s_2 = \pm j\,1.414\omega_0$

$s_3^2 = -(\sqrt{2}+2)\omega_0^2 = -3.414\omega_0^2$ $\quad s_3 = \pm j\,1.85\omega_0$

$s_4^2 = -4.0\omega_0^2$ $\quad s_4 = \pm j\,2.0\omega_0$

$$F(s) = \frac{F}{s}$$

and equation E.29 can be written as follows:

$$X_6(s) = \frac{A}{s} + \frac{Bs}{s^2+0.586\omega_0^2} + \frac{Cs}{s^2+2.0\omega_0^2} + \frac{Ds}{s^2+3.414\omega_0^2} + \frac{Es}{s^2+4.0\omega_0^2}$$

$$A = -\frac{84\omega_0^6}{16\omega_0^8}\frac{F}{m} = -5.25\frac{F}{\omega_0^2 m}$$

$$B = \frac{-7(0.586)^3 + 54(0.586)^2 - 126(0.586) + 84}{8}\frac{F}{\omega_0^2 m}$$

$$= 3.41\frac{F}{\omega_0^2 m}$$

$$C = \frac{-7(2.0)^3 + 54(2.0)^2 - 126(2.0) + 84}{-8}\frac{F}{\omega_0^2 m}$$

$$= 1.0\frac{F}{\omega_0^2 m}$$

$$D = \frac{-7(3.414)^3 + 54(3.414)^2 - 126(3.414) + 84}{-8}\frac{F}{\omega_0^2 m}$$

$$= 0.59\frac{F}{\omega_0^2 m}$$

$$E = -\frac{-7(4.0)^3 + 54(4.0)^2 - 126(4.0) + 84}{(-8)(2)}\frac{F}{\omega_0^2 m}$$

$$= 0.25\frac{F}{\omega_0^2 m}$$

Taking the inverse transform

$$x_6(t) = [3.41\cos 0.765\omega_0 t + 1.0\cos 1.41\omega_0 t + 0.59\cos 1.85\omega_0 t + 0.25\cos 2.0\omega_0 t - 5.25]\,F/\omega_0^2 m$$

$$\ddot{x}_6 = -[2.0\cos 0.765\omega_0 t + 2.0\cos 1.41\omega_0 t + 2.0\cos 1.85\omega_0 t + 1.0\cos 2.0\omega_0 t]\frac{F}{m}$$

from equation E.19:

$$x_1(t) = \frac{1}{2\omega_0^2}\ddot{x}_6 + x_6 + 7/2\omega_0^2 m\,F$$

$$x_1(t) = [2.41\cos 0.765\omega_0 t - 0.41\cos 1.85\omega_0 t - 0.25\cos 2.0\omega_0 t - 1.75]\frac{F}{\omega_0^2 m}$$

$$\ddot{x}_1 = [-1.41\cos 0.765\omega_0 t + 1.41\cos 1.85\omega_0 t + 1.0\cos 2.0\omega_0 t]\frac{F}{m}$$

from equation E.20:

$$x_2(t) = -x_0 + \frac{1}{\omega_0^2}\ddot{x}_1 + 2x_1 - F/m$$

$$= [-1.0\cos 1.41\omega_0 t + 0.25\cos 2.0\omega_0 t + 0.75]\frac{F}{\omega_0^2 m}$$

$$\ddot{x}_2 = [2.0\cos 1.41\omega_0 t - 1.0\cos 2.0\omega_0 t]F/m$$

from equation E.21:

$$x_3(t) = -x_1 + \frac{1}{\omega_0^2}\ddot{x}_2 + 2x_2 - F/m$$

$$= [-2.41\cos 0.765\omega_0 t + 0.41\cos 1.85\omega_0 t - 0.25\cos 2.0\omega_0 t + 2.25]\frac{F}{\omega_0^2 m}$$

$$\ddot{x}_3 = [1.41\cos 0.765\omega_0 t - 1.41\cos 1.85\omega_0 t + 1.0\cos 2.0\omega_0 t]\frac{F}{m}$$

from equation E.22:

$$x_4(t) = -x_2 + \frac{1}{\omega_0^2}\ddot{x}_3 + 2x_3 - F/m$$

$$= [-3.41\cos 0.765\omega_0 t + 1.0\cos 1.41\omega_0 t - 0.59\cos 1.85\omega_0 t + 0.25\cos 2.0\omega_0 t + 2.75]\frac{F}{\omega_0^2 m}$$

$$\Delta x_1 = x_1 - x_0$$

$$= [-1.00\cos 0.765\omega_0 t - 1.0\cos 1.41\omega_0 t - 1.0\cos 1.85\omega_0 t - 0.50\cos 2\omega_0 t + 3.50]\frac{F}{\omega_0^2 m} \qquad (E.30)$$

$$\Delta x_2 = x_2 - x_1$$

$$= [-2.41\cos 0.765\omega_0 t - 1.0\cos 1.41\omega_0 t + 0.41\cos 1.85\omega_0 t + 0.50\cos 2.0\omega_0 t + 2.50]\frac{F}{\omega_0^2 m} \qquad (E.31)$$

$$\Delta x_3 = x_3 - x_2$$

$$= [-2.41\cos 0.765\omega_0 t + 1.0\cos 1.41\omega_0 t + 0.41\cos 1.85\omega_0 t - 0.50\cos 2.0\omega_0 t + 1.50]\frac{F}{\omega_0^2 m} \qquad (E.32)$$

$$\Delta x_4 = x_4 - x_3$$

$$= [-1.0\cos 0.765\omega_0 t + 1.0\cos 1.41\omega_0 t - 1.0\cos 1.85\omega_0 t + 0.5\cos 2.0\omega_0 t + 0.5]\frac{F}{\omega_0^2 m} \qquad (E.33)$$

E.3 SIX-BAY (60') BRIDGE

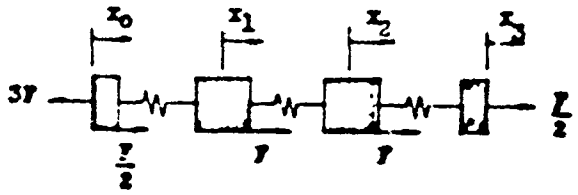

equations of motion:

$$\ddot{x}_0 + 2\omega_0^2 x_0 - 2\omega_0^2 x_1 = -\frac{5}{m} F \qquad (E.34)$$

$$-\omega_0^2 x_0 + \ddot{x}_1 + 2\omega_0^2 x_1 - \omega_0^2 x_2 = F/m \qquad (E.35)$$

$$-\omega_0^2 x_1 + \ddot{x}_2 + 2\omega_0^2 x_2 - \omega_0^2 x_3 = F/m \qquad (E.36)$$

$$-2\omega_0^2 x_2 + \ddot{x}_3 + 2\omega_0^2 x_3 = F/m \qquad (E.37)$$

equivalent Laplace equations:

$$(s^2 + 2.0\omega_0^2) X_0(s) - 2\omega_0^2 X_1(s) = -5\, F(s)/m \qquad (E.38)$$

$$-\omega_0^2 X_0(s) + (s^2 + 2\omega_0^2) X_1(s) - \omega_0^2 X_2(s) = F(s)/m \qquad (E.39)$$

$$-\omega_0^2 X_1(s) + (s^2 + 2\omega_0^2) X_2(s) - \omega_0^2 X_3(s) = F(s)/m \qquad (E.40)$$

$$-2\omega_0^2 X_2(s) + (s^2 + 2\omega_0^2) X_3(s) = F(s)/m \qquad (E.41)$$

solve equation E.41 for $X_3(s)$:

$$X_3(s) = \frac{2\omega_0^2}{s^2 + 2\omega_0^2} X_2(s) + \frac{1}{s^2 + 2\omega_0^2} F(s)/m$$

substitute into equation E.40:

$$-\omega_0^2 X_1(s) + \left[s^2 + 2\omega_0^2 - \frac{2\omega_0^4}{s^2 + 2\omega_0^2}\right] X_2(s) - \left[1 + \frac{\omega_0^2}{s^2 + 2\omega_0^2}\right] F(s)/m$$

$$-\omega_b X_1(s) + \frac{s^4+45^2\omega_b^2+24\omega_b^4}{s^4+24\omega_b^4} X(s) = \frac{s^4+7\omega_b^2}{s^4+24\omega_b^4} \frac{ft}{lb}$$

solve for $X_2(s)$

$$X_2(s) = \frac{\omega_b^2(s^4+24\omega_b^4)}{s^6+45^2\omega_b^2+24\omega_b^6} X(s) + \frac{s^4+7\omega_b^2}{s^6+45^2\omega_b^2+24\omega_b^6} \cdot F(s)/m$$

substitute into equation E.39:

$$-\omega_b^2 X_2(s) + \left[s^2+24\omega_b^2 - \frac{\omega_b^2(s^4+24\omega_b^4)}{s^6+45^2\omega_b^2+24\omega_b^6}\right] X_1(s)$$

$$= \left[1 + \frac{\omega_b^2(s^4+7\omega_b^2)}{s^6+45^2\omega_b^2+24\omega_b^6}\right] F(s)/m$$

$$-\omega_b^2 X_2(s) + \frac{s^6+65^2\omega_b^4+95^2\omega_b^6+24\omega_b^8}{s^4+45^2\omega_b^2+24\omega_b^4} X(s) = \frac{s^4+55^2\omega_b^2+5^4\omega_b^4}{s^4+45^2\omega_b^2+24\omega_b^4} \frac{ft}{lb}$$

solve for $X_1(s)$

$$X_1(s) = \frac{\omega_b^2(s^4+45^2\omega_b^2+24\omega_b^4)}{s^6+65^2\omega_b^4+95^2\omega_b^6+24\omega_b^8} X(s) + \frac{s^4+55^2\omega_b^2+5^4\omega_b^4}{s^6+65^2\omega_b^4+95^2\omega_b^6+24\omega_b^8} \frac{ft}{lb}$$

substitute into equation E.38

$$\left[s^2+24\omega_b^2 - \frac{24\omega_b^8(s^4+45^2\omega_b^2+70\omega_b^4)}{s^6+65^2\omega_b^4+95^2\omega_b^6+24\omega_b^8}\right] X(s)$$

$$= \left[-5 + \frac{24\omega_b^4(s^4+55^2\omega_b^2+5^4\omega_b^4)}{s^6+65^2\omega_b^4+95^2\omega_b^6+24\omega_b^8}\right] \frac{ft}{lb}$$

$$\frac{s^6+85^2\omega_b^4+195^2\omega_b^6+175^4\omega_b^8}{s^6+65^2\omega_b^4+95^2\omega_b^6+24\omega_b^8} X(s) = -\frac{55^4+285^2\omega_b^2+35^4\omega_b^4}{s^6+65^2\omega_b^4+95^2\omega_b^6+24\omega_b^8} \frac{ft}{lb}$$

$$X(s) = -\frac{55^4+285^2\omega_b^2+35^4\omega_b^4}{s^6+85^2\omega_b^4+195^2\omega_b^6+12\omega_b^8} F(s)/m \qquad (E42)$$

the characteristic equation is:

$$s^6+85^2\omega_b^4+195^2\omega_b^6+12\omega_b^8 = 0$$

by inspection, this may be factored to

$$(s^2+4\omega_b^2)(s^2+3\omega_b^2)(s^2+\omega_b^2) = 0$$

$s_1^2 = -\omega_b^2$ $\qquad$ $s_1 = \pm j\omega_b$

$s_2^2 = -3\omega_b^2$ $\qquad$ $s_2 = \pm j1.73\omega_b$

$s_3^2 = -4\omega_b^2$ $\qquad$ $s_3 = \pm j2.0\omega_b$

$$F(s) = \frac{F}{s}$$

equation E.42 may be written as follows:

$$X(s) = \frac{A}{s} + \frac{Bs}{s^2+\omega_b^2} + \frac{Cs}{s^2+3\omega_b^2} + \frac{Ds}{s^2+4\omega_b^2}$$

$$A = -\frac{35\omega_0^4}{12\omega_0^6}\frac{F}{m} = -\frac{35}{12}\frac{F}{\omega_0^2 m}$$

$$B = -\frac{(5-25+35)F}{-(3)(-1+3)\omega_0^2 m} = 2\frac{F}{\omega_0^2 m}$$

$$C = -\frac{(45-84+35)F}{-3(-3+1-3+1)\omega_0^2 m} = \frac{2}{3}\frac{F}{\omega_0^2 m}$$

$$D = -\frac{(80-112+35)F}{4(-1+3)(-1+1)\omega_0^2 m} = \frac{1}{4}\frac{F}{\omega_0^2 m}$$

taking the inverse transform:

$$x_0(t) = [2\cos\omega_0 t + 0.67\cos 1.73\omega_0 t + 0.25\cos 2\omega_0 t - 2.92]\frac{F}{\omega_0^2 m}$$

$$\ddot{x}_0 = -[2\cos\omega_0 t + 2\cos 1.73\omega_0 t + \cos 2\omega_0 t]\frac{F}{m}$$

from equation E.34:

$$x_1(t) = \frac{1}{2\omega_0^2}\ddot{x}_0 + x_0 + \frac{5}{2}F/m$$

$$= [\cos\omega_0 t - 0.33\cos 1.73\omega_0 t - 0.25\cos 2\omega_0 t - 0.42]\frac{F}{\omega_0^2 m}$$

$$\ddot{x}_1 = [-\cos\omega_0 t + \cos 1.73\omega_0 t + 2\cos 2\omega_0 t]\frac{F}{m}$$

from equation E.35:

$$x_2(t) = -x_0 + \frac{1}{\omega_0^2}\ddot{x}_1 + 2x_1 - F/m$$

$$x_2(t) = [-\cos\omega_0 t - 0.33\cos 1.73\omega_0 t + 0.25\cos 2\omega_0 t + 1.08]\frac{F}{\omega_0^2 m}$$

$$\ddot{x}_2 = [-\cos\omega_0 t + \cos 1.73\omega_0 t - \cos 2\omega_0 t]\frac{F}{m}$$

from equation E.36:

$$x_3(t) = -x_1 + \frac{1}{\omega_0^2}\ddot{x}_2 + 2x_2 - F/m$$

$$= [-2\cos\omega_0 t + 0.67\cos 1.73\omega_0 t - 0.25\cos 2\omega_0 t + 1.58]\frac{F}{\omega_0^2 m}$$

$$\Delta x_1 = x_1 - x_0$$

$$= [2.50 - \cos\omega_0 t - \cos 1.73\omega_0 t - 0.50\cos 2\omega_0 t]\frac{F}{\omega_0^2 m}$$

$$\Delta x_2 = x_2 - x_1$$

$$= [1.50 - 2\cos\omega_0 t + 0.50\cos 2\omega_0 t]\frac{F}{\omega_0^2 m}$$

$$\Delta x_3 = x_3 - x_2$$

$$= [0.50 - \cos\omega_0 t + \cos 1.73\omega_0 t - 0.50\cos 2\omega_0 t]\frac{F}{\omega_0^2 m}$$

E.4 FOUR-BAY (40') BRIDGE

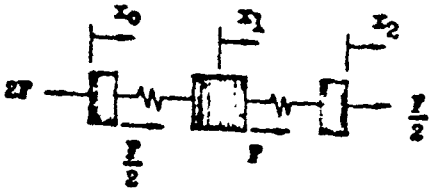

equations of motion:

$$\ddot{x}_0 + 2\omega_b^2 x_0 - 2\omega_b^2 x_1 = -3F/m \qquad (E.43)$$

$$-\omega_b^2 x_0 + \ddot{x}_1 + 2\omega_b^2 x_1 - \omega_b^2 x_2 = F/m \qquad (E.44)$$

$$-2\omega_b^2 x_1 + \ddot{x}_2 + 2\omega_b^2 x_2 = F/m \qquad (E.45)$$

equivalent Laplace equations:

$$(s^2 + 2\omega_b^2) X_0(s) - 2\omega_b^2 X_1(s) = -3F(s)/m \qquad (E.46)$$

$$-\omega_b^2 X_0(s) + (s^2 + 2\omega_b^2) X_1(s) - \omega_b^2 X_2(s) = F(s)/m \qquad (E.47)$$

$$-2\omega_b^2 X_1(s) + (s^2 + 2\omega_b^2) X_2(s) = F(s)/m \qquad (E.48)$$

solve equation E.48 for $X_2(s)$

$$X_2(s) = \frac{2\omega_b^2}{s^2 + 2\omega_b^2} X_1(s) + \frac{1}{s^2 + 2\omega_b^2} F(s)/m$$

substitute into equation E.47

$$-\omega_b^2 X_0(s) + \left[s^2 + 2\omega_b^2 - \frac{2\omega_b^4}{s^2 + 2\omega_b^2} \right] X_1(s) = \left[1 + \frac{\omega_b^2}{s^2 + 2\omega_b^2} \right] F(s)/m$$

$$-\omega_b^2 X_0(s) + \frac{s^4 + 4s^2\omega_b^2 + 2\omega_b^4}{s^2 + 2\omega_b^2} X_1(s) = \frac{s^2 + 3\omega_b^2}{s^2 + 2\omega_b^2} F(s)/m$$

solve for $X_1(s)$

$$X_1(s) = \frac{\omega_0^4(s^2+2\omega_0^2)}{s^4+4.5\omega_0^2s^2+2\omega_0^4} X_0(s) + \frac{s^2+3\omega_0^2}{s^4+4.5\omega_0^2s^2+2\omega_0^4} F(s)/m$$

substitute into equation E.46

$$\left[s^2+2\omega_0^2 - \frac{2\omega_0^4(s^2+2\omega_0^2)}{s^4+4.5\omega_0^2s^2+2\omega_0^4}\right] X_0(s)$$
$$= \left[-3 + \frac{2\omega_0^2(s^2+3\omega_0^2)}{s^4+4.5\omega_0^2s^2+2\omega_0^4}\right] F(s)/m$$

$$\frac{s^4+6.5\omega_0^2s^2+8\omega_0^4}{s^4+4.5\omega_0^2s^2+2\omega_0^4} X_0(s) = -\frac{3s^4+13.5\omega_0^2s^2}{s^4+4.5\omega_0^2s^2+2\omega_0^4} F(s)/m$$

$$X_0(s) = -\frac{3s^2+10.5\omega_0^2}{s^4+6.5\omega_0^2s^2+8\omega_0^4} F(s)/m \qquad (E.49)$$

and the characteristic equation is

$$s^4+6.5\omega_0^2s^2+8\omega_0^4 = 0$$

by inspection, this may be factored

$$(s^2+2\omega_0^2)(s^2+4\omega_0^2) = 0$$

$$s_1^2 = -2\omega_0^2 \qquad s_1 = \pm j\,1.41\omega_0$$
$$s_2^2 = -4\omega_0^2 \qquad s_2 = \pm j\,2.0\omega_0$$

$$F(s) = \frac{F}{s}$$

equation E.49 may be rewritten:

$$X_0(s) = \frac{A}{s} + \frac{Bs}{s^2+2\omega_0^2} + \frac{Cs}{s^2+4\omega_0^2}$$

$$A = -\frac{10}{8}\frac{F}{\omega_0^2 m} = -1.25\frac{F}{\omega_0^2 m}$$

$$B = -\frac{(-6+10)}{-2(-2+4)}\frac{F}{\omega_0^2 m} = \frac{F}{\omega_0^2 m}$$

$$C = \frac{(-12+10)}{-4(-4+2)}\frac{F}{\omega_0^2 m} = 0.25\frac{F}{\omega_0^2 m}$$

taking the inverse transform

$$x_0(t) = \left[\cos 1.41\omega_0 t + 0.25\cos 2\omega_0 t - 1.25\right]\frac{F}{\omega_0^2 m}$$

$$\ddot{x}_0 = -\left[2\cos 1.41\omega_0 t + \cos 2\omega_0 t\right]\frac{F}{m}$$

From equation E.43:

$$x_1(t) = \frac{1}{2\omega_0^2}\ddot{x}_0 + x_0 + \frac{3}{2}F/\omega_0^2 m$$

$$= [-0.25\cos 2\omega_0 t + 0.25]F/\omega_0^2 m$$

$$\ddot{x}_1 = (\cos 2\omega_0 t)F/m$$

From equation E.44

$$x_2(t) = -x_0 + \frac{1}{\omega_0^2}\ddot{x}_1 + 2x_1 = F/m$$

$$= [-\cos 1.41\omega_0 t + 0.25\cos 2\omega_0 t + 0.75]\frac{F}{\omega_0^2 m}$$

$$\Delta x_1 = x_1 - x_0$$

$$= [-\cos 1.41\omega_0 t - 0.50\cos 2\omega_0 t + 1.50]\frac{F}{\omega_0^2 m}$$

$$\Delta x_2 = x_2 - x_1$$

$$= [-\cos 1.41\omega_0 t + 0.50\cos 2\omega_0 t + 0.50]\frac{F}{\omega_0^2 m}$$

TABLE E.1

Incremental Displacement, 100' Bridge

$w_o t$	0	.2	.4	.6	.8	1.0	1.2	1.4	1.6	1.8	2.0
cos .618 $w_o t$	1	.992	.970	.932	.880	.815	.737	.648	.549	.441	.327
cos 1.18 $w_o t$	1	.972	.890	.759	.586	.380	.153	-.082	-.313	-.526	-.711
cos 1.62 $w_o t$	1	.948	.797	.569	.270	-.051	-.366	-.644	-.854	-.975	-.995
cos 1.90 $w_o t$	1	.928	.724	.416	.047	-.325	-.653	-.888	-.995	-.960	-.883
cos 2.0 $w_o t$	1	.921	.696	.360	-.020	-.418	-.740	-.944	-.998	-.894	-.772
2.62 cos .618 $w_o t$	2.62	2.600	2.54	2.441	2.315	2.135	1.930	1.647	1.438	1.155	.856
3.24 cos .618 $w_o t$	3.24	3.210	3.14	3.019	2.851	2.640	2.387	2.099	1.778	1.428	1.059
1.62 cos 1.18 $w_o t$	1.62	1.570	1.441	1.229	.949	.615	.247	-.132	-.507	-.852	-1.151
.38 cos 1.82 $w_o t$	.38	.360	.302	.216	.102	-.019	-.139	-.244	-.324	-.370	-.378
1.24 cos 1.62 $w_o t$	1.24	1.175	.988	.705	.334	-.063	-.453	-.793	-1.058	-1.209	-1.233
.62 cos 1.90 $w_o t$	.62	.580	.448	.257	.029	-.201	-.404	-.550	-.616	-.595	-.547
.50 cos 2.0 $w_o t$	.50	.460	.384	.180	-.010	-.209	-.370	-.472	-.499	-.447	-.386
$\Delta x_1 \frac{w_o^2 m}{y}$	0	.20	.77	1.64	2.71	3.87	5.00	5.94	6.61	6.97	7.15

TABLE E.1 (Continued)

$\Delta x_2 \frac{v_o^2 a}{F}$	0	.01	.01	.05	.16	.36	.69	1.16	1.78	2.53	3.24
$\Delta x_3 \frac{v_o^2 a}{F}$	0	0	0	.01	.01	.01	.03	.08	.16	.31	.69
$\Delta x_4 \frac{v_o^2 a}{F}$	0	0	0	0	0	0	0	0	0	.01	.03
$\Delta x_5 \frac{v_o^2 a}{F}$	0	0	0	0	0	0	0	0	0	0	0

TABLE E.1 (Continued)

$w_o t$	2.2	2.4	2.6	2.8	3.0	3.2	3.4	3.6	3.8	4.0
cos .618 $w_o t$	.208	.086	-.038	-.163	-.282	-.398	-.508	-.610	-.710	-.735
cos 1. 18 $w_o t$	-.856	-.953	-.997	-.986	-.920	-.804	-.642	-.445	-.223	-.097
cos 1.62 $w_o t$	-.910	-.732	-.476	-.171	.151	.459	.717	.902	.992	.201
cos 1.90 $w_o t$	-.503	-.146	.232	.576	.839	.932	.983	.844	.585	.242
cos 2.0 $w_o t$	-.102	.094	.474	.780	.962	.992	.864	.600	.240	.156
2.62 cos .618 $w_o t$	.544	.022	-.095	-.427	-.738	-1.042	-1.330	-1.598	-1.841	-2.056
3.24 cos .618 $w_o t$	.673	.0273	-.0123	-.534	-.913	-1.239	-1.645	-1.976	-2.277	-7.543
1.62 cos 1.18 $w_o t$	-1.386	-1.543	-1.615	-1.597	-1.490	-1.302	-1.040	-.720	-.361	-.157
.38 cos 1.62 $w_o t$	-.345	-.278	-.180	-.064	.0573	.174	.272	.342	.376	.076
1.24 cos 1.62 $w_o t$	-1.120	-.907	-.590	-.013	.187	.569	.889	1.118	1.230	.249
.62 cos 1.90 $w_o t$	-.311	-.090	.143	.357	.520	.577	.609	.523	.362	.150
.50 cos 2.0 $w_o t$	-.051	.047	.237	.390	.481	.496	.432	.300	.120	.078
$\Delta x_1 \frac{w_o^2 m}{f}$	6.61	6.20	5.54	4.85	4.23	3.82	3.52	3.51	3.73	4.86
$\Delta x_2 \frac{w_o^2 m}{f}$	4.33	5.26	5.77	6.34	6.67	6.74	6.64	6.30	5.81	5.87

TABLE E.1 (Continued)

$\Delta x_3 \frac{w_0^{2a}}{F}$	.75	1.52	1.68	2.63	3.12	3.86	4.60	5.29	5.89	5.22
$\Delta x_4 \frac{w_0^{2a}}{F}$	.18	.35	.25	.43	.65	.98	1.34	1.81	2.36	3.25
$\Delta x_5 \frac{w_0^{2a}}{F}$	0	0	.01	.03	.07	.07	.20	.31	.45	1.15

APPENDIX F

STRENGTH OF SWAY BRACE

by Norman G. Hansen

The sway brace is a bar, 1 1/8 in. in diameter, of cold rolled steel, FS 1020, in accordance with Federal Specification QQ-S-671. No specific requirement for physical properties is thereby established. The tensile strength actually obtained varies considerably, but is expected to be usually in the range 60 to 70 thousand pounds per sq in. The overall strength of the brace is limited by the strength of the threaded part where the turnbuckle is applied. These threads are 1 1/8 in. nominal diameter, National Coarse series, having a root diameter of 0.94 in. and a pitch diameter of 1.03 in. Published material indicates that a fair estimate of the thread strength may be based on the mean of these diameters. This area is 0.76 sq in. and on this basis a strength, for the entire brace, of 45,000 to 53,000 lb might be expected. One test was made on 30 January 1953 of a brace with turnbuckle, from the T1 bridge, which is of similar construction but 1 1/4 in. nominal diameter. The threaded portion broke at 55,000 lb pull; this is equal to 57,000 psi on the mean effective thread area. If the Bailey bridge, 1 1/8 in. diameter sway brace were of this material, its strength would be 43,000 lb. It is believed likely that the cold-rolled bars used for Bailey sway braces are slightly stronger, so the value of 50,000 lb. assumed, is rather likely to be realized.

APPENDIX G

OVERTURNING COLLAPSE OF TRUSSES

by Norman O. Hansen

In the report, the assumption was made that bridge failure would occur under lateral force by failure of the sway (i.e., lateral) braces. There is another possible mode of failure, namely overturning of the trusses with failure of the rakers, bracing frames and/or the transom clamps. In the case of the double-single bridges to be tested, there are again two ways in which these parts might fail. Each way involves combined failure of at least two parts. The structure is highly indeterminate in these respects; and, furthermore, an assumption of elastic behavior is unwarranted.

In the case of the single-single construction, the raker alone would resist overturning moment. The tension in this member would be approximately 1.5 times the lateral force less the inertia resistance of the truss itself. The shock impulse is large enough to produce excessive stresses, but as the duration is very small (order of 5 msec) the effects will be probably limited to moderate distortion of the connecting pintles. The drag force will be much smaller; for an overpressure of 12 psi, the total drag force on one truss panel is about 6,700 lb and the raker tension 10,000 lb which should be well within the capacity of the raker.

Double-single bridges have very considerable additional resistance to overturning, although as described above, it is indeterminate. There should be ample strength, however, to resist overturning.

In double-double Bailey construction the overturning moment will be very much greater; nearly four times as great as for the double-single. The resisting strength is no greater except for the increased inertia. Failure of DD bridges by truss overturning seems definitely possible.

APPENDIX E

LOCATION OF BRIDGE SITES

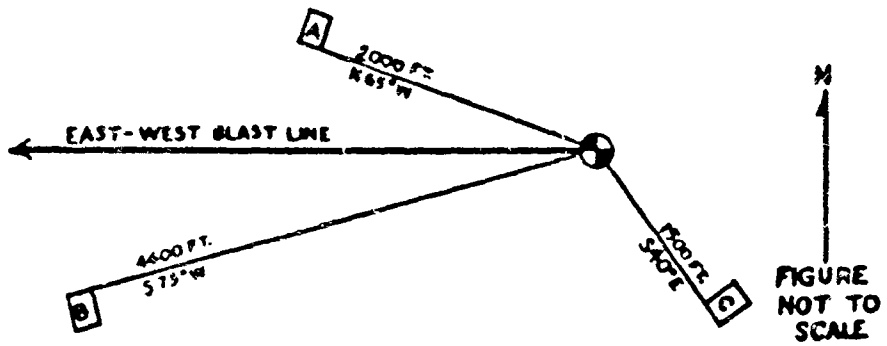

Fig. E.1 Location of Bridge Sites

BIBLIOGRAPHY

1. The Effects of Atomic Weapons, Los Alamos Scientific Laboratory, September 1950, Unclassified.

2. Capabilities of Atomic Weapons, Department of the Army TM23-200 October 1952, Secret, RD.

3. Panel Bridge, Bailey Type, M2, Department of the Army TM5-277, April 1948.

4. Operation UPSHOT-KNOTHOLE, Project 1.1a-1.2, Pressure Measurements in the Air and on the Ground, Dr. W. E. Morris, U. S. Naval Ordnance Laboratory, AFSWP Report WT-716.

5. Operation UPSHOT-KNOTHOLE, Project 1.1b, Air Pressure vs. Time, L. M. Swift and D. C. Sachs, Stanford Research Institute, AFSWP Report WT-711.

6. Operation UPSHOT-KNOTHOLE, Project 1.1d, Dynamic Pressure vs. Time, and Supporting AW Blast Measurements, Carter D. Broyles, Sandia Corporation, AFSWP Report WT-714, Secret RD.

7. Operation UPSHOT-KNOTHOLE, Summary Report of the Technical Director, AFSWP Report WT-782, Secret, RD.

8. Behavior of Truss Bridges Under Blast From an Atomic Bomb, a report submitted in two phases by the Massachusetts Institute of Technology to the Office of Chief of Engineers, Department of the Army, November 1950 and July 1951, Confidential.

9. Gardner and Barnes, Transients in Linear Systems, John Wiley and Sons, New York, 1952.

10. Hildebrand, Advanced Calculus for Engineers, Prentice-Hall, Inc., New York, 1949.

11. Binder, Fluid Mechanics, Prentice-Hall, Inc., New York, 1949.

12. Resume' of the Theory of Plane Shock and Adiabatic Waves with Applications to the Theory of Shock Tubes, Ballistic Research Laboratories, March 1950, Unclassified.

13. Operation GREENHOUSE, Scientific Directors Report, Annex 3.3, U. S. Air Force Structures, Appendix E, Section I, WT-59.